INFLUENCE OF SURFACE ROUGHNESS AND WAVINESS UPON THERMAL CONTACT RESISTANCE

Milan M. Yovanovich
Warren M. Rohsenow

Report No. 76361-48
Contract No. NAS7-100

Department of Mechanical Engineering
Engineering Projects Laboratory
Massachusetts Institute of Technology

June 1967

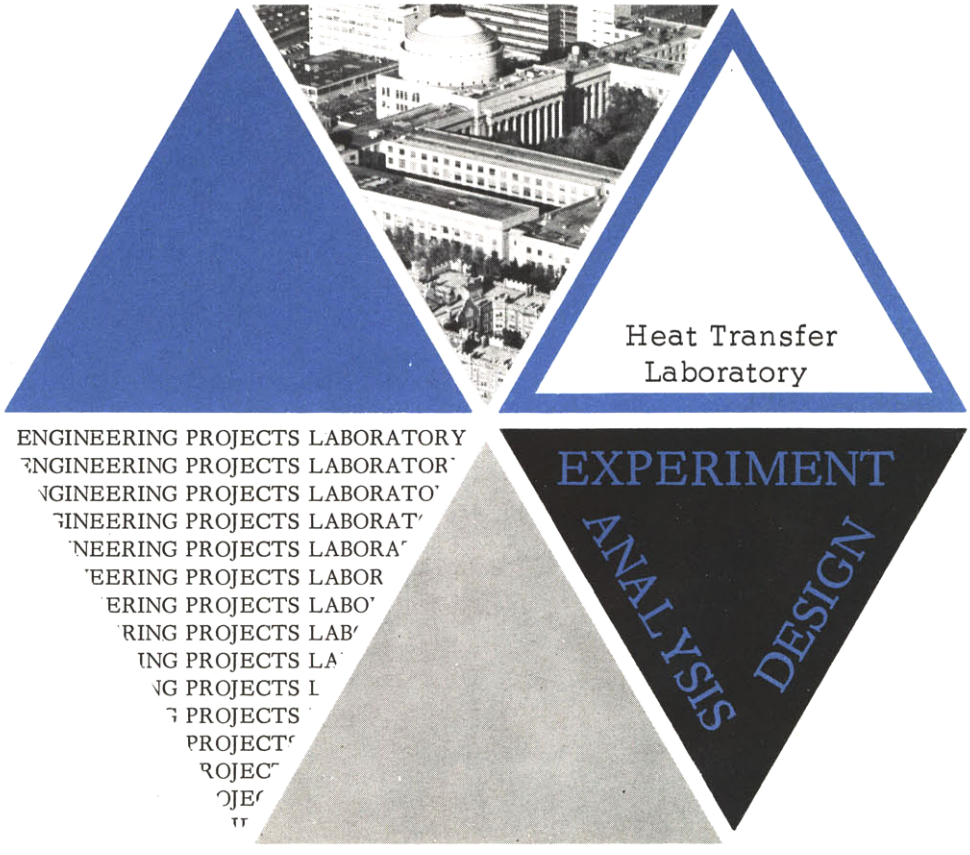

Technical Report No. 6361-48

INFLUENCE OF SURFACE ROUGHNESS AND WAVINESS UPON THERMAL CONTACT RESISTANCE

by

M. Michael Yovanovich

Warren M. Rohsenow

Sponsored by the National Aeronautics

and Space Administration

Contract No. Nas 7-100

June 1967

Department of Mechanical Engineering

Massachusetts Institute of Technology
Cambridge, Massachusetts 02139

ABSTRACT

This work deals with the phenomenon of thermal resistance between contacting solids. Attention is directed towards contiguous solids possessing both surface roughness and waviness. When two such surfaces are brought together under load, they actually touch at isolated microcontacts, and the resulting real area is the sum of these microcontacts. Because of the waviness the microcontacts are confined to a region called the contour area which may occupy some fraction of the total available area. The non-uniform pressure distribution over the contour area results in microcontacts which vary in size and density. In the absence of an interstitial fluid and negligible radiation heat transfer, all the heat crossing the interface must flow through the microcontacts. A thermal analysis, based on size and spatial distribution, results in a thermal resistance equation which differs from previously developed theories. The equation is verified by liquid analog tests which show that the size and spatial distribution are very significant.

A surface deformation analysis considers the influence of surface roughness upon the elastic deformation of a rough hemisphere. An equation is developed which shows the extent of the contour area as a function of the surface geometry, the material properties, and the applied load. The equation is compared with existing theories and qualitatively checked against experimental results.

Experimental heat transfer data were obtained to verify the thermal and deformation theories. The agreement between theory and test is quite good over a large range of surface geometry and applied loads.

ACKNOWLEDGMENTS

The author wishes to acknowledge the assistance and advice of his Thesis Committee which consists of Professors Warren M. Rohsenow, Henri Fenech, Brandon G. Rightmire, and Michael Cooper. He particularly wishes to acknowledge the encouragement of his thesis supervisor, Professor Warren M. Rohsenow, and the many long and fruitful discussions with Professor Michael Cooper.

The author also extends his heartfelt thanks to his colleagues in thermal contact resistance research: Professor Bora Mikic of the Department of Mechanical Engineering, Dr. Thomas J. Lardner of the Department of Mathematics, and Spyros Flengas. Professor Mikic and Mr. Flengas shared with me the results of their liquid analog tests. Dr. Lardner acted as a sounding board for some of my ideas on contact resistance and the deformation of solids.

The author would be remise if he did not acknowledge the advice and aid of Mr. Frederick Johnson of the Heat Transfer Laboratory, whose experience enabled the author to accomplish quickly and efficiently some of the fabrication work.

Finally the author expresses his thanks to his wife for her patience and encouragement.

Sincere appreciation is expressed for the financial support of the National Aeronautics and Space Administration under NASA Contract NAS 7-100 which made this work possible.

TABLE OF CONTENTS

LIST OF FIGURES

NOMENCLATURE

A	area
a	apparent radius
B	curvature, Eq. (4.4)
b	channel radius
C	contour radius
c	contact spot radius
E	modulus of elasticity
E'	complete elliptic integral, Eq. (4.16)
F	force
g	distance between isothermal planes
H	material hardness
h	thermal conductance
J	Bessel Function
K'	complete elliptic integral, Eq. (4.16)
L	length
P	pressure
Q	heat flow per unit time
q	heat flux
R	thermal resistance
r	coordinate
S	number of intersections, Eq. (7.3)
T	temperature
V	potential, Eq. (2.1)
x	coordinate

Y	distance between mean planes
Y_o	separation at zero load, Eq. (4.19a)
y	coordinate

Greek letters

α	compliance, Eq. (4.21)
β	maldistribution factor, Eq. (3.1)
δ	absolute displacement
ϵ	real area ratio, $\epsilon^2 = A_r/A_a$
$\}$	variable, Eq. (4.5a)
η	dimensionless compliance, Eq. (4.28)
λ	contour area ratio, $\lambda^2 = A_c/A_a$
ν	Poisson's Ratio, Eq. (4.5a)
η	variable, Eq. (4.5a)
π	pi
ρ	radius of curvature
σ	surface roughness, (rms or CLA)
ϕ	geometric factor, Eq. (2.8); Eq. (2.10)
ψ	roughness influence factor, Eq. (4.28)
ω	vertical displacement, Eq. (4.4)

Subscripts

a	apparent
c	contour
e	elastic or Hertzian
i	ith component
j	jth component

m	mean harmonic value
o	reference
r	real
t	total
y	yield
1, 2	solids 1 and 2

1. INTRODUCTION

1.1 Historical Background

Heat transfer across a contact interface formed by any two solid bodies is usually accompanied by a measurable temperature difference because there exists a thermal resistance to heat flow in the region of the interface. The temperature difference at the contact interface is obtained by extrapolating the steady state unidirectional temperature distribution from regions "far" from the contact plane. See Fig. 1. Temperatures T_1 through T_6 represent the unidirectional temperature distribution in either solid body. Temperatures T_7 and T_{11} represent the temperature levels at the boundaries of the region of three-dimensional or disturbed temperature distribution. T_8 and T_{10} are the extrapolated temperature levels at the contact interface, and the difference $(T_8 - T_{10})$ represents the pseudotemperature drop at the contact interface. The actual contact interface temperature will be some intermediate temperature T_9. If there were no resistance to heat flow across the interface, temperatures T_8, T_9, and T_{10} would be identical.

The contact coefficient of heat transfer will be defined in the conventional way as

$$h_c = \frac{Q/A_a}{\Delta T_c} \tag{1.1}$$

where Q/A_a is the steady state heat flux as determined by the temperature distribution in the undisturbed temperature region, and T_c is the pseudotemperature drop at the contact interface.

Using the electrical analog the thermal contact resistance is defined by

$$R = \Delta T_c / Q \tag{1.2}$$

and can be related to the contact coefficient of heat transfer or conductance as defined by Eq. (1.1) as

$$R = \frac{1}{h_c A_a} \quad . \tag{1.3}$$

It is seen that the thermal contact resistance is the reciprocal of the contact conductance. Thus, whenever reference is made to the contact conductance, the reciprocal of the thermal contact resistance is implied. The thermal contact resistance concept will be used throughout the body of this work since this concept lends itself to mathematical analysis.

Over the last two decades and in particular the past ten years, a large body of literature has been published which deals, with a few exceptions, primarily with experimental investigations concerning the thermal resistance between contacting solids. The emphasis on experimental investigations indicates that there was a lack of fundamental understanding of the thermal contact phenomenon. The result is that all the experimental data gathered by the various investigators cannot be used to predict thermal contact resistance for joints which differ from those investigated. The experimental data can, however, be used to show the trends as various parameters are changed. The influence of these various parameters is shown in Fig. 2. For a more complete

description of the materials investigated and details of the experimental procedure, this author refers the reader to the very complete bibliographies of references 9, 10, and 11.

1.2 Review of Parameters Affecting Thermal Contact Resistance

Figure 2 shows the influence on the thermal contact resistance as the indicated parameters are increased over some range of values. It is seen that some parameters have a negative influence, i.e., tend to decrease the thermal resistance while others have a positive influence. It will be assumed that whenever the influence of one parameter is considered, all other parameters are constant and, therefore, do not explicitly affect the discussion.

It should be borne in mind that throughout this discussion we will be dealing with real or worked engineering surfaces. By this we mean surfaces which have undergone some engineering process. It is a well-known fact that all "worked" surfaces exhibit waviness and roughness. These surface characteristics can be determined rather easily by means of a surface profilometer, and Fig. 6 shows a typical linear profile of a solid having a wavy, rough surface. An analysis of many linear profiles indicates that most surfaces have essentially a Gaussian distribution of asperity heights about some mean plane lying in the surface, irrespective of the manner in which the surface was prepared, i.e., milling, grinding, lapping. There is, however, a large difference in the way the asperities are distributed over the mean plane.

The surface irregularities are the result of the inherent action of production processes, machine or work deflections, vibrations, and warping strains. The surface irregularities with the large wavelength

are termed waviness, the length of these waves depending upon a number of conditions varying from 0.04 to 0.40 inch. The height can vary from 80 to 1600 microinches. In general, the longer waves (waviness) cannot be seen by either eye or microscopic examination. They may, however, play a controlling part in the behavior of the interface. In addition to these, most surfaces exhibit finely spaced roughness that is superimposed on the waviness and is responsible for the finish of the surface. The finely spaced irregularities are termed roughness and can range from 2×10^{-6} in. rms for the very smooth surfaces to about 600×10^{-6} in. rms for the very rough surfaces. Whenever reference is made to surface asperities, surface roughness is implied. The curvature of all asperities relative to their height is very large; i.e., if the asperities are thought to have peaks, the most characteristic range of the included angle at the peak is between 160° and 164°. The smallest included angle which occurs with the roughest surfaces would seldom be smaller than 150°.

It can be seen that when two solid bodies, exhibiting surface characteristics described above, are brought together under a load, there will be intimate contact at many small discrete spots, and a gap will exist in the regions of no real contact. The gap region will normally be occupied by a fluid, such as air. This brief explanation will suffice to make clear the discussion on the influence of the various parameters on the thermal contact resistance, Fig. 2.

1.2.1 Effect of Apparent Contact Pressure

The first and most obvious parameter to be investigated was the load holding the solid bodies together. As the load was increased,

it was observed that the thermal contact resistance decreased. The decrease was large initially and became less as the apparent contact pressure became quite large. It is expected, from a basic knowledge of strength of materials, that an increase in apparent contact pressure would result in a displacement of one surface relative to the other in the direction of load. This would bring the two surfaces closer together, thus reducing the size of the gap. A reduction in the size of the gap means that the surfaces must be in real contact over a larger region; i.e., the real area of contact has increased. The rate of gap decrease and the rate of real area increase should be large initially when relatively few asperities are in contact, and then the rate of change should decrease as the number of contacts becomes large. Also, as the gap size decreases, the thermal resistance through the fluid in the gap should decrease.

Several attempts were made to correlate the thermal contact resistance against the apparent contact pressure ($R \propto Pa^{-m}$). It was observed that the exponent varied from practically zero to almost one depending on several parameters. Even for a fixed system, the exponent would sometimes be quite different over particular load values. It was noted that initially m was 1/3 and then increased to one when the load was quite large. When the contacting surfaces are very smooth but possess spherical waviness, the contact resistance depends on the load to the minus 1/3 power at moderate contact pressures. This shows that the physical interaction between the solids is primarily elastic. When the contacting surfaces exhibit large roughness with essentially no waviness, the contact resistance varies inversely with the contact

pressure. This indicates that plastic deformation of the asperities is important. When the contacting surfaces are very smooth and a fluid such as air fills the gaps, the contact resistance at high contact pressures is almost independent of load changes.

A loading-unloading effect has been observed by several investigators and studied exclusively by Cordier, et al. (13), at the University of Poitiers. They obtained experimental data for a series of tests in which the contact pressure was increased stepwise by approximately 300 psi over a range from 0 to 1800 psi; then the contact pressure was decreased by the same increments until the load was again zero. The measurements were taken at the rate of one every hour. It was noted that the contact resistance could take on either of two values for any contact pressure, depending upon whether the measurement is made during the loading or unloading cycle.

1.2.2 Effect of Metal Thermal Conductivities

The next obvious parameter to be investigated was the effect of metal thermal conductivities. It was found that the influence of the harmonic mean thermal conductivity was practically linear. The reason that the correlation of thermal resistance with thermal conductivity is not exactly linear is because the mechanical properties of the solid bodies cannot be kept constant as the thermal conductivity is changed. The thermal conductivity effect will not be changed by altering any of the other parameters.

1.2.3 Effect of Surface Roughness

Considering the influence of surface roughness before the influence of surface waviness does not imply that roughness effects are

more pronounced than waviness effects. On the contrary, there are situations where waviness effects dominate. One should, however, recognize that the waviness effect can be minimized or reduced completely by proper preparation of the surface (no waviness present) or by increasing the load on the contact so that the contact occurs over the entire apparent area. Roughness, however, cannot be completely removed by lapping, and its influence on the heat transfer persists even under the largest contact pressures.

It has been observed that roughness plays an important part in determining the thermal resistance of a contact interface. The influence is positive, i.e., increases the resistance. A twofold increase in roughness can result in a four to fivefold increase in the thermal resistance. The influence is greatest when the apparent contact pressures are light and the surfaces are relatively smooth, and least when the contact pressures are high and the surfaces are rougher.

1.2.4 Effect of Surface Waviness

As discussed earlier the influence of surface waviness upon the thermal contact resistance is dominant under certain conditions of surface geometry and/or apparent contact pressure. It has been observed that waviness has a positive influence upon the thermal resistance. The effect is small for small waviness and becomes very important when the waviness is large. It has also been noted that a small amount of surface roughness (which is always present) has a pronounced effect upon the waviness at light apparent contact pressures. Generally the presence of some roughness reduces the waviness influence. This suggests that roughness may act as negative influence on the waviness

because there is an interaction between surface roughness and waviness. By this we mean that the surface waviness influence upon the thermal contact resistance cannot be determined without also considering the effect of surface roughness upon the waviness. Only under limiting conditions, such as very smooth, very wavy surfaces and very light apparent pressures, can surface roughness be neglected.

1.2.5 Effect of Interstitial Fluid Thermal Conductivity

As observed under Item 1.2.2, there is a negative influence of interstitial fluid (usually a gas) thermal conductivity. The effect is linear indicating that the heat transfer is due entirely to conduction of heat through the fluid layer; i.e., there are no convection effects in the fluid. A change in the apparent contact pressure, surface characteristics (roughness), and material properties does not affect the basic influence of fluid conductivity on the thermal resistance.

1.2.6 Effect of Material Hardness

It has been observed that material hardness has a positive influence upon the thermal contact resistance. By hardness we mean the pressure at which the material will yield under a compressive load as determined by any of the standard hardness tests (Brinell, Rockwell, Knoop, Vickers). There is a good linear correlation between the hardness and the thermal resistance for very rough, very flat (no waviness) surfaces over a large, apparent contact pressure range.

1.2.7 Effect of Modulus of Elasticity

A correlation between the thermal contact resistance and Young's modulus or elastic modulus has been noted. There appears to be a

stronger dependence of the resistance on the elastic modulus as the surfaces exhibit more waviness and less roughness. In fact, Clausing and Chao (14) were able to predict the thermal contact resistance for smooth hemispherical contacts using a contact radius calculated by the classical Hertzian theory. Their theory failed to predict the resistance for hemispherical contacts which had substantial surface roughness or when the apparent contact pressure became quite large. The influence of the elastic modulus is positive; i.e., the thermal resistance increases with increasing elastic modulus (increasing mechanical resistance). It is apparent that for certain surface characteristics and load on the contact, Young's modulus will be important, and the classical elastic theory may be used to predict the important parameters determing the thermal contact resistance.

1.2.8 Effect of Mean Contact Temperature Level

It has been observed that there is a correlation between the thermal contact resistance and the mean contact temperature level. The temperature influence is negative; i.e., as the temperature level increases, the thermal resistance decreases. The temperature effect is not very strong over a large temperature range and only becomes significant when the temperature level exceeds 1000 ^{o}F. The temperature trend is not unexpected when one considers the various parameters which can influence the thermal contact resistance and which in turn can be affected by the temperature level. Both metal and interstitial fluid thermal conductivities are affected by the temperature level and thus influence the thermal resistance of the contact. Generally, the metal conductivity influence is slightly positive while the fluid conductivity

influence is negative as the temperature level increases. But more important, the material properties, such as the hardness and the elastic modulus, are influenced by the temperature level. Both effects are negative; i.e., the hardness and elastic modulus tend to decrease the thermal contact resistance with increasing temperature level. This effect is implicitly taken into account when either plastic or elastic deformation of the surfaces is considered.

For mean contact temperature levels which exceed 1000 ^{o}F, radiation heat transfer across the gap becomes significant; i.e., the thermal contact resistance is determined primarily by the radiation resistance. Since this thermal resistance depends upon the mean temperature to the 1/3 power in the linearized form of the radiation equation, it is seen that the thermal resistance will have a very strong negative dependence on the temperature level.

Since most engineering problems are concerned with mean contact temperature levels below 1000 ^{o}F, the temperature influence will be small and will be taken into consideration through the deformation analysis.

1.2.9 Effect of Interstitial Fluid Pressure

There is a striking dependence of the thermal contact resistance upon the interstitial fluid pressure when the fluid is a gas. Consider the typical thermal resistance-gas pressure relationship shown in Fig. 2i. The high, horizontal resistance level corresponds to the thermal resistance for surfaces in a hard vacuum, while the low, horizontal resistance level is typical of surfaces at or near atmospheric pressure. The transition region extends over a very narrow pressure range (about

100 mm Hg) and will be shifted to the left or right depending upon the surface geometry, the type of gas in the gaps, and the load on the contact. For smoother surfaces the shift is to the left. As the load on the contact increases, the transition region also shifts to the left. Also, as the apparent contact pressure increases, the difference between the two horizontal regions decreases. Generally the higher level (vacuum region) decreases sharply while the lower level (atmospheric region) increases slightly. This interesting phenomenon depends upon the relationship between the mean free path of the gas molecules and the average or mean gap width. The gap width depends upon the initial surface geometry, the material properties of the contacting bodies, and the applied load on the contacting interface.

1.2.10 Effect of Relaxation Time

This phenomenon of relaxation time has been investigated extensively by Cordier. He has observed that the thermal contact resistance changes with time after initial contact. The influence is negative and usually takes place over a period of weeks or even months. If the thermal resistance is plotted against contact time, it is observed that the resistance decreases continuously and finally assumes a constant level. It is believed that this phenomenon is intimately connected with the hardness of the material and the initial surface geometry.

1.2.11 Effect of Filler Material

By filler material we mean any solid material which is placed between contacting solid bodies to either reduce or increase the thermal resistance. It is usually assumed that the filler material is smooth and uniform in thickness.

The shaded area in Fig. 2k indicates that there are many ways in which the filler material can influence the thermal contact resistance. The variables at one's disposal are the filler thickness, filler thermal conductivity, and filler hardness or elasticity. It has been observed that increasing the filler material thickness generally decreases the thermal resistance (if the original thickness is small $\sim$ 1 mil). As the thickness is increased further, the resistance goes through a minimum value and then begins to increase. Any further increase in filler material results in yet a higher resistance. The thickness of filler material at which the thermal resistance is a minimum depends on the surface geometry, the filler material properties, and the apparent contact pressure. The filler thermal conductivity can have a negative, zero, or positive influence upon the thermal resistance depending upon several things such as filler thickness, hardness, and the applied load. When the filler thickness is large ($\gtrsim$ 100 mil), the filler conductivity can have either a negative or positive influence depending upon the ratio of the solid body/filler thermal conductivity. When the filler thickness is quite small ($\sim$ 1 mil), the filler thermal conductivity has negligible influence, as the material properties are more important in determining the effect on the thermal resistance.

It is apparent that a knowledge of the physical interaction between a filler and the two solid bodies is needed in order to be able to predict what influence the filler material can have on the thermal contact resistance.

1.2.12 Directional Effect

By directional effect we mean the influence on the thermal contact resistance which may result from heat flowing from A to B, or from B

to A, where A and B are two dissimilar contacting bodies. It has been observed by several investigators that there is a significant directional effect on the thermal resistance when heat flows between aluminum and stainless steel placed in a vacuum. For the same heat flux and apparent contact pressure, there may be over 100 percent difference in the thermal contact resistance for heat flowing from aluminum to stainless steel than from stainless steel to aluminum. The magnitude of this difference is seen to depend upon the surface geometry (roughness, waviness), the material properties, the apparent contact pressure, and the level of heat flux.

It is believed that this phenomenon is the result of local thermal strains due to the relative temperature gradients between the actual contact spots and surrounding material. Due to local thermal strains, the number and size of contacts will be influenced differently as the heat flows from A to B or from B to A. This may result in significant changes in the thermal contact resistance. In order to predict this phenomenon, it is necessary to have knowledge of the interaction of solid bodies under various heating conditions. This includes knowing the effect of surface roughness and waviness, as well as the material properties.

1.3 Summary of Parameters Influencing Thermal Contact Resistance

The brief review of the many parameters which have some influence on the thermal contact resistance clearly shows that this contact phenomenon is quite complex. One would be rather naive to think that any one theory could predict the thermal resistance over all possible ranges of the many parameters considered to be important. Each area of interest

will require special consideration in order to evaluate the relative importance of one parameter over another, e.g., influence of interstitial fluid relative to the influence of the contact spots.

One underlying theme runs through all of the discussions. It becomes very clear that the interaction of solid bodies under loading conditions is of paramount importance. The influence of interstitial fluid, filler material, the radiation effect, and the directional effect will depend upon the gap and, therefore, upon the surface geometry and the interaction of the solid bodies.

The factors which determine the real contact area between contiguous solids can be divided into two areas of importance: surface geometry (roughness, waviness) and surface interaction (plasticity, elasticity, hardness). It is obvious that during the development of contact, both areas are mutually interrelated, and it is impossible to determine some of them without a knowledge of others. For example, the size of the actual contact area, which depends upon the geometrical properties of the contacting surfaces, determines the actual pressure acting on the asperities, while the roughness determines the asperity density over the contacting area. The present knowledge of surface interactions does not permit one to use either the classical elasticity or plasticity theory unless the compressed surfaces are of regular geometrical form with either perfectly elastic properties or for the case of plasticity without roughness.

The contact process for real surfaces cannot be reduced to purely elastic or to purely plastic deformation of the microscopic asperities. Contact interactions of two solids are generally of an elastoplastic

or elastoviscous nature. This is due to the fact that the initial contact usually occurs between the highest asperities which are few in number and which must bear all the applied load. There is subsequent redistribution of the pressure to the other asperities after the first contacting asperities have been crushed, and the total applied load is finally supported by the entire surface layer of the bodies. The possibility is not excluded that the macroscopic surface deviations (waviness) can change during the loading. Also, there may be a permanent change in the characteristics of the roughness during the compression.

It is evident (and bears repeating) that the shape, height, and distribution of the macroscopic (waviness) and microscopic (roughness) surface irregularities are some of the most important factors determining the real contact area under loading conditions.

The most important physical (mechanical) properties are the modulus of elasticity, the hardness or yield pressure of the asperities, and the plasticity in the determination of the following: 1) real contact pressure; 2) the displacement or approach of the surfaces as a result of the deformation of the surfaces under compression; and 3) the actual area of contact (number and size of contact spots).

2. THERMAL CONTACT RESISTANCE

2.1 Introduction

Historically the first individual to consider the effect of constriction of flow lines was Weber (16). He solved the following problem: "If V be the potential due to a circular disk (electrode) of radius c on which there is a charge of electricity in equilibrium unaffected by the action of electricity external to the disk, what is the potential distribution in the region external to the disk?" Weber showed that the following potential distribution satisfies Laplace's equation and the boundary conditions

$$V = \frac{2V_o}{\pi} \int_0^\infty e^{\mp \lambda z} \sin(\lambda c)\, J_o(\lambda r)\, \frac{d\lambda}{\lambda} \qquad (2.1)$$

where the upper sign is to be taken for positive values of z and the lower for negative values, and V_o is the potential of the disk. He further showed that for a constant potential over the disk area, the flux of the potential normal to the disk was proportional to $(c^2 - r^2)^{-\frac{1}{2}}$. It is obvious that the flow will be infinite at the edge of the circular disk unless the condition of constant potential at the edge be relaxed. Weber showed that when the circular disk was very small relative to the external region, the constriction resistance on one side of the disk could be written as

$$R = 1/4kc \qquad (2.2)$$

where c is the radius of the circular disk, and k is the conductivity of the external region.

Many investigators after Weber considered the constriction resistance for either electricity or heat flow to be the result of many small circular contacts. They essentially arrived at the same result that Weber had found many years earlier. The first attempt at determining the constriction resistance of a constant potential circular spot feeding into a coaxial right circular cylinder appears to be that of Roess (18). He considered the effect of increasing the size of the spot relative to the size of the cylinder. Although the problem was formulated as the constriction resistance of a constant potential circular area, the boundary condition which he used was that of a flux distribution over the spot proportional to $(c^2 - r^2)^{-\frac{1}{2}}$. For large contact spots, he used an average temperature over the area. Roess also considered the effect of heat flux distribution on the local temperature over the circular contact area. He solved this problem numerically for several values of contact spot size and heat flux distribution and presented them in tabulated form.

Clausing later used these tabulated results to show that the constriction resistance for either constant temperature or constant heat flux over the contact spot is essentially the same from $\epsilon \leq c/a = 0$ to 0.4. In the limit $\epsilon \to 0$, Clausing showed that the numerical constant was 0.252 for the constant flux condition and compared it with the value 0.250, see Eq. (2.2) obtained for the constant temperature condition over the contact spot. It has been shown by Carslaw (19) that for the region $z > 0$ with constant flux q over the circular area $r < c$ and zero flux over $r > c$, the temperature is

$$T = \frac{qc}{k} \int_0^\infty e^{-\lambda z} J_o(\lambda r) J_1(\lambda c) \frac{d\lambda}{\lambda} \quad . \tag{2.3}$$

The average temperature T_{av} over $0 < r < c$ is

$$T_{av} = \frac{2q}{k} \int_0^\infty J_1^2(\lambda c) \frac{d\lambda}{\lambda^2} = \frac{8qc}{3\pi k} \quad . \tag{2.4}$$

Since the rate of heat flow over the circular spot is $Q = \pi c^2 q$, Eq. (2.4) gives the constriction resistance

$$R = T_{av}/Q = 8/3\pi^2 \, kc = 0.270/kc \quad . \tag{2.5}$$

This indicates that the constant flux boundary condition produces a resistance which is 8 percent greater than the resistance which results from the constant temperature boundary condition.

More recently Mikic (11) reconsidered the problem of a concentric circular hot spot on the end of the right circular cylinder. The walls were adiabatic, and the length of the cylinder was finite. He assumed the constant temperature boundary condition and obtained a result which reduced to Weber's solution for the case of a very small contact spot. When he assumed a constant heat flux boundary condition, he obtained a solution which in the limit $\epsilon \to 0$ the numerical constant was 0.276. This is 4 percent larger than the value given by Carslaw.

Mikic was able to show that the constriction resistance for a finite contact spot on the end of a heat channel is uniquely determined by the temperature distribution over the apparent contact area of the heat channel. He considered the contact spot to be composed

of a very large number of heat sources equally spaced and employed the method of superposition to determine the temperature distribution over the apparent area. Thus in the contact plane the contribution of each source is $Q/4kc$ over its own area and $(Q/2\pi kc)\sin^{-1}(c/r)$ elsewhere where c is the radius of the source, and r is the distance from the center of the source. The heat flow out of each source per unit time is Q. When this temperature distribution is substituted into the expression for the constriction resistance

$$R = \frac{\Delta T}{Q} = \frac{\frac{2}{c^2}\int_0^c T(z=0)\ rdr - \frac{2}{a^2}\int_0^a T(z=0)\ rdr}{Q} , \qquad (2.6)$$

one can obtain a value for the constriction resistance for the constant temperature boundary condition. This method leads to an expression which gives values of the contact resistance similar to those obtained by Weber and Roess for various values of the ratio ϵ.

2.2 General Theory of Thermal Contact Resistance

Since the real contact between two "engineered" solids occurs at a finite number of discrete spots, any heat transfer across the contact interface will be accompanied by an additional temperature drop. This pseudotemperature drop is a manifestation of the thermal contact resistance which is the result of not having a perfect contact; by this we mean that the real contact area is a very small fraction of the apparent area. Another manifestation of this thermal contact resistance is the convergence and divergence of heat flow lines as the heat flows into and out of the contact interface region. This "pinching" effect can

be visualized more easily if we restrict our discussion to contiguous surfaces in a hard vacuum environment and also assume that radiation heat transfer across the gaps is negligible; i.e., the radiation thermal resistance is extremely large relative to the "pinching" effect. All the heat crossing the contact interface can flow only through the real contact area. The pinching effect is maximum when the contact spots are few in number and small in size. It will be shown later in this discussion that the number, size, and distribution of contact spots are more important than the magnitude of the total real area in reducing the thermal contact resistance.

The presence of a fluid in the gaps or radiation effects tends to alleviate the "pinching" effect and thus reduce the thermal contact resistance. The presence of a very thin, very soft metal foil also tends to alleviate the "pinching" effect by increasing the density of contacts over the value without the presence of the foil.

With this "pinching" effect in mind, let us examine closely the physical interaction of two nominally flat, rough surfaces (no waviness present). Since there is no waviness, the small contact spots will appear randomly over the entire apparent area. This picture will not be true if the contiguous surfaces have a definite lay, and they are mated either parallel or perpendicular to this lay. We shall restrict ourselves to a random distribution of contact spots over the apparent area. The diameter of these contact spots will vary over some range from the smallest diameter (probably determined from surface energy conditions) to some maximum diameter (which cannot be determined at this moment). It is expected that the largest diameter

can be (and often is) an order of magnitude larger than the smallest. The frequency of occurrence of the smallest can be orders of magnitude larger than the occurrence of the largest diameter, so that ultimately the total real area due to the smallest contact spots is practically equal to the real area of the largest. But most important, the bulk of the real contact area is due to the many contact spots having some mean contact diameter which is approximately the average of the smallest and largest diameter.

It has been observed that the mean contact spot diameter is practically independent of the apparent contact pressure. This does not mean that the sizes of the contact spots do not change. The smallest diameter may change slightly, and it is expected that the largest size will change significantly as the load on the contact interface is increased. With every increase in apparent pressure, there is an increase in the total number of contacts. The result is that the bulk of the total real area is still due to those contacts having a diameter intermediate to the smallest and largest diameter. This new mean diameter corresponding to the new larger apparent pressure is practically unchanged.

It must be realized that a rough surface consists of many very small peaks and valleys, which are randomly distributed about some mean plane lying in the surface. It has been shown that the contained angle at the peaks is seldom smaller than 150° and is usually about 162°. The value of 150° corresponds to the roughest surface which one may encounter. This means that the peaks are more like very long rolling plains than high mountains. When two such peaks or asperities come

into contact, it resembles the contact between two very large hemispheres touching over a small (relative to the radii of curvature of the asperities) circular spot.

Since we are examining the case of heat transfer only through the contacts (hard vacuum, negligible radiation effect), the heat transfer model which suggests itself for the case of few and small contacts is that of a contact spot on a semi-infinite body. As the apparent contact pressure increases, the number of contacts increases greatly, and the heat transfer model must be changed. Here we can assume that each contact spot is fed by a heat channel having adiabatic walls; i.e., all the heat passing some plane contained by the heat channel and which is far from the contact zone must pass through the contact spot. The mathematic solution to this model should go into the solution for the first model in the limit as the diameter of the contact spot becomes very much smaller than the heat channel diameter.

Throughout this discussion we have referred to contact spot diameter implying that the contacts are circular. We expect the contacting asperities (which need not be hemispherical) will seldom touch along an axis passing through their centers of curvature. They will touch on their shoulders thus producing elliptical contact spots. We believe that these will differ only slightly from circular spots, and, therefore, to facilitate the mathematics we assume circular contact spots throughout the discussion.

It will further be assumed that the contact interface (it is reasonable to assume that the interface can be slightly curved, due to a very hard curved solid contacting a flat soft solid) lies in a surface

which if the contact were perfect would be an isothermal surface. This assumption is important to the argument presented in Appendix A. Here it is shown that the contact spots are all at a uniform temperature (this will yield a particular solution for the thermal contact resistance of an elemental heat channel). It is further shown that all contact spots, irrespective of size, shape, or distribution over the apparent contact area, have the same uniform temperature. This is true only for the restrictions stated above.

2.3 Thermal Contact Resistance for an Elemental Heat Channel

The following discussion will follow closely the work done by Mikic (11), who determined the thermal contact resistance for an elemental heat channel. He assumed that all the contact spots have the same circular area and also that the contact spots are uniformly distributed over the contact interface. This picture of the contact spot size and distribution is not strictly valid and will be discussed later. For contacts in a vacuum and because the contacting asperities usually have a very small slope, Mikic assumed the elemental heat channel to consist of a circular hot spot on the end of a right circular cylinder. For negligible radiation heat transfer, the area beyond the contact spot can be considered to be adiabatic. The sides of the heat channel by definition will also be adiabatic. The radius of the heat channel will be calculated by means of the contact spot density as defined by the constant radius, uniformly distributed contact spot model. One half of the elemental heat channel is shown in Fig. 9 with the boundary conditions which must be satisfied by the solution to Laplace's

differential equation over the entire region defined by the elemental heat channel.

The two cases which he solved differed only in the boundary conditions prescribed over the contact spot. The first case considered a uniform temperature over the contact spot (this requires that the heat flux over the contact spot be hemispherical, i.e., $q = Q/2\pi c\sqrt{c^2 - r^2}$ where c is the contact spot radius). In the second case it was assumed that the heat flux over the contact spot was uniform. These two boundary conditions will determine the minimum and maximum thermal resistances which can be developed due to the contact spot. Any other temperature or heat flux distribution over the contact spot will produce a thermal resistance whose magnitude will lie between the limiting values. It is for this reason that the two cases were studied in great detail. The complete details can be found in reference (11).

Only the salient features of the theory will be presented here in order to show which geometric parameters are needed. It has been shown that the thermal contact resistance for one half an elemental heat channel can be expressed as

$$\bar{R} = \frac{4}{\pi k \bar{c}} \phi\left(\frac{\bar{c}}{a}\right) \tag{2.7}$$

where k is the thermal conductivity of the heat channel material, $\bar{c}$ is the average contact spot radius, and $\phi(\bar{c}/a)$ is the dimensionless factor which depends upon the boundary condition over the contact spot and the ratio of the spot radius to the heat channel radius.

For the case of uniform contact spot temperature or hemispherical heat flux over the contact spot, ϕ can be expressed as

$$\phi_1\left(\frac{\bar{c}}{a}\right) = \frac{1}{2}\left(\frac{a}{\bar{c}}\right) \sum_{n=1}^{\infty} \frac{\sin\left(\alpha_n a \frac{\bar{c}}{a}\right) J_1\left(\alpha_n a \frac{\bar{c}}{a}\right)}{(\alpha_n a)^3 J_o^2 (\alpha_n a)} \tag{2.8}$$

with $J_1(\alpha_n a) = 0$. (2.9)

For the case of uniform heat flux over the contact spot, ϕ can be expressed as

$$\phi_2\left(\frac{\bar{c}}{a}\right) = \left(\frac{a}{\bar{c}}\right) \sum_{n=1}^{\infty} \tanh\left(\alpha_n a \frac{\bar{c}}{a}\right) \frac{J_1^2\left(\alpha_n a \frac{\bar{c}}{a}\right)}{(\alpha_n a)^3 J_o^2(\alpha_n a)} . \tag{2.10}$$

As in Eq. (2.8) the roots are determined by $J_1(\alpha_n a) = 0$.

An examination of Eqs. (2.8) and (2.10) shows that ϕ_2 exceeds ϕ_1 over the entire range of the ratio $\bar{c}/a$. The maximum difference is just slightly less than 10 percent; i.e., the thermal contact resistance for the constant heat flux boundary exceeds the constant temperature boundary condition by about 10 percent.

Since all physical phenomena appear to follow the path of least resistance, it would not be premature to assume that the constant temperature boundary condition is the appropriate one. This boundary condition, however, requires a hemispherical heat flux distribution which has a singularity at the very edge of the boundary, i.e., $r = \bar{c}$. It might be more reasonable to assume that the constant temperature condition is valid over the major portion of the real contact and that in the vicinity of the edge, another condition is valid, say a constant flux. We shall, however, assume throughout the discussion that the

constant temperature condition prevails over the entire real contact area.

In order to determine the depth of the disturbed or three-dimensional temperature distribution region, Mikic solved Laplace's differential equation for a finite heat channel. We shall consider only the thermal resistance for the constant temperature boundary condition. Only the expression for ϕ will be given here

$$\phi_3 = \frac{1}{2}\left(\frac{a}{c}\right) \sum_{n=1}^{\infty} \tanh\left(\alpha_n a \frac{g}{a}\right) \frac{\sin\left(\alpha_n a \frac{\bar{c}}{a}\right) J_1\left(\alpha_n a \frac{\bar{c}}{a}\right)}{(\alpha_n a)^3 J_o^2(\alpha_n a)} . \qquad (2.11)$$

Comparison of ϕ_1 and ϕ_3 shows that the influence of the finite length of the elemental heat channel on the thermal contact resistance is negligible for all values of $g \geq a$, i.e., for heat channel length equal or greater than the channel radius. In other words, the depth of the region of disturbance does not extend beyond a distance from the contact plane approximately equal to the heat channel radius. Since the average heat channel radius depends upon the contact spot density, it is evident that the disturbed region is an extremely narrow region encompassing the contact interface. It is strictly a geometric effect and does not depend upon the thermal conductivity of the material on either side of the contact. When the curvature (waviness) becomes important, the disturbed region extends over a much larger depth and may greatly effect readings of thermocouples located within this region.

To recapitulate, it has been shown that the thermal contact resistance for half an elemental heat channel is given by Eq. (2.7), and

the geometric factor ϕ is given by Eq. (2.8) for the constant temperature boundary condition. The analysis was based on steady-state conditions, hard vacuum, negligible radiation, and the absence of an oxide film. The model is based on the physical contact between typical hemispherical asperities assuming that the circular contact spot is much smaller than the radii of curvature of the contacting asperities.

We can now write the expression for the total contact resistance for an entire typical heat channel which can consist of thermal conductivities k_1 and k_2

$$R = \bar{R}_1 + \bar{R}_2 = \frac{4}{\pi \bar{c}} \phi(\bar{c}/a) \left[\frac{1}{k_1} + \frac{1}{k_2} \right] \tag{2.12}$$

or written more compactly $R = 8\phi(\bar{c}/a)/k_m \pi \bar{c}$ where k_m is the harmonic mean thermal conductivity defined by $k_m = 2k_1k_2/(k_1 + k_2)$. Here it has been assumed from symmetry arguments that the heat channel radius is identical on either side of the contact spot.

If there are N <u>identical</u> contact spots distributed <u>uniformly</u> over the apparent contact area, we can assume that each contact spot has the same thermal resistance as any other spot. The total thermal contact resistance can now be written as

$$\frac{1}{R_t} = \sum_{i=1}^{N} \frac{1}{\bar{R}_i} = \frac{N}{\bar{R}_i} = \frac{N \pi \bar{c} k_m}{8\phi(\bar{c}/a)} \quad . \tag{2.13}$$

Using the relationship between thermal contact conductance and resistance, the conductance can be written as

$$h = \frac{1}{R_t A_a} = \frac{\pi n k_m \bar{c}}{8\phi(\bar{c}/a)} \tag{2.14}$$

where n is the contact spot density.

It can be seen that the conductance or resistance depends upon the contact spot density (which depends strongly on the applied load, $n \propto P_a^{0.8\text{-}0.9}$) and the average radius of contact (which has a weak dependence upon the applied load $c \propto P_a^{0.10\text{-}0.20}$). The strong dependence of the conductance on the apparent contact pressure can be seen by substituting the expression for heat channel radius, $a = 1/\sqrt{\pi}\, n$ into the ratio $\epsilon = \bar{c}/a$ so that the conductance can be written as

$$h = \frac{\sqrt{\pi n}\, k_m}{8\phi(\epsilon)} \quad . \tag{2.15}$$

A slightly different form of this expression had been arrived at by this author (10), who showed that Eq. (2.15) reduces to

$$h = \frac{2}{\sqrt{\pi}} \sqrt{n}\ k_m\ \epsilon \tag{2.16}$$

for the case when $\epsilon << 1$, i.e., $\phi(\epsilon) \simeq \pi/16$, which is valid for very rough surfaces or when the apparent contact pressure is less than 1000 psi.

Equation (2.15) is restricted to nominally flat, rough surfaces (no waviness) having uniformly distributed, constant radius contact spots. This equation always gives the maximum value of the thermal contact conductance. Any deviation from uniform distribution of contact spots will decrease the conductance of the interface. Any variation of contact spot size will also decrease the effectiveness of the

contacts thus reducing the conductance of the interface. The deviation from uniform distribution of constant size contact spots becomes more evident with decreasing surface roughness and/or increasing contact pressure. These effects on the overall thermal contact resistance will be examined in great detail in the following chapter.

When the contiguous surfaces exhibit large curvature (waviness) as well as roughness, the contact spots are confined to a portion of the apparent area, which is called the contour area. The contour area is the projected area determined by the outer limits of the microcontacts. In the region beyond the contour area, there is no physical contact between the touching surfaces. The contour area lying wholly within the apparent area can occupy a fraction or the entire portion of the apparent area depending upon the surface characteristics, the material properties, and the load on the interface. The effect of surface waviness will be discussed in some detail later.

3. THE EFFECTS OF CONTACT SPOT SIZE AND MALDISTRIBUTION

3.1 Contact Between Nominally Flat, Rough Surfaces

Worked metallic surfaces, whether turned, ground, or sandblasted, exhibit a random distribution of asperity heights about some mean plane lying in the surface (9). The distribution of the asperities over the apparent area, in general, will not be random, but will exhibit a lay. The lay or predominant direction of the asperities will depend upon the process (turning, grinding, blasting). A turning process will produce a circular pattern, while a grinding process will produce a linear pattern.

Unless two identical surfaces are matched exactly, it is expected that even those surfaces having a lay will produce microcontacts which are randomly distributed over the apparent area. Since the contacting surfaces are nominally flat, the microcontacts will be found anywhere in the total region defined by the total apparent area.

Let us consider the interaction of two nominally flat, rough surfaces, bearing in mind the facts just presented. Initially the contact will occur at the few highest asperities. As the load increases, these initial contact spots increase in size, and newer and smaller contacts just begin to form. Upon increasing the load still further, the first contacts grow even larger, the second group of contacts also increases in size, and still newer and smaller contacts appear. The process is repeated with each increase of the pressure on the contact interface.

One can see from this description that as nominally flat, rough surfaces come into contact under a load, there will be real contact

over a large number of discrete microcontacts which differ in size, density, and probably shape.

Autoradiographical data (8), Figure 8, show that the microcontacts are almost circular and that they vary in size and frequency of occurrence. The largest microcontacts are sparce, while the smaller ones are many. This is further substantiated by the friction and wear work of Rabinowicz (22) who measured the size distribution of wear particles formed during the relative slip of one metallic solid over another under a contact pressure. He also demonstrated that the size of wear particles formed is directly related to the size of microcontacts present. It was also observed that the size of the largest particle can be an order of magnitude larger than the smallest particle size.

In the following discussion it will be assumed that the microcontacts are circular in shape. This is done because circular shapes are amenable to mathematical analysis, and it is unlikely that the actual shapes differ much from elliptical shapes having major and minor axes approximately equal. Based on these outstanding facts, it is necessary for us to re-examine the existing thermal contact resistance theory to determine whether the contact size distribution is significant.

3.2 Elemental Heat Flux Tube

We define an elemental heat flux tube as a volume which encompasses a contact spot and extends some distance into either solid forming the contact. The surface which bounds the heat flux tube is called the control surface; it is always a closed surface. The surfaces through which the heat enters and leaves the heat flux tube will

be isothermal surfaces while the remaining surface will always be adiabatic. One isothermal surface will be in one solid while the other isothermal surface will be in the second solid. The axis of the heat flux tube will be parallel to the axis of the contact spot. Every elemental heat flux tube can be separated, in the surface of contact, into two parts because the heat flow pattern on either side of the contact is similar, and the surface of contact, as well as the contact spot, is isothermal. The boundary conditions over the surface of contact can be used to determine the contact or constriction resistance. The total resistance of the elemental heat flux tube will be the sum of the resistances of the two parts considered separately. It will be shown shortly that the linear dimension of the contact spot determines the size of the heat flux tube and, therefore, the quantity of heat flowing through the surface of contact. In the absence of an interstitial fluid and negligible radiation heat transfer across the gaps, all the heat entering the heat flux tube must pass through the contact spot. The larger contact spots will conduct more heat than the smaller contacts, Figure 10.

We shall consider in this work that the elemental heat flux tube is a right circular cylinder. The ends of the cylinder are the isothermal surfaces (planes) while the sides which are parallel to the axis of the cylinder are adiabatic. Other shapes of heat flux tubes can arise which are but modifications of the one which we shall use. As examples, consider the contact between concentric pipes or concentric spheres, Figure 11.

There are two possible types of heat flux tubes: one in which the contact spot is placed right in the center of the contact plane or one in which the contact spot is not equidistant to the boundary of the contact plane. We define the symmetric heat flux tube or symmetric contact as the one in which the axis of the contact spot is coincident with the axis of the heat flux tube. There is symmetry in any plane perpendicular to the contact plane. As stated earlier this problem was first considered by Weber (16) who obtained the constriction resistance for a small circular isothermal spot. Later several other investigators considered the effect of the relative size of the contact spot. They showed that when the contact spot was large, the resistance was not only a function of the linear dimension of the contact, but also a function of the relative size of the contact. Thus a contact spot whose radius is 1 percent of the heat flux tube radius would offer 26.5 times more resistance than a contact spot whose radius is 20 percent of the heat flux tube radius. This is 32 percent greater because of the relative size effect, Figure 12.

We now define an asymmetric heat flux tube as one in which the axis of the contact spot is not coincident with the axis of the heat flux tube. There is a finite distance between the axes, and there is symmetry in only one plane--the perpendicular plane which is co-planar with the two axes. The temperature distribution will be different in every other perpendicular plane. The contact plane, as well as the contact spot, will remain isothermal even when the asymmetry is a maximum.

Intuitively one feels that the asymmetric contact should not be able to conduct as much heat as the symmetric contact, especially when the contact spot is in the vicinity of the boundary of the heat flux tube. Also a relatively large contact spot should be more sensitive to small displacements from its symmetric position, while a very small contact spot would be relatively insensitive to a similar displacement.

A series of liquid analog tests were conducted to determine the effect of asymmetry for a typical heat flux tube. An analysis was made to correlate the experimental data with the relative displacement and the relative size of the contact spot, Appendix B. The experimental data showed that the relatively large contact spots are quite sensitive to small displacements, while the relatively small contact spots were less influenced by the asymmetry. It was observed that the asymmetric effect was a maximum when the contact spot displacement was a maximum and that this effect was a constant $\approx\sqrt{2}$, independent of the relative size of the contact spot, Figure 13.

There are two ways of viewing the asymmetric effect when the contact spot is relatively small. One way is to fix the boundary; then the asymmetric effect can be represented by an area over which the contact could be moved to have only a nominal increase in the resistance, Figure 18. The second way is to fix the contact spot in space and allow the boundary to alter its shape about the usual circular boundary, Figure 19. In short, the constriction resistance of a very small contact spot is independent of the shape of the boundary of the heat flux tube as long as the minimum or maximum distance from the contact spot to the boundary is not less than $(b - \delta)$ or greater

than $(b + \delta)$ where b is the linear dimension of the plane of contact, and δ is the displacement corresponding to a nominal increase in the resistance.

It is shown in Appendix B that the liquid analog test data is correlated very well by

$$\beta = \left[1 + \frac{(\delta/b)^2}{(1 - \epsilon)^2} \right]^{\frac{1}{2}} \tag{3.1}$$

where β is the asymmetric coefficient, δ/b the relative displacement, ϵ the relative size of the contact spot, and the constriction resistance for the symmetric contact as reference.

3.3 Effect of Variable Contact Spot Size

The concept of the symmetric heat flux tube will be used to determine the effect of variable contact spot sizes on the thermal resistances. There will be an elemental heat flux tube associated with each contact spot. By definition there will be no heat transfer between adjacent heat flux tubes, and from symmetry arguments, the size and shape of each tube will be identical on either side of the contact spot.

Far from the contact plane, the temperature distribution along the length of each heat flux tube will be identical to the temperature distribution along the heat channel which conducts the total heat flow to all the contact spots. In the vicinity of the contact spots, the temperature distribution in each heat flux tube will be different even though the temperature of each contact spot is the same. The pseudo-temperature drop at the contact plane will be the same for each heat

flux tube. From the definition of thermal contact resistance, we can immediately write

$$R_{c1} Q_1 = R_{c2} Q_2 = \cdots = R_{cj} Q_j = R_c Q \tag{3.2}$$

where Q_1, Q_2, etc. are the quantities of heat flowing through each contact spot. The quantity of heat flowing through each contact spot can also be related to the heat flux and the corresponding apparent area $Q_j = q_j A_{aj}$. The corresponding or appropriate apparent area is defined as that part of the contact plane which is associated with each heat flux tube. Since every heat flux tube has the same temperature distribution far from the contact plane, the heat fluxes in every flux tube must be identical, and we can now write Eq. (3.2) as

$$R_{c1} A_{a1} = R_{c2} A_{a2} = \cdots = R_{cj} A_{aj} = \cdots = R_{cN} A_{aN} = R_c A_a \tag{3.3}$$

where A_{a1}, A_{a2}, etc. are the corresponding apparent areas.

Equation (3.3) gives the relationship which must be satisfied by all the contact spots. It shows how the corresponding apparent areas are related to the contact spots and to each other. We see that the apparent area corresponding to the jth contact spot can be written in terms of the total apparent area

$$A_{aj} = A_a \Big/ \sum_{i=1}^{N} \left(\frac{\phi_j}{\phi_i}\right) \left(\frac{c_i}{c_j}\right) \tag{3.4}$$

where ϕ is the geometric factor of Eq. (2.7). Since the linear dimension of even the largest contact spot is a small fraction of the linear

dimension of the corresponding apparent area, $\phi_j/\phi_i \simeq 1.0$ for any two contact spots. This means that the size of any corresponding apparent area is determined by the linear dimensions of the corresponding contact spot and the entire set of contact spots. The total apparent area is subdivided among the contact spots according to the relation given in Eq. (3.4).

Equation (3.3) also gives the relationship for the thermal contact conductance in terms of the conductance for any contact spot, hence

$$h_c = k_m \pi \sum_{i=1}^{N} c_i/8\phi_j A_a \tag{3.5}$$

where k_m is the harmonic mean thermal conductivity and ϕ_j is the geometric factor for the jth contact spot. Since the jth contact is any contact spot in the total set of contact spots, we can use any ϕ. When there is plastic deformation of asperities, the real area ratio can be determined from $\epsilon^2 = P_a/3\sigma_y$, and so $\phi_j = (\pi/16 - \epsilon/4)$.

The previous theories based on uniform contact spot size result in a conductance equation which can be written as

$$h_c = \frac{\pi k_m}{8\phi(\epsilon)A_a} \left[N \sum_{i=1}^{N} (c_i)^2 \right]^{\frac{1}{2}} \tag{3.6}$$

whereas the new theory based on variable contact spot size results in the following expression

$$h_c = \frac{\pi k_m}{8\phi(\epsilon)A_a} \sum_{i=1}^{N} c_i \quad . \tag{3.7}$$

Liquid analog tests clearly demonstrate that for the same number of contact spots and the same total real area, Eq. (3.6) will over predict the conductance by as much as 34 percent while Eq. (3.7) agrees extremely well with the tests. As the variation in contact spot size becomes smaller, both Eqs. (3.6) and (3.7) predict conductances which agree with test data, and in the limit when all contacts are the same size, Eq. (3.6) reduces to Eq. (3.7).

3.4 Effect of Maldistribution of Contact Spots

We have shown that a certain fraction of the total apparent area corresponds to each contact spot. This function is determined by the linear dimension of the contact spot relative to the sum of the linear dimensions of all the contact spots. The position of the jth corresponding apparent area is determined by every contact spot. Not only the neighboring contact spots but also the most distant contact spots contribute towards determining where the jth corresponding apparent area will be located. If the jth contact spot falls on the center of the jth corresponding apparent area, it forms a symmetric contact, and it is properly distributed. Should the jth contact spot not fall on the center of the jth corresponding apparent area, it forms an asymmetric contact, and it is not properly distributed but maldistributed. The maldistribution will be determined by the relative displacement between the axes of the contact spot and the corresponding heat flux tube.

The constriction resistance for a maldistributed contact spot is now given by

$$R_{cj} = \beta_j \, 8\phi_j / \pi k_m c_j \quad . \tag{3.7}$$

Suppose that all the other contact spots are properly distributed, then only the jth contact spot is maldistributed. The temperature distribution far from the contact plane is the same in the jth asymmetric heat flux tube as in any other heat flux tube. This means that the flux through the jth corresponding apparent area is the same as any other corresponding apparent area; i.e., $(Q_j/A_{aj}) = (Q_1/A_{a1})$. The pseudotemperature drop at the contact plane must be the same for every heat flux tube including the jth tube, therefore,

$$A_{aj} = \frac{A_{a1}}{c_1} \frac{c_j}{\beta_j} \tag{3.8}$$

where $\phi_j \approx \phi_1$. The contribution of the jth contact spot has been reduced due to its maldistribution. Every contact spot which is maldistributed can be treated in a similar fashion. If every contact of the total set of contact spots shows some maldistribution but there is no preferred direction, the conductance can now be written as

$$h_c = \frac{\pi k_m}{8\phi(\epsilon) A_a} \sum_{i=1}^{N} c_i / \beta_i \quad . \tag{3.9}$$

It is seen that the maldistribution correction appears as a reduction in the linear dimension of the contact spot; i.e., the effective radius of the contact spot is smaller than the actual radius by the factor β. When the maldistribution is such that all the contact spots are displaced in a particular pattern, then an additional correction will

have to be made. This can occur with a wavy surface where the contact spots are crowded together towards the center of the apparent area. This situation cannot be handled directly by the maldistribution factor β.

A series of liquid analog tests were conducted to check the validity of Eq. (3.9). In one series the number and size of the contact spots were fixed, but their position in the contact plane was varied. It is seen that a positive or negative displacement in the radial direction results in an increase in the contact resistance. For the tests conducted the maldistribution varied from 9 to 18 percent, and the theory agreed reasonably well with the test data. As stated above the theory would not predict the effect of displacing all the contact spots to the boundary or to the center of the apparent area.

3.5 Contact Resistance Between Rough, Wavy Surfaces

It was noted earlier that the contact spots are confined to a particular region of the apparent area if the contacting surfaces have large curvature (waviness). For hemispherical waviness, the contact spots will appear in a circular region which is defined as the contour area. The contour area is determined by the outer limits of the contact spots, Figure 16. By definition there is no physical contact beyond the contour area. In the absence of an interstitial fluid and negligible radiation heat transfer across the gaps, the heat flow across the interface will be confined to the contour region in the vicinity of the contact plane. The total resistance is postulated to consist of the waviness resistance (constriction of the heat flow lines to the contour area) and the roughness resistance (pinching of the heat flow lines

due to the contact spots). We assume that these two effects can be linearly added to obtain the overall thermal contact resistance.

It has been proved that the contact spots are all at a uniform and common temperature independent of their size, shape, and distribution. The only restrictions are that they be in a plane which would be an isothermal plane if the contact were perfect. If there is no waviness, the contour area is identical with the apparent area, and the contact spots by definition will be found over the entire contact plane. An isothermal plane (1) will exist at some distance g_1 from the contact plane (0). This distance is quite small being proportional to the radius of the elemental heat flux tube (the contact spot radius is much smaller than the heat flux tube radius; i.e., $\epsilon \ll 1$). If the contact were perfect, planes (0) and (1) would be coincident, and there would be no thermal contact resistance.

Consider now the situation where the contact spots completely fill the contour area, but the contour area is smaller than the apparent area. Planes (0) and (1) are coincident and isothermal. Another isothermal plane (2) will exist at some distance g_2 from the contact plane (0). This distance is large, being proportional to the radius of the heat channel if the contour area is very small. In the limit as the contour area becomes as large as the apparent area, plane (2) is coincident with the contact plane and, therefore, coincident with planes (0) and (1). Thus for perfect contact, all three isothermal planes are coincident ($g_1 = 0$ and $g_2 = 0$), and there is no contact resistance.

When both roughness and waviness are present, we hypothesize that all three isothermal planes exist and that the effect of roughness can

be determined by considering the thermal contact resistance between planes (0) and (1), while the effect of waviness can be determined by considering the thermal contact resistance between planes (1) and (2). The total contact resistance will be the sum of the two resistances.

We also assume that the distances g_1 and g_2 are linearly proportional to the difference between the radius of the heat channel (or flux tube) and the contour radius (or contact spot radius). It is obvious that as the contour area approaches the size of the apparent area, g_2 decreases, becoming zero in the limit, and, therefore, the waviness resistance is zero.

Since the contact spot is always much smaller than the heat flux tube area, $g_1 > 0$, and it is approximately equal to the heat flux tube radius. Only in the limit of very smooth surfaces (mirror finish) does $g_1 \approx 0$. We conclude that the effect of surface roughness is always present, but that its overall effect will be dependent upon the magnitude of the waviness resistance. For lightly loaded, very wavy "smooth" surfaces, the waviness resistance will be dominant, and the roughness resistance will be negligible. The surface roughness may, however, have a significant effect upon the size of the contour area. When the contacting surfaces are very rough with slight "out-of-flatness," and heavily loaded, the roughness resistance will be dominant while the waviness resistance is negligible. The surface waviness may be quite important in determining the pressure distribution over the contact plane and thus indirectly affects the roughness resistance.

We can now state that for rough, wavy contacting surfaces in a vacuum and negligible radiation heat transfer, the overall thermal contact resistance is

$$R = \frac{8\phi_1}{\pi k_s \sum_{i=1}^{N} c_i/\beta_i} + \frac{8\phi_2}{\pi k_s C} \tag{3.10}$$

where the first term represents the thermal resistance due to the contact spots, and the second term represents the thermal resistance due to the contour area. We have shown that because of the waviness influence, the resistance of the contact spots will have to be corrected for size variation as well as maldistribution. The geometric factor for the contact spots can be approximated by $\phi_1 = (\pi/16 - \epsilon/4)$. The thermal resistance of the contour area is inversely proportional to the contour radius. This radius will depend upon the geometry of the contacting surfaces, the material properties, and the applied load. Unless the surfaces are quite smooth and quite wavy, the contour radius will generally be a large fraction of the apparent radius. The contour geometric factor ϕ_2 can be obtained from Figure 12.

An equation similar to Eq. (3.10) has been proposed by Holm (21) and Kragel'ski (29) for the total contact resistance of rough spheres

$$R = \frac{1}{2Nk_s c} + \frac{1}{2k_s c} \tag{3.11}$$

where c is the radius of a contact spot, and C is the contour radius. This equation is restricted to a contact which consists of many very

small contact spots (all the same size) properly distributed in a very small contour area. A contact which satisfies these conditions is quite uncommon and would occur only if the contacting surfaces were quite rough and quite wavy, and the contact load were very light. It can be seen that Eq. (3.10) will reduce to Eq. (3.11) when all these restrictive conditions are met. Eq. (3.10) is therefore a more general expression for the overall thermal contact resistance for a rough, wavy contact.

Multiple contour regions will occur whenever periodic waviness is present. Equation (3.10) should then be changed to take this into consideration. For small out-of-flatness, the contour areas will be almost as large as the corresponding apparent areas, and the maldistribution correction will have to be applied to the contour resistance. It has been shown that the asymmetry effect is most important when the contour area is large relative to the apparent area. We believe that the contour asymmetry effect will not directly affect the roughness resistance. Since the contour asymmetry effect becomes important for large contour areas when the roughness resistance is usually dominant, the overall resistance may be little influenced by maldistribution of contour areas.

4. SURFACE DEFORMATION

4.1 Introduction

Real surfaces exhibit roughness and waviness. As a consequence of the roughness, the real contact between two solids always occurs at discrete spots which are finite in number and very small. As a consequence of the waviness, the discrete contact spots are generally confined to a particular region of the apparent area called the contour area. The extent of the contour area will depend upon the surface waviness, roughness, material properties, and the applied load. At the points of real contact, generally at the highest parts of contacting asperities, the local pressure is extremely large, resulting in plastic yielding of the softer material (if a soft and hard material are in contact). The stress over the contour area will usually be very much less than the local stresses, so that the formation of the contour area can be considered as an elastic process. The application of a greater load decreases the distance and separation between the surfaces, thereby increasing the number of discrete contact spots and also increasing the contour area. The contacting asperities themselves, however, may either be deformed plastically, with some workhardening taking place, or elastically. Elastic deformation occurs only in those asperities, usually those coming into contact last, in which the local stresses are relatively low. They generally occur at the boundary of the contour area where the stress distribution over the contour area approaches a zero value.

Since the shape and size of the asperities depend upon the mechanical process used to generate the surface, the number, shape, and size

of individual contacts will depend upon the geometry and material properties. Table 4.1 gives an indication of the maximum height of asperities $j\sigma$, and the radius of curvature ρ, transverse and parallel to the direction of mechanical preparation.

Table 4.1

Process	$j\sigma$ (microns)	ρ (microns) Transverse	Longitudinal
Casting	30 - 120	1000 - 1500	1000 - 1500
Shot Blasting	3 - 12	100 - 150	100 - 150
Turning	3 - 12	20 - 80	60 - 120
Milling	6 - 20	40 - 100	80 - 150
Planing	6 - 20	40 - 100	80 - 150
Grinding	1 - 5	5 - 20	250 - 15,000
Lapping	0.08 - 0.3	15 - 250	7000 - 35,000

It can be seen in Table 4.1 that those mechanical processes which have a definite direction, usually in the plane of the surface, produce asperities which have radii of curvature which are different in the transverse and longitudinal direction. In general, the radius of curvature measured in a direction longitudinal to the process direction is at least twice as large as the radius of curvature in the transverse direction. For the grinding and lapping processes, this difference in the radii of curvature is even larger, resulting in asperities which appear to be cylindrical. The mechanical processes which do not have a definite direction of application result in asperities which

have radii of curvature which are the same in mutually perpendicular directions. These asperities can be considered to have a hemispherical shape. Since the surfaces used in this study have been prepared by glass blasting, it will be assumed that we always have hemispherical asperities coming into contact.

The waviness of surfaces encountered in practice is the result of many mechanical and thermal factors and is, therefore, quite variable. When the surface waves are smooth and have regular shapes, such as semicylinders or hemispheres, the contour area can be calculated from the classical Hertz theory. If the waviness is not regular, then the contour area must be determined empirically. In this work it will be assumed that the waves are hemispherical, so that when two such waves contact, the resulting contour area will be circular.

4.2 Elastic Deformation of a Smooth Hemispherical Surface

In this section we shall review the basic theory of the elastic deformation of smooth hemispherical surfaces. The results of this analysis will be used to determine the deformation of a rough, hemispherical surface. Let two smooth solid hemispheres be in contact at a point O as shown in Figure 22. The surfaces have a common tangent plane at O, which we take as the xy-plane. Take the positive Z-direction as being in either solid and denote the corresponding coordinates as Z_1 and Z_2. Near a point of ordinary contact with the xy-plane, the equation of the surfaces can be written with sufficient accuracy as

$$z_1 = r^2/2\rho_1 , \qquad z_2 = r^2/2\rho_2 \tag{4.1}$$

where ρ_1 and ρ_2 are the radii of curvature of the two solids.

Let us assume that the two solids are now pressed together by an applied force and approach each other by a short distance α. A deformation occurs near the original point of contact, and the two solids will be in contact over a small but finite portion of their surfaces. Let w_1 and w_2 be the components (along the Z_1 and Z_2 axes, respectively) of the corresponding displacements for points on the surfaces of the two solids. The broken lines in Figure 22 show the surfaces as they would be in the absence of any deformation, while the solid lines show the surfaces of the deformed bodies. It is seen from the figure that the equation

$$(z_1 + w_1) + (z_2 + w_2) = \alpha \tag{4.2}$$

holds everywhere in the region of contact. At points outside the region of contact, we have

$$z_1 + w_1 + z_2 + w_2 > \alpha \tag{4.3}$$

The local displacement can be related to the approach of the solids and the equation of the surfaces as

$$w_1 + w_2 = \alpha - \frac{r^2}{2}\left[\frac{1}{\rho_1} + \frac{1}{\rho_2}\right] = \alpha - \frac{r^2}{2B} \quad . \tag{4.4}$$

We denote by $P_z(x, y)$ the pressure between the two deformed solids at points in the region of contact; outside this region, $P_z = 0$. To determine the relation between P_z and the local displacements w_1 and w_2, we can with sufficient accuracy regard the surfaces as plane and use the results of point loading on the half space.

A. E. H. Love (23) has shown that Boussinesq's solution for a point load can be extended to the case of a distributed load of intensity $P_z(\xi, \eta)$ acting on the boundary of the half space, where ξ, η are the coordinates of a point in the loaded region of the boundary.

Summing up the effects of such forces, we obtain the displacements in the elastic half space due to the given distributed load.

$$\omega_1 = \frac{1 - \nu_1^2}{\pi E_1} \iint \frac{P_z(\xi, \eta)}{r} \, d\xi \, d\eta \tag{4.5a}$$

$$\omega_2 = \frac{1 - \nu_2^2}{\pi E_2} \iint \frac{P_z(\xi, \eta)}{r} \, d\xi \, d\eta \tag{4.5b}$$

where ν and E are the Poisson ratio and the elastic modulus, respectively, of the two solids, and $r = \sqrt{(x - \xi)^2 + (y - \eta)^2}$. Since $P_z = 0$ outside the region of contact, the integration extends only over the loaded region. It should be noted that from these formulae, the ratio ω_1/ω_2 is constant, independent of loading,

$$\omega_1/\omega_2 = \left(\frac{1 - \nu_1^2}{\pi E_1}\right) \Big/ \frac{(1 - \nu_2^2)}{\pi E_2} \tag{4.6}$$

and are identical for the same materials.

The relations (4.2) and (4.6) together give the displacements ω_1 and ω_2 at every point of the contact region, while relations (4.5a, b) and (4.6) relate to points outside the contact region.

Substituting the expressions (4.5a, b) in (4.4) we obtain

$$\left[\frac{1-\nu_1^2}{\pi E_1}+\frac{1-\nu_2^2}{\pi E_2}\right]\iint \frac{P_z(\xi,\eta)}{r}\,d\xi\,d\eta = \alpha-\frac{r^2}{2B}\,. \quad (4.7)$$

This integral equation determines the distribution of the pressure P_z over the region of contact. A. E. H. Love showed that the solution to (4.7) can be found by analogy with the following results of potential theory. The idea of using this analogy arises as follows: (1) The integral on the left-hand side of Eq. (4.7) is of a type commonly found in potential theory, where such integrals give the potential of a charge distribution; (2) the potential inside a uniformly charged ellipsoid is a quadratic function of the coordinates. Love deduced that the region of contact (i.e., the region of integration in (4.7)) is bounded by an ellipse of the form

$$x^2/a^2 + y^2/b^2 = 1 \quad (4.8)$$

and that the function $P_z(x, y)$ must be of the form

$$P_z(x, y) = \text{constant} \times \left[(1 - x^2/a^2 - y^2/b^2)\right]^{\frac{1}{2}}\,. \quad (4.9)$$

Taking the constant such that the integral $P_z\,d\xi\,d\eta$ over the region of contact is equal to the given total force F which moves the solids together, we find that the constant in Eq. (4.9) is $3F/2\pi ab$. It should be noted that the pressure at the center of this region is 3/2 times the mean pressure $F/\pi ab$.

When these formulae are applied to the case of contact between two hemispheres of radii ρ_1 and ρ_2, it is clear from symmetry that

a = b; i.e., the region of contact is a circle. We find the radius a of this circle to be

$$a = \left[\frac{3\pi}{4} \frac{F(k_1 + k_2)\rho_1\rho_2}{(\rho_1 + \rho_2)} \right]^{1/3} \tag{4.10}$$

and the total displacement to be given by

$$\alpha = \left[\frac{9\pi^2}{16} \frac{F^2(k_1 + k_2)^2 (\rho_1 + \rho_2)}{\rho_1\rho_2} \right]^{1/3} \tag{4.11}$$

where $k_1 = (1 - \nu_1^2)/\pi E_1$ and $k_2 = (1 - \nu_2^2)/\pi E_2$.

The pressure distribution over the contact region because of symmetry can now be written as

$$P_z = \frac{3F}{2\pi a^2} \left[1 - r^2/a^2 \right]^{1/2} . \tag{4.12}$$

Similar arguments will be used to show that the pressure distribution over the contour area formed by contacting rough hemispheres is also of the form $P_z \propto \left[1 - r^2/a^2 \right]^{1/2}$.

4.3 Contact Between Nominally Flat, Rough Surfaces

The mechanical interaction between nominally flat, rough surfaces is an exceedingly complex phenomenon. The complexity arises from the fact that rough surfaces consist of asperities which vary in height about a mean plane in the surface and also vary in shape due to the mechanical process forming them. The shape variation can exist in the direction normal to the surface as well as in the direction tangent to the surface. The variation in the tangent plane is usually dominant.

The asperities come into contact at different times in the history of the contact. The highest will contact first, and throughout the remainder of the contact will experience the largest load. The smaller asperities will contact at some later time and will experience lower pressures. One would therefore expect that the highest asperities will be loaded to the yield or flow pressure while the last asperities to come into contact will be elastically deformed. Those asperities which are smaller than the highest, but larger than the last asperities to contact, can experience stresses which run the gamut from purely plastic deformation through a combination of elastic and plastic deformation down to the purely elastic deformation.

Where purely plastic deformation ends and the elasto-plastic deformation begins will depend to a large extent upon the assumed distribution of asperity heights and shape about the mean plane as well as the shape of the contacting tips. The load at which the remaining contacts are deformed elastically will depend upon the assumptions made concerning the plastic and the elasto-plastic deformation.

The analysis of the deformation of rough surfaces will depend strongly upon the previous history of the surface. If the surface has experienced work hardening so that the yield or flow stress is greater than three times the yield stress under tension, then the loads at which purely plastic deformation ends and purely elastic deformation begins will be shifted, usually in the direction of greater contact pressures. If the surface has been loaded to some arbitrary pressure, then completely unloaded, a subsequent loading will produce contact areas which are not the same as those produced during the first loading.

There is a hystersis in the first loading-unloading cycle due to the irreversibility of plastic deformation. The highest asperities are crushed and do not recover upon unloading as do the elastically deformed asperities.

The deformation of the surface asperities will also be strongly influenced by the bulk deformation of the supporting material. Greenwood, et al. (26), found that asperities on a "penny-shaped" speciman when compressed between smooth rigid anvils underwent extreme plastic deformations, while the same asperities on the end of a tall cylinder experienced very little plastic deformation even though the bulk material underwent plastic deformation. He concluded that the contacting asperities will be flattened if the plastic deformation of the bulk material extends to the interface. He was unable to explain why the plastic deformation of the bulk material for a tall cylinder did not penetrate to the interface or how the contacting asperities were capable of transmitting the total load necessary to cause bulk plastic flow. It would appear that the effective hardness of the contacting asperities was about $6\sigma_y$ or twice as large as expected. Another variation, therefore, is the geometry of the supporting material, and we conclude that compressed rough plates may not experience the same deformation as rough solids.

For convenience we shall list the most important items which must be taken into account when developing a deformation model which will completely describe the contact between nominally flat, rough surfaces:

I. Height Distribution of Asperities
   1. linear
   2. exponential
   3. Gaussian

II. Shape of Asperity Tips

1. cones
2. spheroids
3. ellipsoids

III. Material Deformation

1. plastic
2. elastic
3. elasto-plastic

IV. Deformation History

1. initial loading
2. subsequent loading
3. work hardening

V. Bulk Geometry

1. very thin plates
2. thick plates

We might add under the heading "Shape of Asperity Tips" that we must make some assumption concerning the distribution of the radii of curvature of the contacting asperities, usually assumed to be constant.

Most worked surfaces have a Gaussian distribution of asperity heights. Some surfaces, e.g., bead-blasted ones, are Gaussian while some are not. Over a limited range the Gaussian distribution approximates to an exponential distribution. This occurs in the highest asperity range where the distribution may be exponential. Thus a Gaussian distribution is a good approximation even for the exponential distribution. Of course, the distribution will be neither Gaussian or exponential if the asperities have experienced plastic deformation

during some previous contact. Most deformation theories have been based on a Gaussian distribution of asperity heights about some mean plane.

The assumption that the contacting asperities are spheroids has been used by almost all the investigators. It was further assumed that the force between the contacting asperities was transmitted along a line passing through the centers of the spheroids. This assumption precludes any contact which might occur on the shoulders of the asperities. For bead-blasted surfaces these assumptions are probably quite good in predicting the physical interaction between nominally flat, rough surfaces over a large load range. For surfaces prepared in some other manner, new assumptions will have to be made.

If plastic deformation of the contacting asperities is assumed, then only the yield pressure of the softer material (if a soft and hard material are in contact) is required to predict the total real area of contact. No information about the height distribution nor the shape of the asperity tips is required for purely plastic deformation. On the other hand, the plastic deformation theory will not yield any information regarding the number or sizes of the contact spots which make up the total real area. In conjunction with the plastic deformation theory, we need some information about the topography of the contacting surfaces and how the topography changes with relative approach of the contacting surfaces. Only in this way can information be obtained about the number and size of the individual contact spots.

If one assumes elastic deformation of the contacting asperities, then both height distribution and asperity shape are necessary to predict the contact size, the number of contacts, and the relative approach

of the contacting surfaces. These three parameters can be related to the radii of curvature of the contacting asperities and the compliance of the contacting surfaces. Greenwood and Williamson (26) used this approach to determine the criterion for the onset of plastic deformation of the asperities. They were able to show that the contact behavior of a surface can be described in terms of two material properties: the hardness or flow pressure at the asperity tips and the elastic modulus; and two topographic parameters: the radii of curvature of the contacting asperities and the spread of asperity heights. They have called this parameter the plasticity index. The plasticity index merely determines the load at which the asperity deformation changes from purely elastic to plastic. They concluded that actually the plasticity index completely dominates the behavior, and the load has little effect. When the plasticity index is less than 0.6 (very smooth surfaces), plastic contact could be caused only if the surfaces were forced together under very large nominal pressures. When the index exceeds 1.0 (most worked surfaces fall in this category), plastic flow of contacting asperities will occur at even the lowest nominal pressures.

Mikic (11) also concluded that during initial contact over 95 percent of the total real area results from plastic deformation of the contacting asperities while 5 percent of real area is due to elastic deformation. His analysis was based on arguments similar to the ones used by Greenwood.

No theory to date has taken into consideration the effects of subsequent loadings or work hardening. It is well known that when the load on a contact is reduced to some lower level, the real area of contact

is larger than the value which would correspond to the same load on the first loading cycle. This agrees with the assumption that there is plastic deformation of asperities during the initial loading. After several loading-unloading cycles, the contact between the surfaces becomes completely elastic. The topography has been altered due to the plastic deformation, and the distribution of the highest asperities is no longer exponential or Gaussian. The radii of curvature have become very large, almost infinite for those asperities which have been completely flattened.

Work hardening is always present to a small or large degree depending upon the material and the method of preparation. It is not clearly understood how important work hardening is or when it becomes important in the loading/deformation cycle.

No surface deformation theory has included the effect of bulk geometry, i.e., the effect of the support material upon the deformation of the contacting asperities. As stated earlier, it has been observed experimentally that asperities which rest on a very thick layer of material can support very large loads before plastic deformation occurs. On the other hand, asperities which rest on a very thin layer of material will undergo complete plastic deformation.

It can be seen that the mechanical interaction between nominally flat, rough surfaces is quite complex, and no theory has been developed which can predict the number and size of individual contact spots under any load condition. We shall, therefore, restrict our attention to bead-blasted surfaces (Gaussian distribution, spheroidal asperity tips), undergoing initial loading (predominantly plastic deformation). The

contacting solids are quite thick (no bulk geometry effect), and we assume that the effect of work hardening is negligible.

4.4 Depth of Distributed Stress Region

The contacts are small in size and far apart. The deformation of a contacting asperity is initially plastic so that the pressure over the contact is uniform and equal to the flow pressure, approximately $3\sigma_y$.

Since the maximum slope of any asperity is less than 10^o measured from the horizontal plane, assume that the contact is made on a half space. To simplify the mathematics, assume that the contact is circular of radius a. The compressive stress σ_z in the direction of loading at any point z on the axis of symmetry is

$$\sigma_z = 3\sigma_y \left[1 - z^3/(a^2 + z^2)^{3/2}\right] \tag{4.13}$$

where a is the radius of the contact.

We now ask, "At what level below the actual contact does the compressive stress approach the average or apparent stress in the body of the half space?" It is expected that the level should be at least an order of magnitude larger than the contact radius. Substituting P_a for σ_z and expanding the bracketed term by means of the binomial theorem, we find that

$$\frac{z}{a} = 1.25/(Pa/3\sigma_y)^{\frac{1}{2}} \tag{4.14}$$

A substitution of practical pressures and yield stresses shows that the depth of the distributed stress region is 10 to 100 times

the radius of the contact. We can arrive at a more interesting expression which relates the depth to the radius of the corresponding apparent area by means of $Pa/3\sigma_y = \epsilon_p^2 = a^2/b^2$

$$z/b = 1.25 \tag{4.15}$$

It is obvious that the distributed stress region is very thin. For most engineering surfaces the maximum depth will range from about 100 mils for very light loading down to about 10 mils for large contact pressures. When the thickness of the distributed stress region is compared with the radius of curvature of the waviness component of the surface finish, it is seen that the ratio is much less than unity.

We can now consider the deformation of a rough, wavy surface to consist of two parts: the plastic or elasto-plastic deformation of the contacting asperities (which is a local phenomenon), and the elastic deformation of the surface lying beyond the distributed stress region.

4.5 Local Displacements Due to Plastic Deformation of Asperities

Whenever a region of the half space is loaded, there occur local displacements in the direction of loading. The surface of the half space at some distance from the axis of loading will also experience displacements in the vertical direction, Figure 24. We ask, "At what distance from the axis of symmetry does this effect become negligible?"

We again consider the case of a uniform load (due to plastic deformations of contacting asperities) distributed over the area of a circle of radius a and consider the displacement, in the direction of loading, of a point P on the surface of the half space at a distance r from the center of the circle. By superposition of point loads, the total displacement at P is given by (24)

$$w(r) = \frac{4(1 - \nu^2)qa}{\pi E} \frac{r}{a} \left[E' - \left(1 - \frac{a^2}{r^2}\right) K' \right] \tag{4.16}$$

where ν and E are the material properties, q is the pressure on the circle, and E' and K' are the complete elliptic integrals with modulus $k = a/r$

$$K' = \int_0^{\pi/2} \frac{dx}{\sqrt{1 - k^2 \sin^2 x}}, \quad \text{and} \quad E' = \int_0^{\pi/2} \sqrt{1 - k^2 \sin^2 x}\, dx$$

To obtain the displacement at the boundary of the loaded circle, we take r = a in Eq. (4.16) and find

$$(r = a) = \frac{4(1 - \nu^2)qa}{\pi E} \tag{4.17}$$

A more interesting and useful expression can be obtained by taking the ratio of the displacements at point P and at the boundary

$$\frac{w(r)}{w(r = a)} = \frac{r}{a} \left[E' - \left(1 - \frac{a^2}{r^2}\right) K' \right] \tag{4.18}$$

This expression is independent of the material properties and the magnitude of the uniform stress over the circle. The displacement at any point P depends upon the radius of the loaded circle. Equation (4.18) could be rewritten, replacing the term r/a by (r/b)(b/a) and letting $r \rightarrow b$. The expression would then give the ratio of the displacement at r = b to the displacement at the boundary of the loaded circle. The displacement ratio then becomes a function of the ratio of the

loaded circle (contact spot) to the area of interest (apparent contact area).

The integrals can be evaluated for any ratio a/b, and it can be seen that the displacement at r = b is a strong function of the ratio a/b, Table 4.2. Notice that in the range $0.01 < \frac{a}{b} < 0.10$, the ratio of the displacements ranges from 0.008 to 0.079. We can conclude from this that local deflections have very little influence at points far away, or in other words a contact is not influenced by the load and displacement of an adjacent contact.

Table 4.2

$\frac{a}{r}$	$\omega(r)/\omega(r = a)$
.01	.008
.05	.0468
.10	.0786
.20	.158
.40	.321

In this and the previous section we have assumed that the stress distribution and the vertical displacement due to the plastic deformation of an asperity can be modelled as a loaded circle on an elastic half space. A rigid right circular cylindrical indenter will produce stress distributions and displacements which are more severe than would occur under a curved elastic indenter. We have, therefore, determined the maximum vertical displacements of the free surface and the maximum stress variation with depth.

4.6 Elastic Deformation of a Rough Hemispherical Surface

We shall consider the mechanical interaction of two rough hemispherical surfaces bearing in mind the conclusions of the previous sections. In Figure 25 we have shown how two rough hemispheres would first contact. The roughness and out-of-flatness have been exaggerated in this sketch. Actually, the slopes of the asperities are much less ($\leq 10^{o}$) and the out-of-flatness less pronounced. The roughness, out-of-flatness, and the contour radius will be much smaller than the radii of curvature of the rough hemispheres. As shown in the sketch, there is a mean surface running through the asperities of either surface and an envelope which is tangent to the highest asperities. The mean surface is defined as that surface about which the distribution of asperity heights is normal or Gaussian. If there were no gross curvature (out-of-flatness), the contacting surfaces would be called nominally flat surfaces, and the mean surface would be called the mean plane. Since the radii of curvature are considerably greater than the roughness, it is immaterial whether the mean surface or the envelope is used as a reference. In this analysis we have used the mean surface as the reference.

It is a well-known fact that the interaction of two rough surfaces can be mathematically treated as the interaction between a smooth surface and a new rough surface which has the characteristics of the two original rough surfaces. In Figure 26 we have shown the contact model which will be used in the remainder of this discussion. When the surfaces contact under a very light load (essentially zero load contact), the smooth surface and the envelope will contact at one point O located on the tangent plane. The tangent plane will be fixed in space during

the deformation, and the origin will be taken from the point of first contact between the envelope and the tangent plane. The distances from the tangent plane of points, such as M and N, on a meridian section of the hemispheres at a very small distance r from the axes Z_1 and Z_2 can be represented with sufficient accuracy by the formulae

$$z_1 = Y_o + r^2/2\rho_1, \quad z_2 = r^2/2\rho_2 \tag{4.19a,b}$$

where Y_o is the initial separation between the mean plane and the envelope. The mutual distance between these two points is

$$z_1 + z_2 = Y_o + \frac{r^2}{2}\left[\frac{1}{\rho_1} + \frac{1}{\rho_2}\right] = Y_o + r^2/2B \quad . \tag{4.20}$$

Let $\omega_1(r)$ denote the displacement due to the local deformation in the direction Z_1 of a point, such as M on the mean surface of the upper hemisphere, and $\omega_2(r)$ denote the same displacement in the direction Z_2 for a point, such as N on the lower hemisphere. Assuming that the tangent plane at O remains immovable during local compression, then, due to this compression, any two points of the bodies on the axes Z_1 and Z_2 at large distances from O will approach each other by a certain amount α, and the distance between two points, such as M and N, will decrease by $\alpha - (\omega_1 + \omega_2)$. If finally, due to local compression, the points M and N come inside the area of contact (i.e., $r = c_1$), we have

$$\alpha - (\omega_1 + \omega_2) = Z_1 + Z_2 \quad . \tag{4.21}$$

Thus from purely geometric considerations, we find for any point of the surface of contact, that the total elastic displacement in the direction of loading is

$$\omega(r) = \frac{c_1^2}{2B}\,(2 - r^2/c_1^2) - Y_o, \quad r \leq c_1 \tag{4.22}$$

where c_1 is the contour radius. This equation does not imply that there is perfect contact in the region $r \leq c_1$; on the contrary, the real area will consist of many discrete contact spots varying in size and number over the region. Locally at the surface the pressure will be discontinuous, being maximum at the contact spots and much smaller over the free surface. At a very small distance below the contact surface, however, the pressure will be continuous and elastic. Although the contour radius is well defined mathematically, in reality it is rather difficult to directly measure this quantity. The contour radius is determined by the presence of contact spots which at the edge of a contour region are sparsely distributed and small in size. These shortcomings of the analyses are minor when it is realized that the contour radius can, and often is, several times larger than the Hertzian radius.

The compliance ratio for any point of the surface of contact can be expressed as

$$\omega(r)/Y_o = \left[\, c_1^2(2 - r^2/c_1^2) - 1 \,\right] /2BY_o, \quad r \leq c_1 \ , \tag{4.23}$$

and for smooth hemispherical contacting surfaces, the total elastic displacement in the direction of load is found to be

$$\alpha(r) = c_e^2(2 - r^2/c_e^2)/2B, \quad r \leq c_e \tag{4.24}$$

where c_e is the radius of contact as predicted using the classical Hertzian theory.

The radius of contact for rough hemispheres can be expressed as a function of the elastic displacement at the origin (r = 0)

$$c_1^2 = BY_o(1 + \omega(0)/Y_o) \quad , \tag{4.25}$$

and for smooth hemispheres as

$$c_e^2 = B\alpha = 1.23 \left[\frac{F^2}{E_m^2} \frac{1}{B} \right]^{1/3} B \tag{4.26}$$

where F is the total load on the interface, and $E_m = 2E_1E_2/E_1 + E_2$ is the harmonic mean modulus of elasticity. We can now very easily obtain the ratio of the contour radius to the radius of contact between smooth hemispheres

$$c_1^2/c_e^2 = \frac{Y_o(1 + \omega(0)/Y_o)}{1.23 \left[\frac{F^2}{E_m^2} \frac{1}{B} \right]^{1/3}} = \psi^2 \quad . \tag{4.27}$$

This equation can be rewritten into a more useful form by letting η be the compliance ratio at the origin, $\rho_1 = b^2/2d_1$, $\rho_2 = b^2/2d_2$ where b is the radius of the apparent area, and d_1, d_2 are the out-of-flatness values. Realizing that $F = P_a \pi b^2$, we can write

$$\psi^2 = Y_o(1 + \eta)/4.15 \left[\frac{P_a^2 b^2 (d_1 + d_2)}{E_m^2} \right]^{1/3} \quad . \tag{4.28}$$

The compliance ratio η takes on values from 0 to a maximum of 1. It depends upon the surface geometry, the material properties, and the

applied load. We now have an expression which can be used to predict the contour radius which depends upon the surface geometry (b, d, Y_o), the material properties (E, H), and the applied load P_a. The dimensionless ratio η can only be determined by iterative means as it depends upon the maximum pressure at the origin, and the pressure at the origin depends upon the load and the contour radius which depends upon η.

If we define $\lambda^2 = A_c/A_a$ or $\lambda = c_1/b$, then we can say that

$$\lambda = \frac{c_1}{c_e} \frac{c_e}{b} = \psi \lambda_e \tag{4.29}$$

where λ_e is the ratio of the radius of contact to the apparent area radius based solely on the smooth surface theory

$$\lambda_e = 1.285 \left[\frac{P_a b}{E_m (d_1 + d_2)} \right]^{1/3} . \tag{4.30}$$

As stated earlier the pressure distribution over the surface is discontinuous, but some small distance below the surface, the stresses are elastic and continuous. The pressure distribution because of the surface roughness will extend over a much larger region than would be predicted by the smooth surface theory. The pressure will be lower at the center of the contour region and go to zero at the edge. It will be a modified parabolic distribution and can be written as

$$P_c(r) = \frac{3}{2} \left[1 - \frac{1}{\psi^2} \left(\frac{r}{c_e} \right)^2 \right]^{1/2} \frac{F}{\psi^2 \pi c_e^2} . \tag{4.31}$$

As in the smooth surface case, the maximum pressure $P_c(0) = \frac{3}{2} P_c$ (average). It is obvious that the maximum pressure can be written in terms of the apparent pressure and the dimensionless ratio λ as

$$P_c(0) = \frac{3}{2} \frac{P_a}{\lambda^2} \quad . \tag{4.32}$$

We note that due to surface waviness, the pressure at the origin is greater than the average pressure in the bulk of the material. When the contour area fills the entire apparent area, then the pressure at the origin becomes equal to the apparent pressure.

It is obvious that during initial loading the contour area will be small and the contact spots few in number. They will deform plastically. If the hardness or flow pressure is approximately $3\sigma_y$ where σ_y is the yield stress under tensile loading, then the real area ratio at the origin can be written as

$$\epsilon_c^2(0) = \frac{P_c(0)}{3\sigma_y} = \frac{3}{2} \left(\frac{P_a}{3\sigma_y}\right) \frac{1}{\lambda^2} \quad . \tag{4.33}$$

To generate this real area, the surfaces must have approached each other a certain amount. At light loads (λ small) the approach is due to the flattening of the asperities, while at large loads ($\lambda \sim 1$) the approach is the result of bulk elastic deformation, and the flattening of asperities is negligible.

Using linear profiles of rough surfaces, one can determine the relationship between ϵ^2 and the distance Y between mean surfaces (or planes), Figure 27. Knowing ϵ^2 one can determine the relative displacement from

$$\eta = 1 - \frac{Y}{J\sigma} \quad . \tag{4.34}$$

Figure 30 shows in detail the relationship between the Hertzian radius, the contour radius, and the apparent radius as the roughness and load are varied. It can be seen that during the initial portion of the loading cycle, the contour radius can be two-five times as large as the Hertzian radius. The difference is largest with the surface which has the larger roughness. As a result of this roughness effect, the pressure distribution over the contour area is greatly altered from the pressure distribution predicted by the smooth surface theory. Since the force on the interface acts over a larger region, the pressure at the origin will be somewhat smaller than would be predicted by the smooth surface theory. As the load on the interface is increased, the difference between the contour and Hertzian radius becomes less; for the surfaces studied in Figure 30, the difference disappears at about a nominal pressure of 5500 psi. For pressures above 5500 psi, the two radii are identical, and, therefore, the pressure distribution is also identical.

5. DESCRIPTION OF THE APPARATUS

5.1 Introduction

Several devices were required to verify experimentally the validity of the conclusions arrived at from the thermal and deformation analyses. These devices can be separated into five distinct categories.

1. Preparation of the specimen surfaces by blasting with glass beads.
2. Measurement of the surface geometry.
3. Experimental determination of contact resistance.
4. Experimental determination of surface deformation.
5. Liquid analog apparatus.

Some of the devices had been designed and fabricated by previous investigators, some were purchased, while others were designed and fabricated by the author.

5.2 Surface Preparation Device

The system shown schematically in Figure 31, used to prepare the specimen surfaces, was designed and built by the author. This device can produce a stream of high velocity glass beads which can be directed normal to the specimen surface. The system consisted of a hardened 1/4-inch, stainless steel nozzle connected to a venturi. A regulator and a valve located before the nozzle controlled the air pressure and flow rate at the nozzle outlet. A specimen holder was attached to a long, finely threaded rod, so that the distance between the nozzle outlet and the specimen surface could be adjusted.

The nozzle which was part of a flange connection was located at one end of a 5-5/8-inch OD steel shell and a threaded open holder was located at the other end. A large hopper was located beneath the outlet of the steel shell. The hopper served two purposes: to catch the glass beads which had come from the nozzle and to act as the supply for the return line. The return line was connected to the venturi and to an air breathing pipe which was located at the bottom of the hopper. The entire system was covered with a hood to prevent the glass dust from contaminating the air.

The three variables in order of importance were: (1) the size of the glass beads; (2) the air pressure (0-120 psi); and (3) the distance between the nozzle outlet and the specimen surface.

5.3 Surface Measurement Device

A surface analyzer had been designed and built by Henry (9) which is capable of producing voltages analogous to the vertical variations of the surface asperities. The specimen is drawn at a constant speed of 0.1 inch per minute under a diamond stylus having a tip radius of 0.1 to 0.5 mil and a tip angle of 60°. In order to isolate the specimen from background noise and mechanical vibrations of the drive mechanism, the specimen holder rests on a foam rubber cushion, and the specimen is drawn by a length of polyester tape. The stylus is attached to the core of a linear variable differential transformer and can be adjusted by means of a micrometer. With a primary excitation of 3 volts at 2400 cps provided by a Sanborn recorder carrier preamplifier, the secondary voltage varies approximately three millivolts per mil core displacement.

The basic vertical sensitivity of the analyzer was determined to be 0.94 in. per mm Sanborn recorder deflection.

5.4 Experimental Apparatus for Obtaining Contact Resistance Data

The experimental apparatus for obtaining contact resistance data is shown in Figure and consists of: (1) a vacuum system; (2) power supply; (3) refrigeration unit; (4) loading mechanism; and (5) an instrument console. Each of these will be discussed separately below.

Vacuum System

All tests were performed in a chamber which is vacuum tight. The chamber consists of a top plate and upper cylinder and a baseplate bolted to the support structure. The vacuum components are attached to the baseplate and consist of a mechanical forepump, a 4-inch diffusion pump with a water-cooled optical baffle, and a three-way vacuum valve. Pressures between 5 and 1000 microns Hg are read with a thermocouple vacuum gauge, and the pressure between 5 microns and 10^{-7} mm Hg is determined by means of an ionization gauge. The foreline pressure between the mechanical forepump and the diffusion pump is obtained by means of a thermocouple vacuum gauge. An adjustable leak is available to provide a variation in the chamber pressure from 10^{-6} mm Hg when fully closed to 10^{-3} mm Hg when fully open. The range between 10^{-3} mm Hg and 1 atmosphere may be obtained by throttling the pumping system.

Power Supply

The heat supplied to the test specimens was provided by impressing a constant voltage across a Chromalox Ring Heater Element. The element consists of nickel chromium alloy resistor embedded in a special high density refractory. The ring element was used so that high loads could

be transmitted to the test specimens without loading the element. The voltage source was the main 220 volt direct current line. The voltage to the heater element was controlled by a voltage regulator and a variac. The ring element was encased in an aluminum can which was completely insulated except for the region where the aluminum can contacted the test specimens. This assembly insured that practically all the heat produced in the heater element went to the test specimens.

Refrigeration Unit

A closed cycle refrigeration unit was used to ensure that we had a constant low temperature sink. Theunit consisted of a Copeland Corporation Unit, Model 155 WFC, 1-1/2 HP water cooled. It is capable of handling 16,840 BTU/HR at 25^{o}F evaporator temperature. The refrigerant fluid used was Freon-12. With this particular unit we were able to maintain the contact interface temperature as low as 150^{o}F and still produce large heat fluxes through the specimens. The large heat fluxes were required for highly loaded specimens such as aluminum. At the high loads a large heat flux is necessary to produce measurable temperature drops across the interface.

Loading Mechanism

A relatively rigid structure is provided to support the system. A welded steel frame supports the lever system which provides the dead weight loading to the test section. Dead weight loading is independent of thermal strains resulting when the test section is heated. The mechanical advantage of the level system is designed to be 100:1. The load to the test section is applied through a bellows attached to the top plate. The force is transmitted to the test section by a rod which is aligned

by means of a bushing. The system is balanced so that when no weights are on the lever, no load is transmitted to the test section. For tests at one atmosphere the load range is 0-20,000 pounds. When the tests are run in a vacuum environment, the minimum load becomes 103 pounds (or 131 psi in the 1-inch diameter test section) due to atmospheric pressure acting across the 3-inch diameter bellows.

5.5 Surface Deformation Apparatus

The apparatus for the surface deformation was very simple because only the contour radius was needed to check the validity of the equation which had been developed. The apparatus consisted of a dead weight loading mechanism, a rigid, smooth flat support surface, bond paper (4-1/2-mil thick), and carbon paper (1-1/2-mil thick). With this simple arrangement it was possible to obtain qualitative data on the contour radius for smooth and for rough hemispherical surfaces.

5.6 Liquid Analog Apparatus

Liquid analog tests were conducted to substantiate the assumptions made in Chapter 3 regarding the effects of variable contact spot size and contact spot distribution upon the overall contact resistance. The size effect tests were conducted using the apparatus shown schematically in Figure 21, reference (12). The heat flux tube was represented by the plexiglass tube. The copper electrodes at the ends of the tube represented the isothermal planes which exist at distances from the interface equal to the channel radius. The interface was simulated by a perforated 5-mil thick Mylar sheet located midway between the two electrodes. The holes in the Mylar sheet were punched out and ranged in size from 16 to 209 mils diameter. The fluid through which the current flowed was

distilled water with a few grams of table salt. Since both the plexiglas and Mylar have resistivities orders of magnitude larger than the resistivity of the fluid, the current was, therefore, constrained to flow from one electrode to the other through the holes in the Mylar via the conducting fluid. The overall resistance was measured with an AC Impedance Bridge. The use of a DC Bridge would have allowed electroysis to occur, which would result in erratic, nonreproducible data.

The apparatus used to show the effect of maldistribution of contact spots is shown in Figure 20. Two identical devices were constructed. One had no barrier to electrical flow at the interface and gave the total resistance of the material forming the elemental heat channel. This one is called the reference heat channel. The second device had a Mylar sheet placed at the interface. The sheet had one hole to simulate a single contact spot.

6. EXPERIMENTAL PROCEDURE AND TEST RESULTS

6.1 Liquid Analog Tests

6.1.1 Maldistribution Tests

The first series of liquid analog tests employed the device shown schematically in Figure 20. Initially one contact spot was considered, and the effect of asymmetry was obtained as the spot was moved from its symmetric position to the boundary of the test device. The variables for this series of tests were the relative size of the contact spot and its relative displacement from the central location. The reference resistance for each contact spot was the constriction resistance for a centrally located contact. The results of these tests are shown on Figure 17 where the dimensionless constriction resistance is plotted against the dimensionless displacement with the dimensionless contact spot size as a parameter. The results of these tests were used to predict the effect of maldistribution of multiple contact spots.

In the second series of tests, several contact spots all of equal size were tested for maldistribution. Two tests were conducted. In both cases we considered seven equal size contact spots with one of them located in the middle of the contact plane. The remaining six contacts were located on a circle. In the first test we obtained the constriction resistance for what we considered to be the appropriate spatial distribution. Then the six contact spots were placed on a smaller diameter circle, and the new constriction resistance was measured. Next the six contact spots were placed on a larger diameter circle, and again we

measured the total constriction resistance. In Table 6.1 we have shown the results of these tests and a comparison between the predicted and test values of the maldistribution effect.

Table 6.1

	Test No. 1			Test No. 2		
	7 contact spots			7 contact spots		
	52 mil diameter			104 mil diameter		
	$\epsilon^2 = 4.05 \times 10^{-3}$			$\epsilon^2 = 1.62 \times 10^{-2}$		
	Circle Diameter (inches)			Circle Diameter (inches)		
	21/32	16/32	25/32	21/32	16/32	25/32
R_c	5.50	6.29	6.00	2.75	3.20	3.05
β (test)	1	1.14	1.09	1	1.16	1.105
β (theory)	1	1.13	1.085	1	1.14	1.09

6.1.2 Effect of Variable Contact Spot Size

In this series of liquid analog tests, we considered the effect of variable contact spot size but maintained the proper distribution of contact spots over the contact plane. Throughout these tests we considered seventeen contact spots with one spot always located in the middle of the contact plane. Here we used the liquid analog apparatus built by Flengas (12), Figure 21. In Table 6.2 we have shown the results of these liquid analog tests.

Table 6.2

Test No. 3		Test No. 4
17 contact spots		17 contact spots
6-26 mil diameter		11-26 mil diameter
6-52 mil diameter		--
4-104 mil diameter		5-104 mil diameter
1-209 mil diameter		1-209 mil diameter
$\epsilon^2 = 3.6 \times 10^{-3}$		$\epsilon^2 = 3.53 \times 10^{-3}$
h(test)	1.63	1.72
h_1(Weber)	2.19	2.19
h_2(Mikic)	2.50	2.50
h_3(new theory)	1.65	1.79

The results are shown as thermal contact conductance $h = 1/R_c A_a$ to reveal the difference between test values and theoretical values as predicted by the several thermal conductance equations available. The range of contact spot sizes and densities are representative of real contact spots. The smallest contact spots are always more numerous than the largest contact spots.

6.2 Thermal Contact Resistance Tests

6.2.1 Preparation of Test Specimens

Specimens about 1-1/2 inches long are cut from 1-inch diameter bar stock. After turning the specimens on a lathe, the ends are finely ground until they are 1-1/2 inches long. The ends are now lapped to produce a nominally flat surface having a roughness of about 5 microinches. During

the lapping process the surfaces are periodically checked for waviness; the lapping process is continued until no waviness is present. For the nominally flat, rough surface tests, the lapped surfaces are blasted with glass beads with the apparatus shown in Figure 31. The surface characteristics are obtained by means of the Talysurf. The prepared specimens are stored in dessicators to prevent oxidation until they are used in the heat transfer tests.

The wavy, rough surfaces are prepared in a slightly different manner. After the lapping process, one end is made hemispherical by placing the specimens in a lathe and spinning them at very high rpm against a polishing cloth supported by a rigid, flat support. The cloth is covered with varying coarseness polishing compounds, beginning with the coarse and ending with the extremely fine compound. Because of the relative speeds of the points on the surface, the points at the periphery wear more than those located near the center. In this manner hemispherical waviness can be generated. The out-of-flatness is now obtained by means of the Talysurf. The surfaces are now blasted with the glass beads to produce a rough, wavy surface. It is assumed that the waviness or out-of-flatness is not drastically altered by the blasting process. The waviness of the blasted surface is taken to be the same as the waviness before blasting. As in the case of the nominally flat, rough specimens, the wavy, rough specimens are stored in dessicators until used in the heat transfer tests.

6.2.2 Vacuum Tests

The procedure for obtaining thermal contact resistance data is the same whether the specimens have nominally flat, rough or wavy, rough

surfaces. The thermocouples (four in each specimen) are placed and secured by means of Sauereisen. To insure proper alignment, the specimens are placed in a holder which is removed once the specimens are located in the test section. The holder keeps the specimens aligned (in particular the wavy, rough surfaces) and insures there is no relative slip between the surfaces. Having aligned the complete test section, the vacuum chamber is closed, and a vacuum of about 5×10^{-6} mm Hg is attained by means of the mechanical and diffusion pumps. At a nominal pressure of 131 psi (determined by the load bellows), the heater is turned on to produce an interface temperature of about $500^{\circ}F$. The system and interface are permitted to outgas for about thirty-six hours.

After the outgassing has been accomplished, the heaters and cooling system are adjusted to give the desired heat flux. The thermocouple readings are taken every half hour. After two identical successive readings, it is assumed that steady state conditions prevail. The loads are increased by increments of about 500 psi until the maximum load is obtained. The temperature at the interface is maintained relatively constant by increasing the power to the heaters.

The results of tests performed with different materials and various surface geometries are shown in tables and curves and will be discussed in detail in Chapters 8 and 9.

6.3 Surface Deformation Tests

The specimens are prepared in exactly the same manner used in the thermal contact resistance tests. Since the object of these tests was to check the validity of the equation which predicts the relation between the contour and Hertzian radius, two specimens were prepared having

approximately the same waviness. One specimen was smooth, and the other was bead blasted. It was determined by means of the equation at what nominal pressure there would be contact over the entire apparent area for the wavy, rough surface. For the same nominal pressure, the smooth surface would contact over a small fraction of the apparent area. The bond paper is placed upon the rigid, flat smooth support. The carbon paper is now placed face down upon the bond paper. One of the specimens is placed on top of the carbon paper, and the system is placed in a holder until loaded. The holder is removed after a small load is placed on the system. The desired load is placed on the system and held for a few minutes. Upon removal of the load, the bond paper is examined to determine the extent of the region over which the specimens contacted. This procedure showed qualitatively the effect of roughness upon the contact of a wavy surface.

7. SURFACE PROFILE ANALYSIS

7.1 Introduction

The mathematical analysis of the thermal contact resistance of many small circular contact spots requires a knowledge of their number, size, and spatial distribution. In the absence of surface waviness, only their number and radii are necessary to determine completely their resistance to heat transfer for the vacuum case. The surface deformation analysis, for the completely plastic yielding of contacting asperities, requires only a knowledge of the total real area of contact. Thus, it is seen that in order to correlate thermal contact resistance (or conductance) with the nominal contact pressure (or load, it is necessary that we obtain information on the total real area and the number and radii of all the contacts corresponding to the surface geometry and the material properties of the surface. In this analysis it is assumed that the surfaces do not have a dominant lay.

7.2 Surface Profile Theory

There are two methods of measuring the surface topography. One method employs optical techniques while the second method employs mechanical means to probe the surface. In the first method a beam of collimated light is projected at the surface, and then the diffuse reflected beam is inspected by means of a photocell. Irregularities in the surface appear as features in the reflected beam. This method does not damage the surface being examined but is restricted by the wavelength of light to surfaces which are rougher than 20×10^{-6} inches. The most widely

used method of measuring surface roughness employs a diamond stylus. The surface is drawn under the stylus or the stylus is passed over the surface. The vertical movements of the probe are amplified electronically and recorded on a chart. It has been shown by Dr. J. B. P. Williamson that with proper care even the softest metals can be probed with negligible damage to the surface. The performance characteristics are determined by the shape and size of the probe. The basic resolution in the vertical direction is of the order of a microinch. Although it is highly improbable that a single trace of a surface will reveal the highest points of the traversed asperities, it is highly probable that the linear profile does represent the surface to a high degree, in particular, the spatial distribution of the asperities.

7.3 Number, Size, and Real Area of Contact Spots

Consider an arbitrary traverse of length L across a surface. We assume that the probed length L is a representative sample of the surface and that the contact spots are distributed randomly over the nominal contact area. When a nominally flat, smooth plane is brought into contact with the representative profile, we note that the profile penetrates the plane at a number of locations. It is also noted that the lengths of the intersection vary in magnitude. As the plane is moved closer to the profile (simulating a load on the surface), the intersections increase in number, and the variation in the incremental intersections becomes more pronounced. For every trace through the surface at a particular separation of the two planes, it can be shown from probability arguments that the sum of the intersects per unit length of trace is proportional to the real area ratio, Cooper (31),

$$\sum_{i=1}^{N} \frac{l_i}{L} = \frac{A_r}{A_a} = \epsilon^2 \quad . \tag{7.1}$$

This statement is true for any trace as long as the trace length L is representative of the surface.

If the real area is produced by the plastic deformation of the contacting asperities, we can immediately write the relationship between the nominal pressure, the yield pressure of the asperities, and the measured quantity

$$\sum_{i=1}^{N} \frac{l_i}{L} = P_a / 3\sigma_y \quad . \tag{7.2}$$

Following similar probability arguments, we can show that the number of contacts per unit apparent area can be written in terms of the measured number of intersections per unit length of trace and the real area ratio

$$\frac{N}{A_a} = \sqrt{\frac{\pi}{4}} \frac{S}{L} \frac{1}{\epsilon} \quad . \tag{7.3}$$

Cooper (31) very elegantly showed that the number of intersections per unit length of trace could be expressed as

$$\frac{S}{L} = \sum_{i=1}^{N} \frac{2c_i}{A_a} \tag{7.4}$$

where the c_i represents the radii of all the contact spots.

We now recall that the thermal conductance Equation (3.7) for properly distributed contact spots is expressed in terms of $\sum_{i=1}^{N} c_i/A_a$. This means that the thermal conductance of a nominally flat, rough surface can be obtained directly from a trace.

8. COMPARISON OF PREDICTED AND EXPERIMENTAL RESULTS

8.1 Introduction

We shall in this chapter make a comparison between the published studies and the present analysis in the light of the previously obtained test data and the newly acquired experimental results.

8.2 Theoretical Heat Transfer Models

Almost all previously published analyses on thermal contact resistance were based upon the assumption that the real area of contact consisted of a large number of small equal size contact spots distributed uniformly over the contact area whether it be the entire apparent area or a fraction of the apparent area. The one major exception is the macroscopic resistance theory proposed by Clausing (14). He states that the macroscopic constriction effect is of importance and dominates the thermal contact resistance of a majority of engineering surfaces. Clausing's model is based upon the assumption that the apparent contact area can be separated into a contact and noncontact region. In the noncontact region there are few or no microcontacts while the contact region contains a high density of microcontacts. He further assumes that the thermal resistance of the macroscopic area is much greater than the pinching effect of the microcontacts. He determines the macroscopic area by assuming it is the result of elastic contact between hemispheres. As expected he found good agreement between his theory and his test data; in particular, those surfaces which were very smooth, very wavy, and which had a high elastic modulus. With aluminum specimens he had far less success; his theory

predicted thermal resistance orders of magnitude lower than actually observed. Other investigators were even less successful in applying his theory to their problems. This was especially true when the surfaces possessed roughness as well as waviness, and the nominal contact pressures were in excess of 1000 psi. We conclude that Clausing's macroscopic constriction resistance theory is valid only under very restrictive conditions not generally met in industry.

Let us now return to the theories based on the pinching effect of the contacting asperities. Some of the first attempts at predicting contact resistance of rough surfaces in a vacuum were based on the assumption that the constriction resistance of a single circular contact spot is inversely proportional to the contact spot size (Weber solution). Assuming uniform distribution of equal size contact spots over the apparent area, they obtained the following equation for the thermal contact conductance

$$h_l(\text{Weber}) = \frac{2 k_m \sqrt{N(c_1^2 + c_2^2 + \ldots + c_N^2}}{A_a} \qquad (8.1)$$

We have written the conductance in this form so that it can be compared with the other theories. Since the contact spots are all the same size, the term under the square root is actually Nc.

More recently Mikic (11) and Roess (18) considered the effect of the relative size of a single contact spot. They obtained a geometric factor and applying it obtained a new expression for the thermal conductance, again assuming equal size and uniform distribution,

$$h_2 = \frac{\pi k_m \sqrt{N(c_1^2 + c_2^2 + \ldots . c_N^2}}{A_a 8\phi} \quad . \tag{8.2}$$

Equation (8.2) reduces to Eq. (8.1) in the limit when the contact spots are very small.

We have proposed that both the actual sizes of the contact spots as well as spot maldistribution must be considered in determining the thermal contact conductance. Whenever the contact spots are properly distributed, the thermal conductance can be written as

$$h_3 = \frac{\pi k_m (c_1 + c_2 + \ldots . c_N)}{A_a 8\phi} , \tag{8.3}$$

but when maldistribution is also present to some degree, the conductance will be

$$h_4 = \frac{\pi k_m (c_1/\beta_1 + c_2/\beta_2 + \ldots . c_N/\beta_N)}{A_a 8\phi} \quad . \tag{8.4}$$

The liquid analog test results in Table 6.2 clearly demonstrate the importance of the actual sizes of the contact spots. It is interesting to note that the thermal conductance equation based on the Weber solution overpredicts by 34 percent while the thermal conductance equation based upon a more realistic model overpredicts by 54 percent.

None of the previous theories considered maldistribution which can reduce the thermal conductance even more. The liquid analog test results in Table 6.1 show that this effect can be as large as 16 percent for a moderately small amount of maldistribution.

When the contact spots appear as a number of clusters, and the clusters are distributed over the apparent area, we have to propose that the total resistance consists of the constriction resistance based upon the size of the cluster (contour area) and the pinching effect of the contact spots. Several investigators, notably Barkan (20), Holm (21), Kragel'ski (29), and Greenwood (30), have proposed the following expression for the thermal contact resistance of one cluster of contact spots

$$R = \frac{1}{2 k_m Nc} + \frac{1}{2 k_m C} \quad . \tag{8.5}$$

It is obvious that this is based on the Weber solution and is applicable to a very special contact.

We have proposed the following expression which is based upon the actual size of the contact spots and also takes into consideration the relative size of the contact spots and also of the contour area

$$R = \frac{8\phi_1}{\pi k_m \sum_{i=1}^{N} c_i} + \frac{8\phi_2}{\pi k_m C} \quad . \tag{8.6}$$

This equation reduces to the above equation in the limit that the contact spots are very small, and the contour area is extremely small relative to the apparent area. The equation agrees quite well with the liquid analog test data obtained by Flengas (12). The geometric factor ϕ_1 for very small contact spots can be approximated by $\pi/16$, but the geometric factor ϕ_2 must be obtained from Figure (12) especially when $\lambda \leq 0.2$.

8.3 Comparison of Models with Heat Transfer Data

In Figure 32 we have shown the heat transfer data plotted against the nominal pressure on the interface. Although data were obtained for several different materials, we have chosen to show only the data for the stainless steel specimens. It can be seen that for a particular nominal pressure the thermal contact conductance can differ by as much as 100 percent. This difference is due primarily to the difference in the surface roughness. The smoother the surface, the greater the thermal contact conductance appears to be the dominant feature of Figure 32.

We next plotted the same data in a slightly different manner to show how strongly the thermal contact conductance depends upon the surface geometry and the hardness of the material. We chose the surface roughness and the slope of the asperities to be characteristic of the surface and the yield strength under tensile loading to be characteristic of the material. If we assume plastic deformation of the contacting asperities, the ratio of nominal pressure to yield pressure can be related to the area ratio ϵ^2. Figure 33 shows the data plotted as a thermal conductance number ($\sigma h/\tan\theta\ k_m$) versus the area ratio ϵ^2. It is interesting to note how well this correlates the test data over the pressure range. It appears that for values of the area ratio exceeding 2×10^{-3}, all the data fall with a narrow band ($\pm$ 25 percent) on a straight line having a slope of about 0.89 indicating that the conductance is practically proportional to the nominal pressure. This implies that the deformation of the asperities is most probably plastic for the high loads. It is not surprising that we get such a good correlation when it is realized that the parameter ($\sigma/\tan\theta$) is a measure of

the size of the most probable contact. Since it does not change with loading, the increase in the conductance must be due to the increase in the number of contact spots. But it has been shown that the number of contact spots is almost proportional to the nominal pressure (8).

For values of the area ratio below 2×10^{-3}, the spread between the data is much greater, and the slope is considerably less, about 0.49. It is believed that for nominal pressures below those corresponding to $\epsilon^2 = 2 \times 10^{-3}$, the contact is not strictly a contact between nominally flat, rough surfaces. The waviness (which may not be detected by examinations of linear profiles) may be present to some degree. If the waviness were dominant, the slope of the data versus the load would be about 0.33. Since the slope is actually between the slopes for completely wavy and nominally flat surfaces, we conclude that the contact occurs over a contour area which is relatively large, but the pressure distribution over the contour area produces many contacts near the center of contact and fewer near the edge of the contact.

We have shown in Figure 34 the same test data used in Figure 33. In this case we have used the equation developed by Mikic (11) which is based on the solution for an elemental heat channel, equal size contact spots uniformly distributed over the apparent area, and plastic deformation of the contacting asperities. For all the test data for values of the area ratio greater than 2×10^{-3}, the theory predicts values greater than observed. The discrepancy between theory and test data increases with increasing load, and there can be as much as 125 percent difference between the two values. It was believed that neglecting the variable contact spot size and the spatial distribution resulted in the

discrepancy between theory and test data. It can also be seen in Figure 34 that the theory underpredicts for values of $\epsilon^2 < 2 \times 10^{-3}$. As noted above this is probably due primarily to the waviness effect, i.e., the pressure distribution over the contour area.

In Figure 35 we have shown how the thermal contact conductance prediction is affected by considering the variable contact spot size and the maldistribution. The contact spot size variation can be determined by examination of linear profiles. The maldistribution effect, however, cannot be determined from the linear profiles. We have shown a band of the probable predicted values which is based upon assuming little or no maldistribution for the smaller values of the area ratio and almost the maximum correction for maldistribution for the very large values of the area ratio. It is seen that the test data agree quite well with the predicted band.

8.4 Surface Deformation Models

Several investigators have considered the effect of surface roughness upon the contact between hemispheres (or spheres). Barkan (20) showed experimentally that the contour size can be considerably larger than the size predicted using the classical elasticity theory. He showed that there can be contact because of the roughness beyond the Hertzian radius. In his theory of contact resistance between hemispheres, he assumed that the contour radius was always 1.7 times as large as the Hertzian radius. Greenwood, et al., (27) developed a mathematical theory which showed that the Hertzian results are valid at sufficiently high loads, but at lower loads the effective pressure distribution is much lower and extends much further than for smooth surfaces. They showed

that the contour radius could be five times as large as the Hertzian radius. Their equation is very difficult to use as it depends upon a complex iterative procedure. For the example considered in their paper, we were able to show that their theory and ours are approximately the same. The other investigator is Goodman (28) who considered the contact stress of normally loaded rough spheres. His analysis did not result in an equation which would predict the contact region as a function of the surface geometry, the material properties, and the applied load. In one figure he showed that for low contact loads, the observed compliance at the origin was smaller than predicted using the Hertz theory. This corresponds to the fact that since the load is distributed over a larger region, the pressure at the origin is much smaller, and hence the compliance at the origin will be smaller.

9. CONCLUSIONS

9.1 Discussion of Results

It has been shown that the temperature of the microcontacts is uniform and equal for all microcontacts irrespective of their shape, relative size, or spatial distribution. It has also been shown that the total apparent area is subdivided among the microcontacts according to their size (radius). Every microcontact in the total field of microcontacts contributes towards determining what portion of the total apparent area corresponds to a particular microcontact. A thermal contact resistance equation was developed for appropriately distributed microcontacts. It was seen that the resistance is inversely proportional to the sum of the radii of all the microcontacts. The equation agreed extremely well with liquid analog tests.

It was next shown that a single microcontact could be maldistributed within its corresponding apparent area. The maldistribution effect is more apparent with relatively large microcontacts, but the maximum change in the constriction resistance appeared to be about $\sqrt{2}$ whenever the microcontact was displaced to the boundary of the heat flux tube. We were able to correlate the maldistribution effect with the relative size and relative displacement of the microcontact by postulating that the distance between the isothermal surfaces which bound the disturbed temperature region is proportional to the difference between the radii of the corresponding apparent area and the microcontact. The maldistribution effect appears as a reduction in the effective size of a maldistributed microcontact. The theory was compared with liquid analog tests, and the agreement was excellent.

It was next assumed that the thermal resistance of a wavy, rough contact was due to two resistances which could be added linearly. This result is based upon the assumption that there exist three isothermal planes: one in the plane of contact, one a small distance from the contact plane, and one a large distance away. When no waviness is present, the second and third planes are coincident, and there is no waviness resistance. This assumption was checked with liquid analog tests and proved to be an accurate description of the real situation.

The surface deformation analysis showed that the surface roughness can have a significant influence upon the deformation of an hemispherical surface. When the loads are light and the surface roughness large, the contour radius can be five times as large as the Hertzian radius. For sufficiently large nominal pressures, the contour radius is identical to the Hertzian radius, and the pressure distribution over the contact area is the Hertzian pressure distribution. The theory agreed qualitatively with test data for the conditions that were examined.

The thermal analysis and deformation analysis agreed with the thermal contact resistance data. In particular, the theory showed that the assumption of plastic deformation of contacting asperities is valid after the entire apparent area has come into contact. The thermal analysis showed why the previously developed theories overpredict the thermal contact conductance at large nominal pressures.

9.2 Recommendations for Future Research

It is recommended that further work be done to extend the concept of size effect and appropriate distribution to contacts made in a fluid

environment. The author recommends that a study be undertaken to see whether the basic concept of an asymmetric heat flux tube can be extended to include the wavy, rough contact. A preliminary study along these lines resulted in an equation which had the same shape as the liquid analog test data, but underpredicted the thermal resistance by about 30 percent.

It is also recommended that the surface deformation of rough, wavy surfaces be compared with heat transfer data for nominal pressures in the 1 to 50 psi range. In this pressure range the surface roughness has significant influence upon the material deformation and upon the thermal resistance.

This work considered the case of bead-blasted hemispherical surfaces in which there were no lay. It is recommended that the thermal and deformation analyses be performed upon surfaces which have a predominant lay.

BIBLIOGRAPHY

Section 1: M.I.T. Theses

1. Fenech, Henri, "The Thermal Conductance of Metallic Surfaces in Contact," M.I.T. Sc.D. Thesis, May, 1959.
2. Henry, John Jewett, "Thermal Resistance of Metals in Contact," M.I.T. M.S. Thesis, August, 1961.
3. Carroll, Tom Wentworth, "Statistical Calculation of Geometric Parameters for Semi-Smooth Contiguous Surfaces," M.I.T. M.S. Thesis, January, 1962.
4. Kaszubinski, Leonard Joseph, "Determination of the Number of Contacts Between Two Surfaces Pressed Together," M.I.T. M.S. Thesis, August, 1963.
5. Velissaropoulos, Pandelis D., "Apparatus for Measurement of Contact Resistance," M.I.T. M.S. Thesis, August, 1963.
6. Horn, Stefan Schulze, "Thermal Contact Resistance of Graphite," M.I.T. M.S. Thesis, September, 1963.
7. Flammang, Dennis Craig, "The Use and Comparison of Autoradiographical and Statistical Methods of Determining the Number of Contacts Between Two Surfaces Pressed Together," M.I.T. B.S. Thesis, June 1963.
8. Foster, Edward Terence, "Prediction of Contact Population in Bimetallic Surface Junctions," M.I.T. M.S. Thesis, August, 1964.
9. Henry, John Jewett, "Thermal Contact Resistance," M.I.T. Sc.D. Thesis, August, 1964.
10. Yovanovich, M. M., "Thermal Contact Conductance in a Vacuum," M.I.T. M.E. Thesis, February, 1966.

11. Mikic, B. B., "Thermal Contact Resistance," M.I.T. Sc.D. Thesis, September, 1966.

12. Flengas, S., "Analog Study of Thermal Contact Resistance for Wavy and Rough Surfaces," M.I.T. M.S. Thesis, June, 1967.

Section 2: Other Contact Resistance References

13. Cordier, H., "Experimental Study of the Influence of Pressure on Contact Thermal Resistance," Redstone Scientific Information Center, (RSIC - 116) 1961. (Translated from Acad. des Sciences, Compts. Rendus 250, April 25, 1960.)

14. Clausing, A. M. and Chao, B. T., "Thermal Contact Resistance in a Vacuum Environment," University of Illinois, ME-TN-242-1, August, 1963.

15. Clausing, A. M., "Some Influences of Macroscopic Constrictions on Thermal Contact Resistance," University of Illinois, ME-TN-242-2, April, 1965.

16. Weber, H., "Ueber Bessel'sche Functionen und ihre Anwendung auf die Theorie der elektrischen Strome," Crelle, Bd. 75, 1873. See reference (17).

17. Gray, A. and Mathews, G. B., A Treatise on Bessel Functions and Their Applications to Physics," Dover Publications, Inc., New York, 1966.

18. Roess, L. C., "Theory of Spreading Conductance," Appendix A of an unpublished report of the Beacon Laboratories of Texas Company, Beacon, New York.

19. Carslaw, H. S. and Jaeger, J. C., Conduction of Heat in Solids, London: Oxford University Press, Second Edition, 1959.

20. Barkan, P. and Tuohy, E. J., "A Contact Resistance Theory for Rough Hemispherical Silver Contacts in Air and in Vacuum," IEEE Trans. on Power Apparatus and Systems, Vol. PAS-84, No. 12, December 1965.

21. Holm, R., Electric Contacts Handbook, Springer-Verlag, Berlin/Gottingen/Heidelberg, 1958.

Section 3: Subjects Pertinent to Contact Resistance

22. Rabinowicz, E., "A Quantitative Study of the Wear Process," Proceedings of the Physical Society, B, Vol. LXVI, 1953.

23. Love, A. E. H., The Mathematical Theory of Elasticity, Dover Publications, Inc., New York, 1944.

24. Timoshenko, S. and Goodier, J. N., Theory of Elasticity, McGraw-Hill Book Company, Inc., New York, 1951.

25. Greenwood, J. A., "On Area of Contact Between Rough Surfaces and Flats," A.S.M.E. Paper No. 65-Lub-10, 1965.

26. Greenwood, J. A. and Williamson, J. B. P., "Contact of Nominally Flat Surfaces," Proc. Roy. Soc., A, vol. 295, 1966.

27. Greenwood, J. A. and Tripp, J. H., "The Elastic Contact of Rough Spheres," A.S.M.E. Paper No. 66-WA/APM-28, 1966.

28. Goodman, L. E., "Contact Stress Analysis of Normally Loaded Rough Spheres," Jour. of Appl. Mech., pp. 515-522, September, 1962.

29. Kragel'ski, IV. and Demkin, N. B., "Contact Area of Rough Surfaces," Wear, Vol. 3, pp. 170-187, 1960.

30. Greenwood, J. A., "Constriction Resistance and the Real Area of Contact," Brit.J. Appl. Phys., Vol. 17, 1966.

31. Cooper, M. G., "Interfacial Contact Resistance: Some Mathematical Notes," M.I.T. Report.

APPENDIX A

CONTACT SPOTS ARE ALL ISOTHERMAL

When the contact spots lie in a surface which, if there were complete physical contact, is an isothermal surface, then the actual contact spots are at a uniform and common temperature irrespective of their relative shape and size, their distance from each other, and the thermal conductivities of the materials forming the contact.

Let us consider a typical heat channel which consists of two materials of different thermal conductivities touching only at two circular (the argument is not dependent upon the shape of the contact spot) contact spots having different radii, Figure 10.

The apparent contact area A_a consists of two regions: the non-contacting area A_b and the contacting area A_c. Let us assume A_b is thermally insulated; i.e., $\partial T/\partial n = 0$ over A_b. This is true only in the limit when there is a perfect vacuum in the voids and the radiation transfer across the voids is negligible. Over A_c there will be heat transfer, and we assume that each contact spot is uniform in temperature. (It is intuitively difficult to believe that radial heat transfer can exist in the plane of the contact.)

Far upstream of the contact plane, there will exist a surface 1 with constant temperature v_1. The heat flux over this surface is uniform, and the quantity of heat which passes through this surface in unit time is Q_1. Similarly far downstream of the contact plane, there will exist a surface 3 with constant temperature v_3. Here also the heat flux is uniform, and the heat which flows through the surface in

unit time is Q_3. All other bounding surfaces are defined by heat flow lines and are, therefore, thermally insulated; i.e., $\partial T/\partial n = 0$ everywhere. In the absence of sources or sinks within the defined boundaries, $Q_1 = Q_3$.

Let us assume that one contact spot is several times larger than the second contact spot and that they are at some finite distance apart. They are in thermal communication with either isothermal surface 1 and 3 and with each other through the two solids having thermal conductivities k_1 and k_2, where $k_1 = k_2$. There is no thermal communication between the contact spots in the contact plane, i.e., through the plane of A_b.

Let the larger contact spot with radius c_1 have uniform temperature v'_{c1}, and the smaller contact spot with radius c_2 have the uniform temperature v'_{c2}, where $v'_{c1} > v'_{c2}$. A certain quantity of heat Q'_{1c1} will flow in unit time between the surface 1 and the larger contact spot. This quantity of heat will be dependent upon the temperature difference $(v_1 - v'_{c1})$ and the total thermal resistance R_{1t1} to heat flow between the two isothermal planes. The total resistance R_{1t1} is the sum of two thermal resistances, the bulk resistance R_{1m1}, and the constriction resistance due to the contact spot c_1; i.e., $R_{1t1} = R_{1m1} + R_{1c1}$. Similarly the heat flow per unit time between surface 1 and the second contact spot will be Q'_{1c2}, and it also will depend upon the temperature difference $(v_1 - v'_{c2})$ and the total resistance $R_{1t2} = R_{1m2} + R_{1c2}$. The heat which flows across surface 1 must flow through the contact spot; i.e., $Q_1 = Q'_{1c1} + Q'_{1c2}$. Following the same reasoning, it can be shown that the heat which passes through the contact spots must flow through surface 3; i.e., $Q'_{1c3} + Q'_{2c3} = Q_3$. The net heat flow

per unit time between the larger contact spot and surface 3 is Q'_{1c3} which depends upon $v'_{c1} - v_3$ and $R_{1t3} = R_{1m3} + R_{1c3}$. Also, the net heat flow per unit time between the smaller contact spot and surface 3 is Q'_{2c3} with corresponding temperature difference $v'_{c2} - v_3$ and total resistance $R_{2t3} = R_{2m3} + R_{2c3}$.

Since we assumed that the temperature of the larger contact spot is greater than the temperature of the smaller contact spot, there will be heat flow between the contact spots. The quantity of heat flowing per unit time will depend upon the temperature difference $(v'_{c1} - v'_{c2})$ and the thermal resistance between these two contact spots. The heat flow through solid 1 will be $Q_{112} = (v'_{c1} - v'_{c2})/R_{112}$ and through solid 2 will be $Q_{122} = (v'_{c1} - v'_{c2})/R_{122}$. Q_{112} need not be equal to Q_{122} as R_{112} need not be equal to R_{122}. Figure 36 shows the quantities of heat exchanged between the various isothermal surfaces and the corresponding thermal resistances.

Let us assume that the two contact spots are at uniform temperatures v_{c1} and v_{c2}, respectively, where $v_{c1} < v'_{c1}$ and $v_{c2} > v'_{c2}$ and also $v_{c1} = v_{c2}$. In the light of the previous discussion, the heat flows become $Q_{1c1} > Q'_{1c1}$ and $Q_{1c3} < Q'_{1c3}$ for the larger contact spot, and $Q_{1c2} < Q'_{1c2}$ and $Q_{2c3} > Q'_{2c3}$ for the smaller contact spot. Since $v_{c1} = v_{c2}$, the net flow of heat between the contact spots through either solid goes to zero; i.e., $Q_{112} = Q_{122} = 0$.

Let us now consider the steady-state heat transfer per unit time through two control surfaces completely surrounding either contact spot. One can determine the following two heat balances for the case of unequal contact spot temperatures

$$- Q'_{1c1} + Q_{112} + Q_{122} + Q'_{1c3} = 0 \tag{A.1}$$

$$- Q'_{1c2} - Q_{112} - Q_{122} + Q'_{2c3} = 0 \tag{A.2}$$

Adding and transposing terms result in

$$2(Q_{112} + Q_{122}) = (Q'_{1c1} - Q'_{1c3}) - (Q'_{1c2} - Q'_{2c3}) \tag{A.3}$$

Since $Q'_{1c1} < Q_{1c1}$ and $Q'_{1c3} > Q_{1c3}$, one can write $(Q'_{1c1} - Q'_{1c3}) < (Q_{1c1} - Q_{1c3})$, and similarly one can write $- (Q'_{1c2} - Q'_{2c3}) < - (Q_{1c2} - Q_{2c3})$.

Equation (A.3) can now be rewritten in quantities which relate the heat flow between contacts to the heat flow into and out of each contact spot under steady-state conditions.

$$2(Q_{112} + Q_{122}) < (Q_{1c1} - Q_{1c3}) - (Q_{1c2} - Q_{2c3}) \tag{A.4}$$

For steady-state conditions and equal contact spot temperatures, the total heat flow per unit time into and out of the control surfaces must be equal

$$Q_{1c1} + Q_{1c2} = Q_{1c3} + Q_{2c3} \tag{A.5}$$

which can be rewritten as

$$(Q_{1c2} - Q_{2c3}) = (Q_{1c3} - Q_{1c1}) \tag{A.6}$$

Substituting Eq. (A.6) into (A.4), one obtains the following relationship.

$$Q_{112} + Q_{122} < Q_{1c1} - Q_{1c3} = 0 \tag{A.7}$$

This inequality can only be satisfied if one or the other quantity is negative; i.e., the heat flow takes place in a direction which is opposite to the assumed direction. This would require that the temperature of one contact spot be greater than the other when considering heat flow in one solid and that the temperature inequality be reversed when considering heat flow in the second solid. This is physically impossible, and, therefore, the two contact spot temperatures must be identical.

The argument can be extended to include a third contact spot lying in the same plane and having yet another size quite different from the sizes of the other two spots. It can be shown that $v_{c1} = v_{c2} = v_{c3}$. By inductive reasoning it can be shown that the temperature of all the contact spots must be the same value independent of the contact spot shape, size, distance between contacts, and the quantity of heat flowing through the spot. The assumption of equality of contact spot temperature is valid whether the materials forming the contact have equal thermal conductivities or not. This argument can now be used to prove the assumption that the temperature over the contact spot is uniform. A uniform temperature over a circular contact spot requires a parabolic heat flux distribution over the contact spot.

In this analysis it was assumed that the isothermal planes were flat and parallel to the contact plane. The adiabatic walls of the heat channel were defined by the outermost heat flow lines which pass through the contact and are assumed to be parallel. Two special cases arise in which the isothermal planes and contact plane are not flat and the adiabatic heat channel walls are not parallel. Figure 11

shows either the case for coaxial cylinders or concentric spheres. The inner surface is isothermal at temperature v_1, and the outer surface is isothermal at temperature v_2 where $v_1 > v_2$. The broken surface represents either a coaxial cylinder or a concentric sphere. If there were perfect contact along this surface, it would be an isothermal surface. Based on the arguments developed for flat surfaces, we can assume that contact spots distributed on this surface will be uniform in temperature and will all be at the same temperature independent of their shape, size, distribution, and magnitude of the heat flow through the contact spots and the thermal conductivities of the materials on either side of the contact surface.

APPENDIX A

ALTERNATE ARGUMENT

Consider the contact problem shown in Figure 37, which shows two unequal sized contact spots transferring all the heat which flows between isothermal surfaces 1 and 2 which are parallel to the contact plane and the same distance from the plane. There is no flow of heat through the bounding walls of the heat channel and none through the contact plane beyond the contact spots. Let the broken lines indicate the heat flux tubes feeding heat to the contact spots. By definition no net heat will flow across the common boundary.

Separate the problem shown in Figure 37 into two sections at the contact plane as shown in Figure 37. The two sections are coupled by the fact that the temperature of the smaller contact spot a and a' must be the same, and the heat flow out of a must be equal to the heat flow in a'. Similar statements can be made concerning contact spot b and b'. Assume isothermal surface 1 is at temperature 1 while isothermal surface 2 is at temperature 0 and that the thermal conductivities of the two sections are identical. Further assume that the thermal conductivity is independent of the temperature.

Consider the heat transfer problem through contact spot 2 (the larger one). In the upper section one can write that $Q_2 = (1 - b)/R_2$ where R_2 is the thermal resistance of heat flux 2 in the upper section. A similar expression can be written for the lower section, $Q_2 = (b' - 0)/R'_2$. The thermal resistance is directly proportional to the normal flow area and the distance through which the heat flows. We assume that there is

symmetry of heat flow about the contact plane; i.e., the heat flow pattern in the heat flux tube 2' is the mirrorimage of the heat flow pattern in heat flux tube 2. From this we conclude that the total thermal resistances of the heat flux tubes 2 and 2' are identical; i.e., $R_2 = R_2'$. Then $b + b' = 1$. Since $b = b'$, $b = b' = 0.5$.

We now consider heat flux tubes 1 and 1'. In the upper section the heat flow is related to the thermal resistance R_1 and the temperature difference $(1 - a)$ by $Q_1 = (1- a)/R_1$. Similarly for the lower section, $Q_1 = (a' - 0)/R_1'$. Since the heat flow pattern in the heat flux tubes feeding contact spot 2 is identical in sections 1 and 2, we conclude that the heat flow pattern in the heat flux tube feeding contact spot 1 is identical. This means that $R_1 = R_1'$. Therefore, $a + a' = 1$ from the coupling of Q_1. But $a = a'$, and this means that $a = a' = 0.5$, the same as the larger contact spot.

The argument can be extended to contacts which consist of dissimilar materials; i.e., the thermal conductivities are unequal. The assumption of heat flow symmetry about the contact plane is still valid. It can be shown that the temperatures of the contact spots are equal but that because of the different thermal conductivities, their levels will be higher or lower than the value determined for identical thermal conductivities.

The assumption of heat flow symmetry will always be true if there is perfect contact.

APPENDIX B

ASYMMETRIC HEAT FLUX TUBE

When the definition of an elemental heat flux tube was established, it was noted that the existence of an asymmetric contact was possible. The asymmetric contact was defined as that contact spot whose axis of symmetry is not coincident with the axis of the elemental heat flux tube. We ask the following questions:

1. What is the effect of asymmetry on the contact resistance?
2. How does the relative size of the contact spot affect the change in the contact resistance?

Ideally we should resolve this problem by finding solutions to Laplace's equation which satisfy the appropriate boundary conditions. Since by definition there is no axis of symmetry, the solution will depend upon three coordinates. The problem is not amenable to a rigorous mathematical approach, and, therefore, we must resort to some engineering approximations.

First, let us establish the fact that the temperature of the contact spot is uniform irrespective of its relative size (ϵ), its shape (we assume circular contacts), and its asymmetry. Consider a small circular contact spot which lies near the boundary of the elemental heat flux tube. There is no heat transfer in the region outside the contact spot. All the heat passing through an isothermal plane some distance above the contact flows through the contact spot and out through another isothermal plane some distance below the contact spot. The heat flow pattern on either side of the contact spot will be

identical, and the isotherms will have the same spacing if the thermal conductivity on either side of the contact is the same. If the thermal conductivities are not the same, the heat flow pattern on either side will still be the same, but now isotherms will not have the same spacing on both sides of the contact. The only way that the flow pattern and temperature distribution can be satisfied on both sides of the contact is to have a uniform temperature over the contact spot.

The potential problem has now been reduced to a three-dimensional region bounded by an isothermal plane, adiabatic walls, and a second plane which consists of a small circular isothermal spot surrounded by an adiabatic region, Figure 15. This represents one half of the asymmetric problem. The region between the two planes is the region of three-dimensional temperature distribution. Heat passing between the isothermal planes experiences a resistance to flow. The total resistance can be separated into the material resistance and the constriction or contact resistance.

It was shown earlier for the symmetric contact that when the contact spot is very small ($\epsilon \ll 1$), the distance from the contact plane to the isothermal plane is equal to the radius of the elemental heat flux tube. It is obvious that as the size of the contact spot increases, the isothermal plane will approach the contact plane, and in the limit when the contact spot fills the contact plane ($\epsilon \approx 1$), the isothermal plane will be coincident with the contact plane. This implies that as the contact spot becomes larger the disturbed temperature region becomes thinner, Figure 14. As a first approximation assume that the distance between the contact plane and the isothermal plane is linearly

related to the difference between the heat flux tube radius and the contact spot radius; i.e., $g/b = (1 - \epsilon)$. This relation satisfies the limiting values of ϵ and probably gives a good approximation for intermediate values of ϵ.

The effect of asymmetry will be resolved by using the concept of thermal resistance as a function of the flow area and the flow path. The total resistance will be an integrated value of the elemental resistance between the isothermal planes. It is obvious that the optimum situation occurs when the contact is symmetric; i.e., the integrated value of the combination of flow area and flow path is a minimum, and hence the resistance is a minimum. When the contact spot is displaced from its symmetric position, the flow area and the path are both changed, and it is expected that the integrated value should be larger. The maximum value will occur when the contact spot has been displaced to within a contact spot radius of the boundary. For each displaced position of the contact spot, there will be a different value for the resistance. If we assume that the integrated flow area does not change significantly between the symmetric and maximum asymmetric cases for all contact sizes, then the resistance will be proportional to the integrated flow path. As a first approximation assume that the integrated flow path can be represented by the straight line joining the center of the contact spot, Figure 15. The total resistance at any displaced position δ relative to the total resistance for the symmetric case can be written as

$$\frac{R(\delta) + R_m}{R(0) + R_m} = \frac{\rho}{g} = \left[1 + \frac{(\delta/b)^2}{(1 - \epsilon)^2} \right]^{\frac{1}{2}} \qquad \text{(B.1)}$$

where R_m is the material resistance ($2g/\pi b^2$ km), (δ/b) is the measure of asymmetry, and ϵ is the relative size of the contact spot.

The left-hand side can be rewritten as

$$\bar{R}\left[1 + (R_m/R(0))/\bar{R}\right] / \left[1 + R_m/R(0)\right] \tag{B.2}$$

The ratio $R_m/R(0)$ can be expanded to show that this ratio is solely dependent upon the geometry of the contact; i.e.,

$$R_m/R(0) = \epsilon(1 - \epsilon)/4\phi \tag{B.3}$$

where ϕ depends upon ϵ only.

When the contact is small ($\epsilon \approx 0$), the ratio of the bracketed terms approaches the value 1. As the contact becomes large ($\epsilon \approx 1$), the ratio again becomes approximately one. It is expected that for any intermediate value of ϵ, the ratio will be approximately one, and so Eq. (B.2) becomes

$$R(\delta)/R(0) \approx \left[1 + \frac{(\delta/b)^2}{(1 - \epsilon)^2}\right]^{\frac{1}{2}} \tag{B.4}$$

For a symmetric contact, $\delta = 0$, the ratio becomes unity. The maximum displacement is $\delta_{max} = b\text{-}c$, or $(\delta/b)_{max} = 1 - \epsilon$, and the ratio becomes $\sqrt{2}$. Using the concept of images, one can argue that for the very small contact spots, the maximum increase in the resistance will be $\sqrt{2}$ times the value for the symmetric contact, which confirms the limiting value given by Eq. (B.4). This equation has been substantiated fully by the liquid analog tests, Figure 17 for all values

of ϵ and the range of δ/b. Equation (B.4) can be rewritten to give the maximum asymmetry allowable for a particular value of the ratio $R(\delta)/R(0)$

$$(\delta/b) = (1 - \epsilon) \left[(R(\delta)/R(0))^2 - 1 \right]^{\frac{1}{2}} \qquad (B.5)$$

It is seen that the small contacts can be displaced a large distance from the symmetric position before there is a significant increase in the resistance. This means that the small contact spots are relatively insensitive to the boundary of the heat flux tube; i.e., the boundary could have the shape shown in Figure 19, and the assumption of a circular heat flux tube is a very good approximation. The large contact spots are very sensitive to the boundary of the heat flux tube, and a relatively small displacement is reflected in a large change in the resistance.

APPENDIX C

AVERAGE CONTACT SIZE INDEPENDENT OF LOAD

In this section it will be shown that the average contact spot radius is a weak function of the apparent pressure on the interface. The analysis will be based upon autoradiographic data obtained by Foster (8). These data consist of contact spot density versus the apparent pressure for nominally flat, rough aluminum surfaces.

The surface interaction will be based upon completely plastic deformation of the asperities or completely elastic deformation of the asperities. It is expected that the surfaces will actually deform elasto-plastically, but that the two limiting cases of either completely plastic or completely elastic deformation will give us an idea of what the limiting results will be.

For completely plastic deformation of the contacting surface asperities, a simple force balance, based upon the assumption that the real contact area can support only the stress at which the material begins to yield, gives the following simple relationship between the average contact spot radius, the contact spot density, the apparent pressure, and the yield stress of the material.

$$n\pi\bar{c}^{2} = P_a/3\sigma_y \qquad (C.1)$$

This expression implicitly takes into consideration the surface geometry (surface roughness) through the relationship between the contact spot density and the apparent pressure. For the same material properties and load, a smoother surface will produce a larger contact

spot density than a rough surface. This leads to the conclusion that a smoother surface will have a smaller average contact spot radius than a rough surface. It should be noted that the factor before the yield stress may exceed the value 3 if the surface has been work-hardened or if the root mean square slope of the contacting asperities becomes quite small. In the first case, the correction may not be more than 30 percent greater, while in the second case the correction may be substantial. For most nominally flat, rough surfaces a value of 3 is good enough.

Table C.1

P_a (psi)	n (No/in^2)	$\bar{c}$ (microns)
100	380	16.4
500	1620	17.8
1000	2510	20.0
5000	8120	25.0
10,000	11,120	30.0

The experimental values in the above table are based upon the interaction of two nominally flat, rough aluminum specimens having surface roughnesses of 107 and 115 μin rms and slopes of 0.118 and 0.119, respectively. The yield stress for aluminum 2024-T4 is 66,000 psi. A plot of the average contact spot radius versus the apparent pressure shows that the radius depends upon pressure to the 0.176 power, a rather weak function of the load.

If the surface deformation is assumed to be completely elastic, the analysis becomes more complex. Assumptions have to be made regarding

the shape of the contacting asperities, their radii of curvature, and the contacting asperities touching at the apex only; i.e., they do not touch at the shoulder.

The average load per asperity is simply the apparent pressure at the interface divided by the contact spot density; i.e., $F_c = Pa/n$. The radius of curvature of the contacting asperities depends upon the surface roughness and slope and the distance from the mean plane.

$$\rho = j\sigma(1 - \omega/Y_o)/2(\tan\theta)^2 \qquad (C.2)$$

This relationship states that the asperities which are furthest from the mean plane have the largest curvature. For elastic deformation of hemispherical asperities, the average contact radius according to the classical theory of Hertz is

$$\bar{c} = 1.109 \left[\frac{F_c}{E} \frac{\rho}{2} \right]^{1/3} \qquad (C.3)$$

assuming that both asperities have the same elastic properties and $\nu = 0.3$ and have identical radii of curvature. For most real surfaces, the factor j, which is the ratio of the maximum asperity height to the root mean square value, ranges between 2.5 and 4. For this analysis we assumed that $j = 3.0$. ω/Y_o is the relative displacement of the mean planes under the load at the interface and ranges between 0 and 0.7 over the apparent pressure range from 0-10,000 psi.

Table C.2

P_a (psi)	n (No/in^2)	F_c (lb_f/asperity)	ρ (microns)	$\bar{c}$ (microns)
100	380	0.513	215	16.8
500	1620	0.555	185	16.5
1000	2510	0.630	169	16.6
5000	8120	0.785	136	16.6
10,000	11,120	0.949	124	17.5

The contact spot radii in Table C.1 are based upon completely plastic deformation of the contacting asperities. It is seen that the size varies by a factor of two as the apparent pressure varies by a factor of 100. The size is indeed a weak function of the applied load. For aluminum surfaces the radius of contact lies in the 10-30 micron range.

Table C.2 shows the contact spot radii which are based upon an analysis that assumes completely elastic deformation of the contacting asperities. It is clearly evident that the average contact spot radius is quite independent of the load over a very large range. The size, as predicted by elastic deformation, is smaller than the size predicted by plastic deformation, but the sizes are of the same order of magnitude.

Since a surface is expected to undergo elasto-plastic deformation, the actual average contact spot radius should be within the limits indicated by completely plastic or elastic deformation. One can conclude from this preliminary analysis that the average contact spot radius for elasto-plastic deformation of the contacting asperities has a very weak dependence upon the apparent pressure.

It should be borne in mind that for any particular load and surface geometry, there will be a spectrum of contact spot sizes. The average contact spot size represents the largest percentage of actual contacting asperities. It is as yet unknown what the maximum contact spot could be produced, and it is believed that the minimum size may be related to the surface energy of the contacting asperities (22). As the load is increased, the total number of contacting asperities increases, and although the average contact spot size increases very little, the range of contact spot size increases.

APPENDIX D

HEAT TRANSFER DATA

TABLE OF PROPERTIES

Material	Temp. ($^{\circ}$F)	k(BTU/HR-FT -$^{\circ}$F)	E(psi)	σ_y(psi)
Stainless Steel (303)	100	9.0	29×10^6	120,000
	300	9.8	27.6×10^6	114,000
	500	10.6	26.5×10^6	110,000
Aluminum (2024 T4)	100	72.5	10.5×10^6	66,000
	300	88.0	10.0×10^6	63,000
	500	100.0	8.5×10^6	53,500
Magnesium (AZ 31B)	100	46.0	6.5×10^6	28,000
	300	54.0	5.5×10^6	23,700
	500	58.5	4.2×10^6	18,100
Leaded Brass (Anaconda 271)	100	65.0	14.2×10^6	68,000
	300	71.0	13.0×10^6	62,200
	500	80.0	12.5×10^6	60,000

Table 1: Stainless Steel (303)

σ_1 = 190 μin, d_1 = 95 μin, tan θ_1 = 0.150

σ_2 = negligible, d_2 = 55 μin, tan θ_2 = 0

σ = 190 μin, d = 150 μin, tan θ = 0.150 Δ

k_m = 10 BTU/HR-FT-^{o}F

P_a(psi)	h(BTU/HR-FT^2-^{o}F)
131	100
395	200
770	265
1100	410
1700	505
2000	630
2700	810
3200	1000
4800	1300

Table 2: Stainless Steel (303)

$\sigma_1 = 132\ \mu in, \quad d_1 = 80\ \mu in, \quad \tan \theta_1 = 0.163$

$\sigma_2 = 76\ \mu in, \quad d_2 = 0\ \mu in, \quad \tan \theta_2 = 0.137$

$\sigma = 152\ \mu in, \quad d = 80\ \mu in, \quad \tan \theta = 0.163$ ×

$k_m = 10$ BTU/HR-FT-$^{\circ}$F

P_a(psi)	h(BTU/HR-FT^2-$^{\circ}$F)
131	140
200	190
275	195
400	255
620	330
1050	610

Table 3: Stainless Steel (303)

$\sigma_1 = 292\ \mu$in, $d_1 = 80\ \mu$in, $\tan\theta_1 = 0.100$

$\sigma_2 = 174\ \mu$in, $d_2 = 35\ \mu$in, $\tan\theta_2 = 0.100$

$\sigma = 340\ \mu$in, $d = 115\ \mu$in, $\tan\theta = 0.100$

$k_m = 10$ BTU/HR-FT-$^\circ$F

P_a(psi)	h(BTU/HR-FT^2-$^\circ$F)
131	49
200	52
260	59
400	70
650	87
1100	110
1950	190
3900	345
5100	470
10,000	1050

Table 4: Stainless Steel (416)

$\sigma_1 = 42\ \mu in, \quad d_1 = 0\ \mu in, \quad \tan \theta_1 = 0.78$

$\sigma_2 = 0\ \mu in, \quad d_2 = 0\ \mu in, \quad \tan \theta_2 = 0$

$\sigma = 42\ \mu in, \quad d = 0\ \mu in, \quad \tan \theta = .078$

$k_m = 14.6$ BTU/HR-FT-^{o}F

P_a(psi)	h(BTU/HR-FT^2-^{o}F)
131	158
190	292
950	1080
2100	2480
3800	3280

Table 5: Stainless Steel (416)

$\sigma_1 = 131\ \mu in, \quad d_1 = 0\ \mu in, \quad \tan\theta_1 = .107$

$\sigma_2 = 108\ \mu in, \quad d_2 = 0\ \mu in, \quad \tan\theta_2 = .097$

$\sigma = 170\ \mu in, \quad d = 0\ \mu in, \quad \tan\theta = .107$ ∇

$k_m = 14.6$ BTU/HR-FT-$^\circ$F

P_a(psi)	h(BTU/HR-FT^2-$^\circ$F)
131	170
334	238
500	326
871	432
1359	510
1831	613
2586	736
3376	933
4131	1040
7452	1385
10,000	1960

Table 6: Aluminum (2024 T4)

$\sigma_1 = 42\ \mu$in, $d_1 = 500\ \mu$in, $\tan\theta_1 = .079$

$\sigma_2 = 80\ \mu$in, $d_2 = 420\ \mu$in, $\tan\theta_2 = .120$

$\sigma = 90\ \mu$in, $d = 920\ \mu$in, $\tan\theta = .120$

$k_m = 87.5$ BTU/HR-FT-$^\circ$F

P_a(psi)	h(BTU/HR-FT^2-$^\circ$F)
131	1150
250	1750
500	2500
1000	4100
3000	9300

Table 7: Aluminum (2024 T4)

$\sigma_1 = 60\ \mu in,\quad d_1 = 1250\ \mu in,\quad \tan\theta_1 = .08$

$\sigma_2 = 57\ \mu in,\quad d_2 = 1300\ \mu in,\quad \tan\theta_2 = .082$

$\sigma = 58.5\ \mu in,\quad d = 2550\ \mu in,\quad \tan\theta_1 = .082$

$k_m = 88.0$ BTU/HR-FT-^{o}F

P_a(psi)	h(BTU/HR-FT^2-^{o}F)
246	1220
703	1810
2200	4100
3600	6700
5900	9600

Table 8: Magnesium (AZ 31B)

$\sigma_1 = 55\ \mu in, \quad d_1 = 2000\ \mu in, \quad \tan \theta_1 = .085$

$\sigma_2 = 62\ \mu in, \quad d_2 = 1800\ \mu in, \quad \tan \theta_2 = .086$

$\sigma = 80\ \mu in, \quad d = 3800\ \mu in, \quad \tan \theta = .086$

$k_m = 55.0$ BTU/HR-FT-$^{\circ}$F

P_a(psi)	h(BTU/HR-FT^2-$^{\circ}$F)
131	600
246	660
703	1020
2200	2750
3600	4300
6000	7200

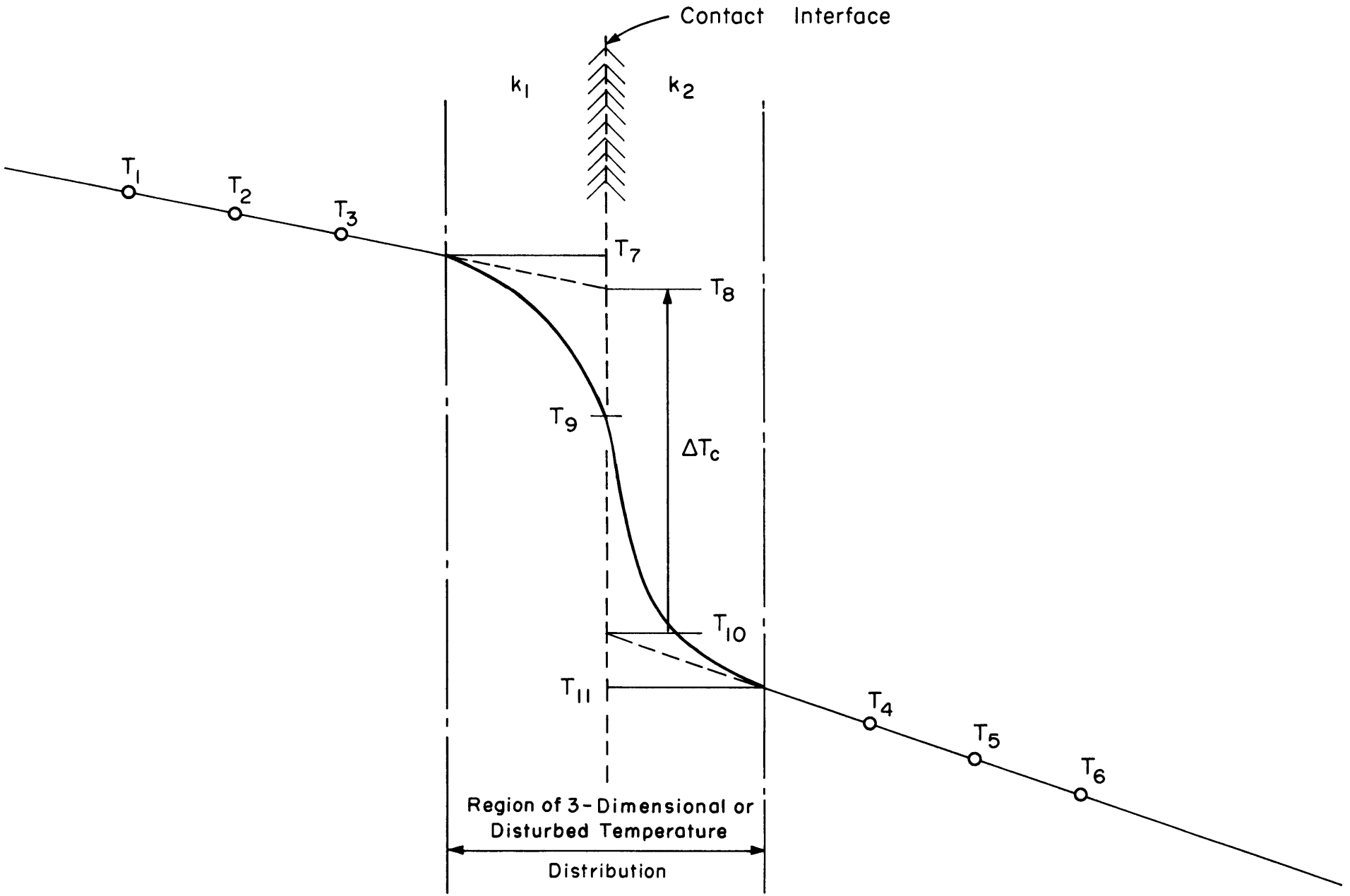

Fig.1 Temperature Distributions in Contacting Solids

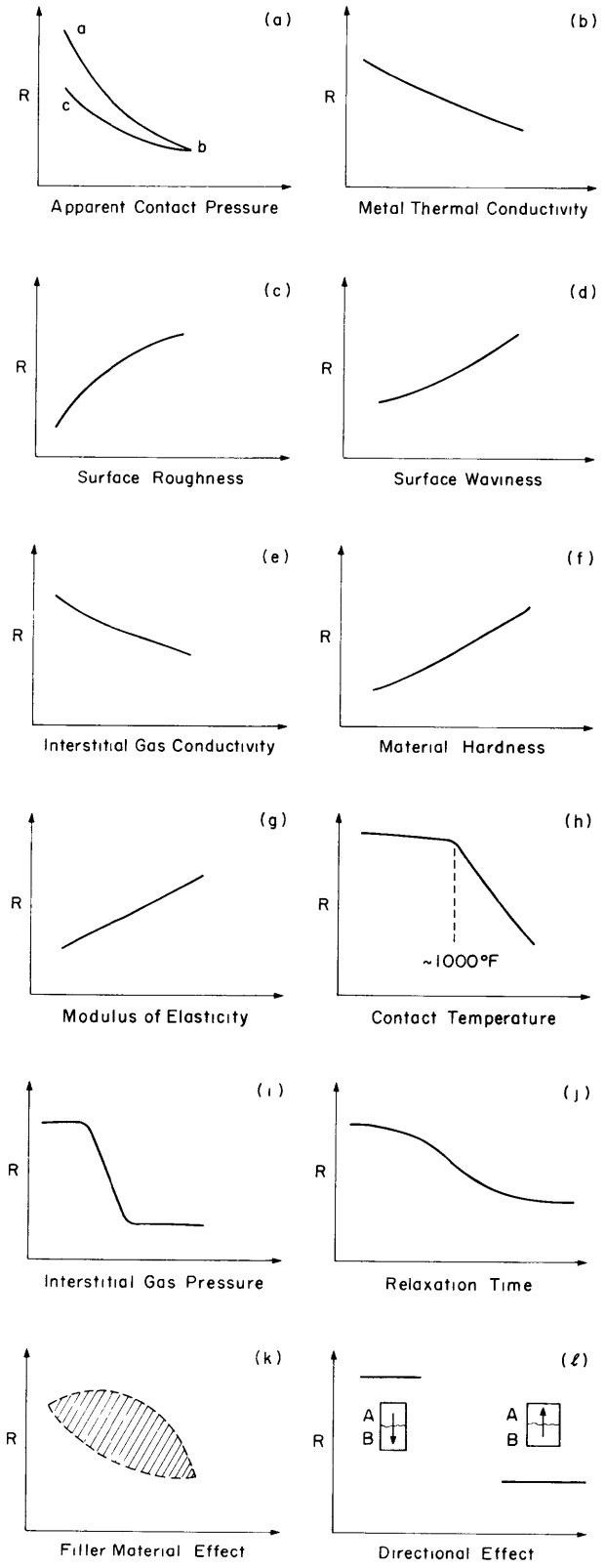

Fig. 2 Parameters Influencing Overall Thermal Contact Resistance

Fig. 3 Typical Linear Profile of Ground Surface

Blanchard Ground: 22 μ in rms, stainless steel 303

Profile Scale Vertical: 18.8 μ in/mm
Horizontal: 1600 μ in/mm
Upper Profile: D1 Direction
Lower Profile: D2 Direction

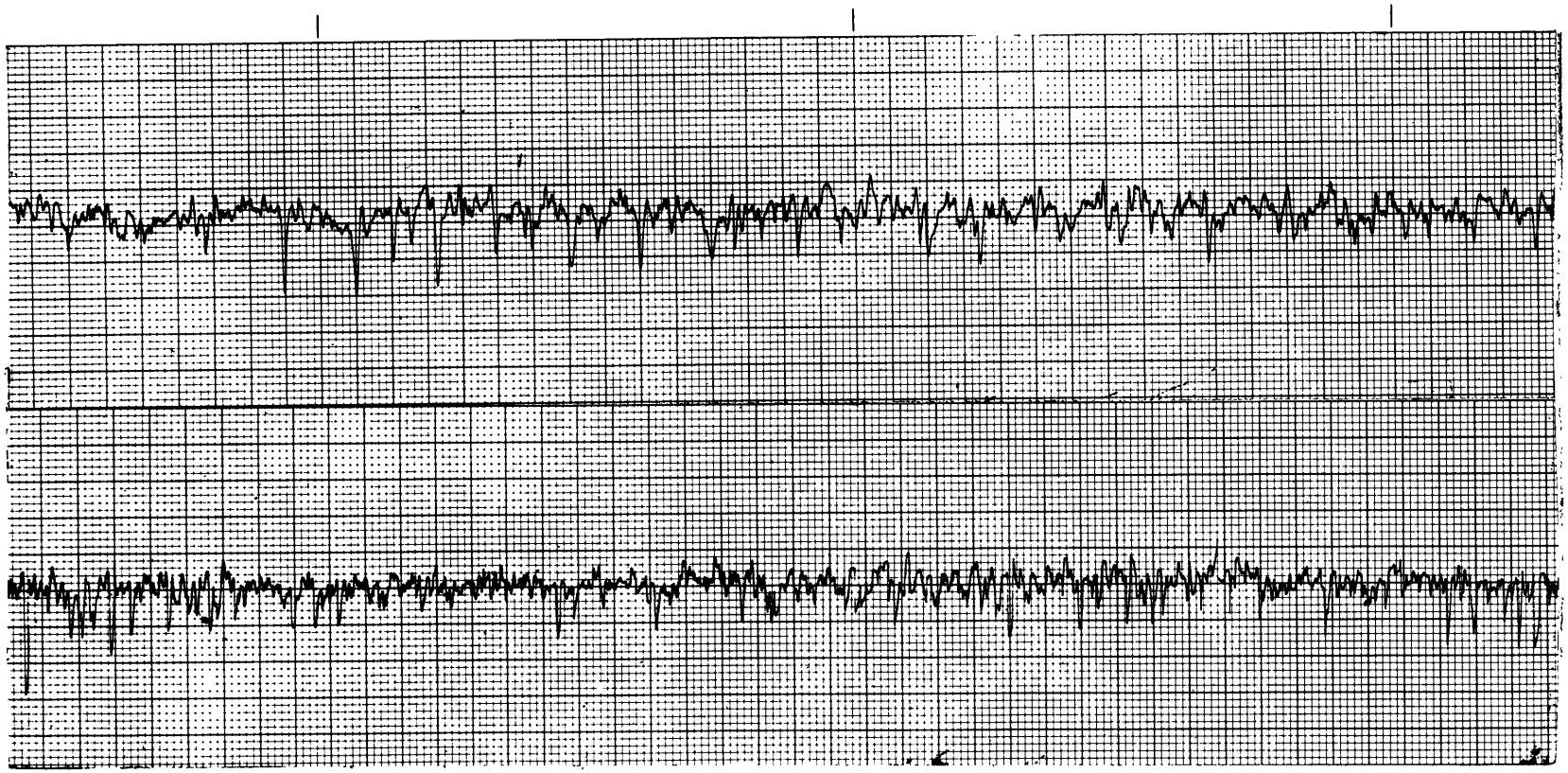

Fig. 4 Typical Linear Profile of Bead Blasted Surface

Bead Blasted: H Beads at 60 psi
45 μ in rms, stainless steel 303

Profile Scale: Vertical: 18.8 μ in/mm
Horizontal: 1600 μ in/mm (upper)
320 μ in/mm (lower)

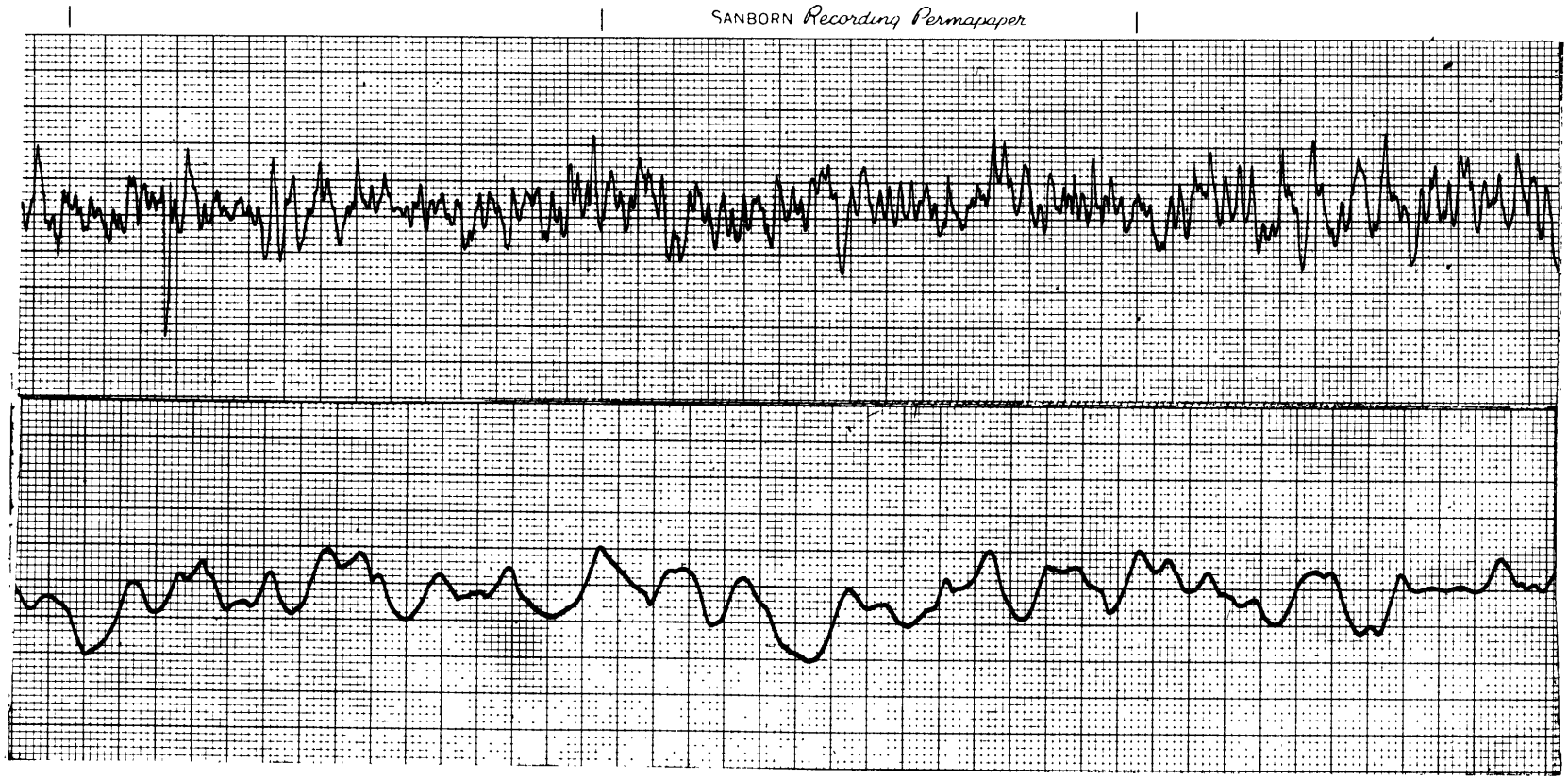

Fig. 5 Typical Linear Profile of Bead Blasted Surface

Bead Blasted: XP Beads at 90 psi
65 μ in. rms, stainless steel 303

Profile Scale: Vertical: 18.8 μ in/mm
Horizontal: 1600 μ in/mm (upper)
320 μ in/mm (lower)

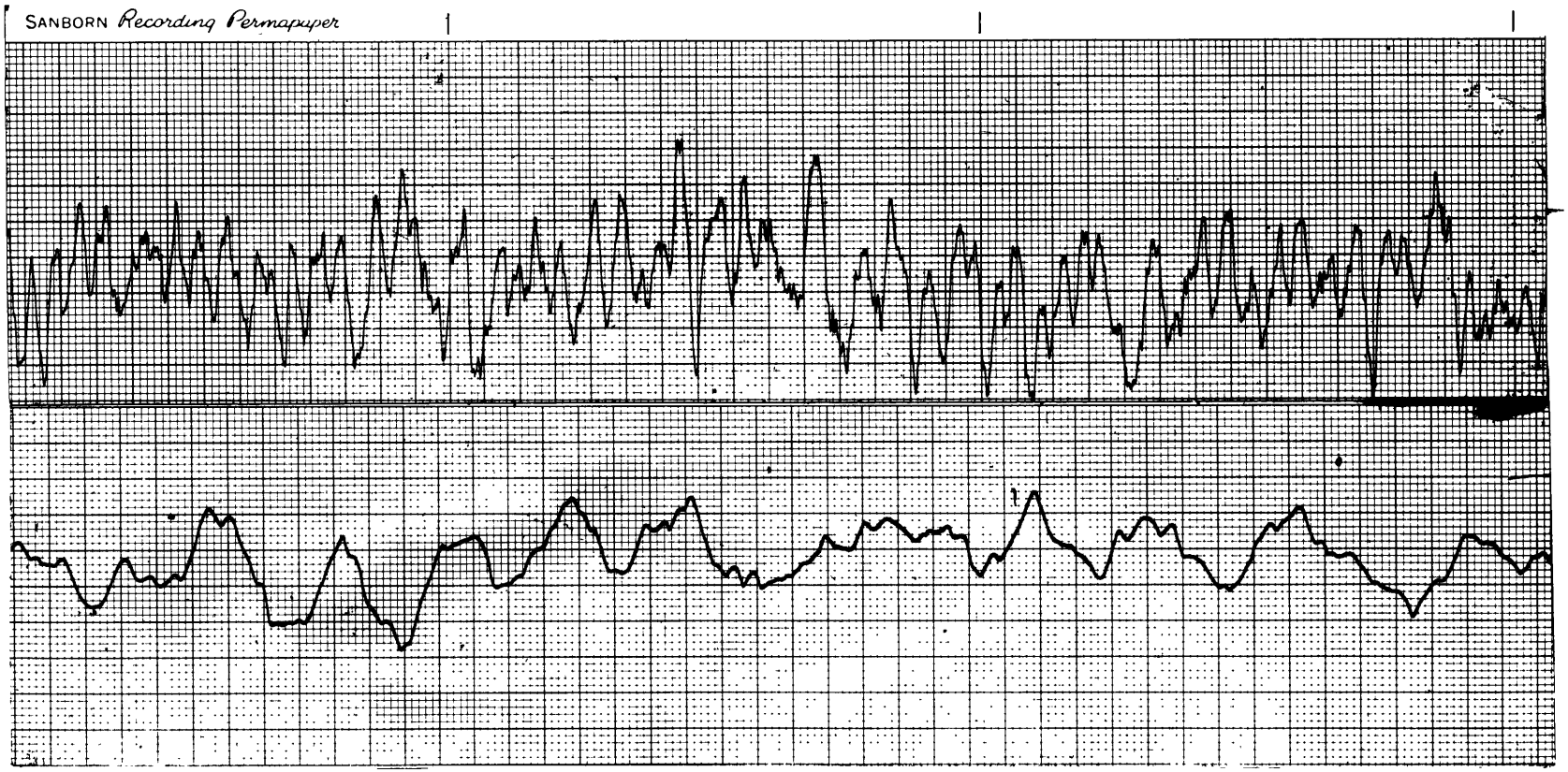

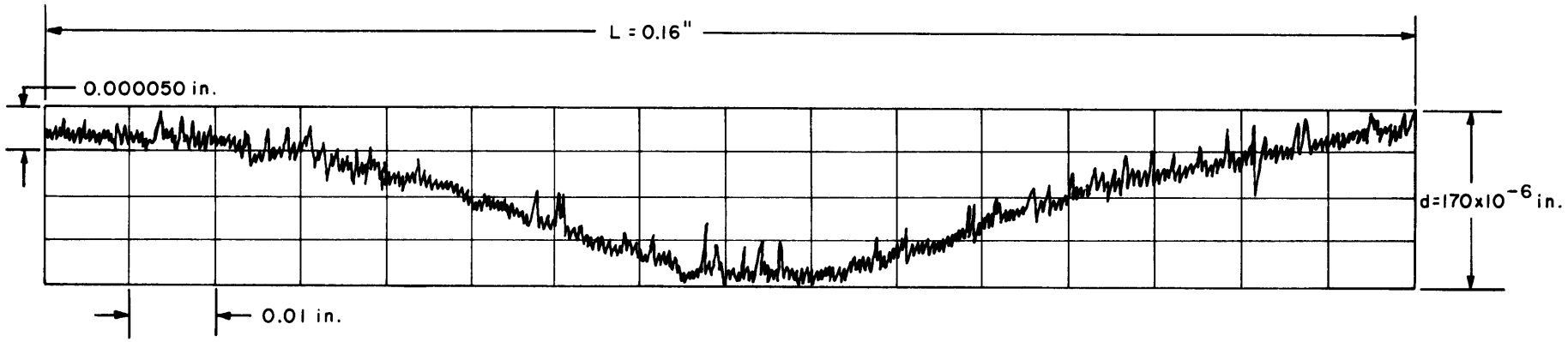

Fig. 6 Typical Trace Showing Waviness and Roughness

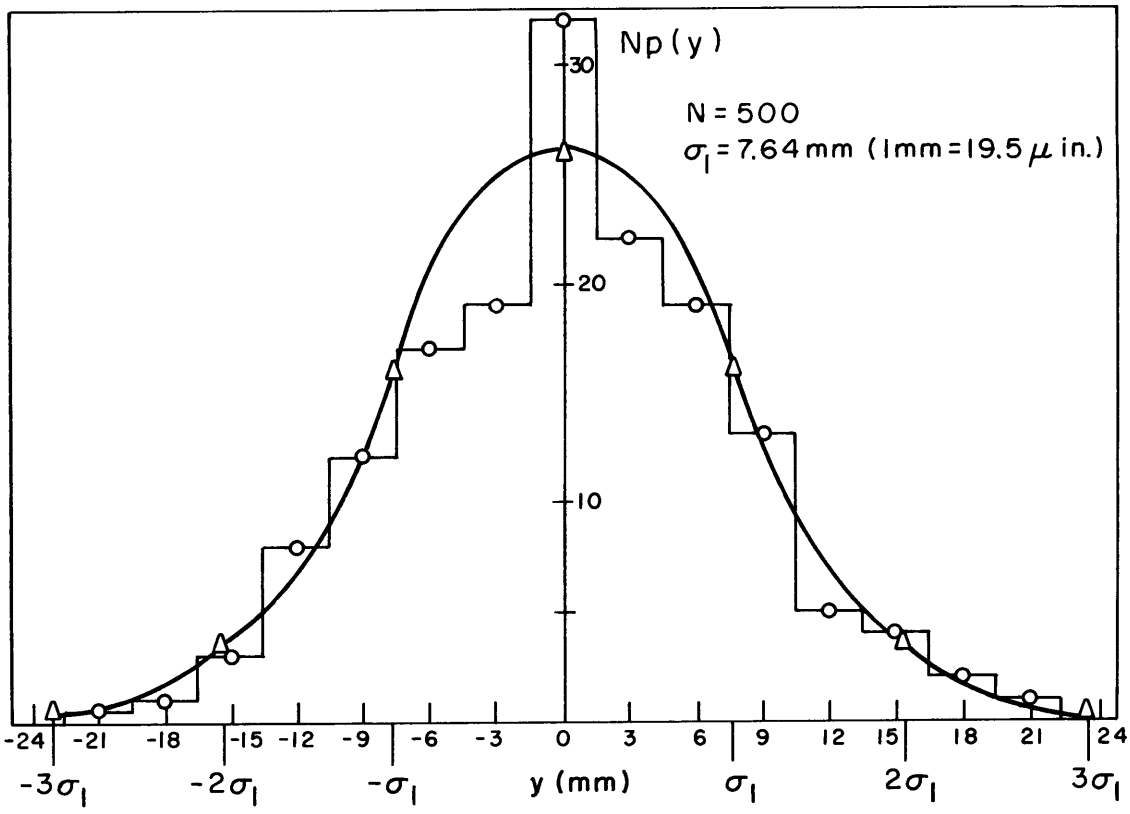

a) 149 μ in. Blasted Stainless Steel

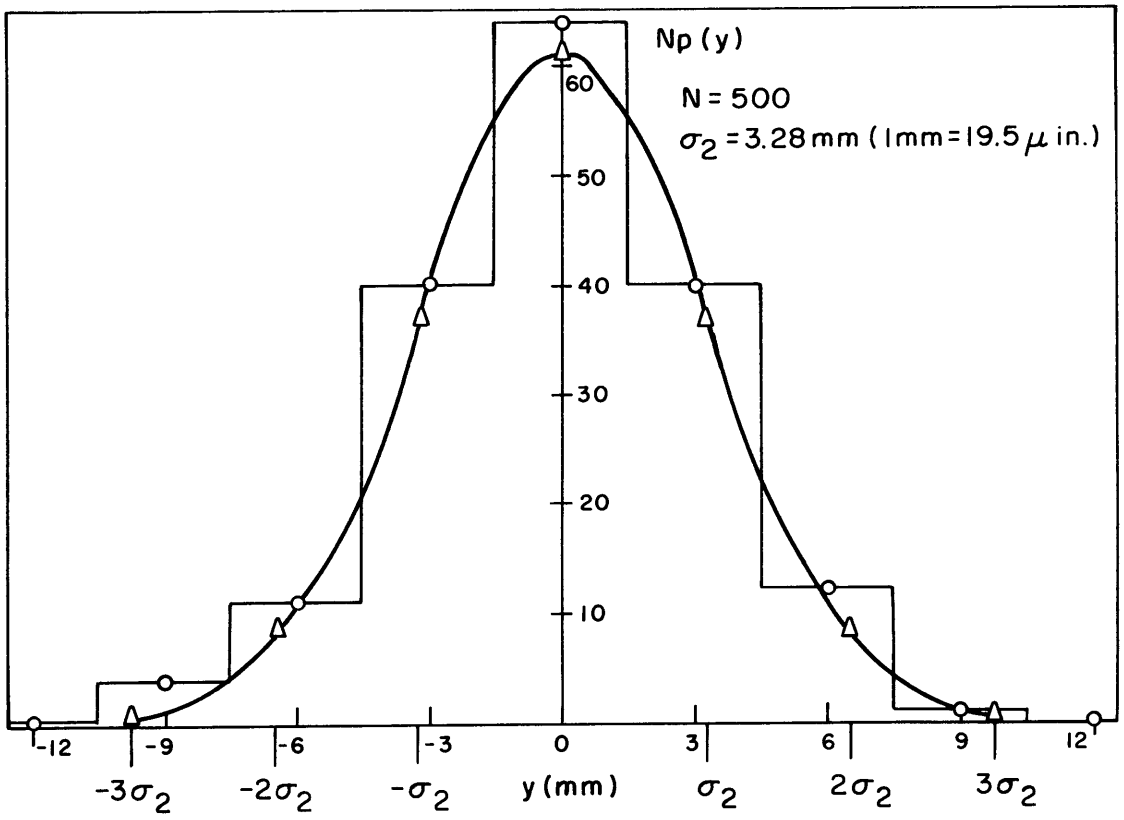

b) 64 μ in. Blasted Stainless Steel

Fig. 7 Distribution of Asperity Heights

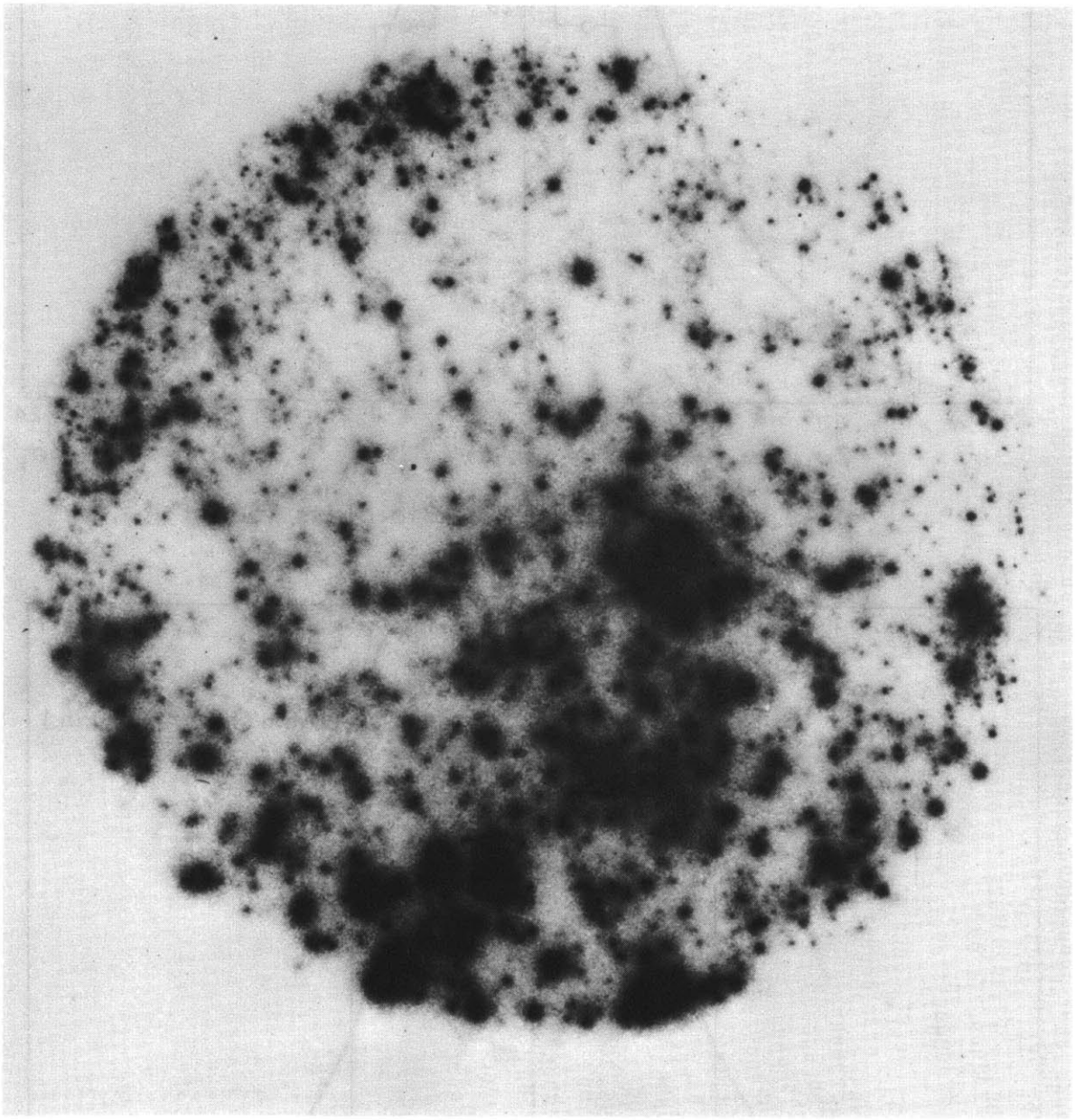

Fig. 8 Enlargement of Exposed X-Ray Film

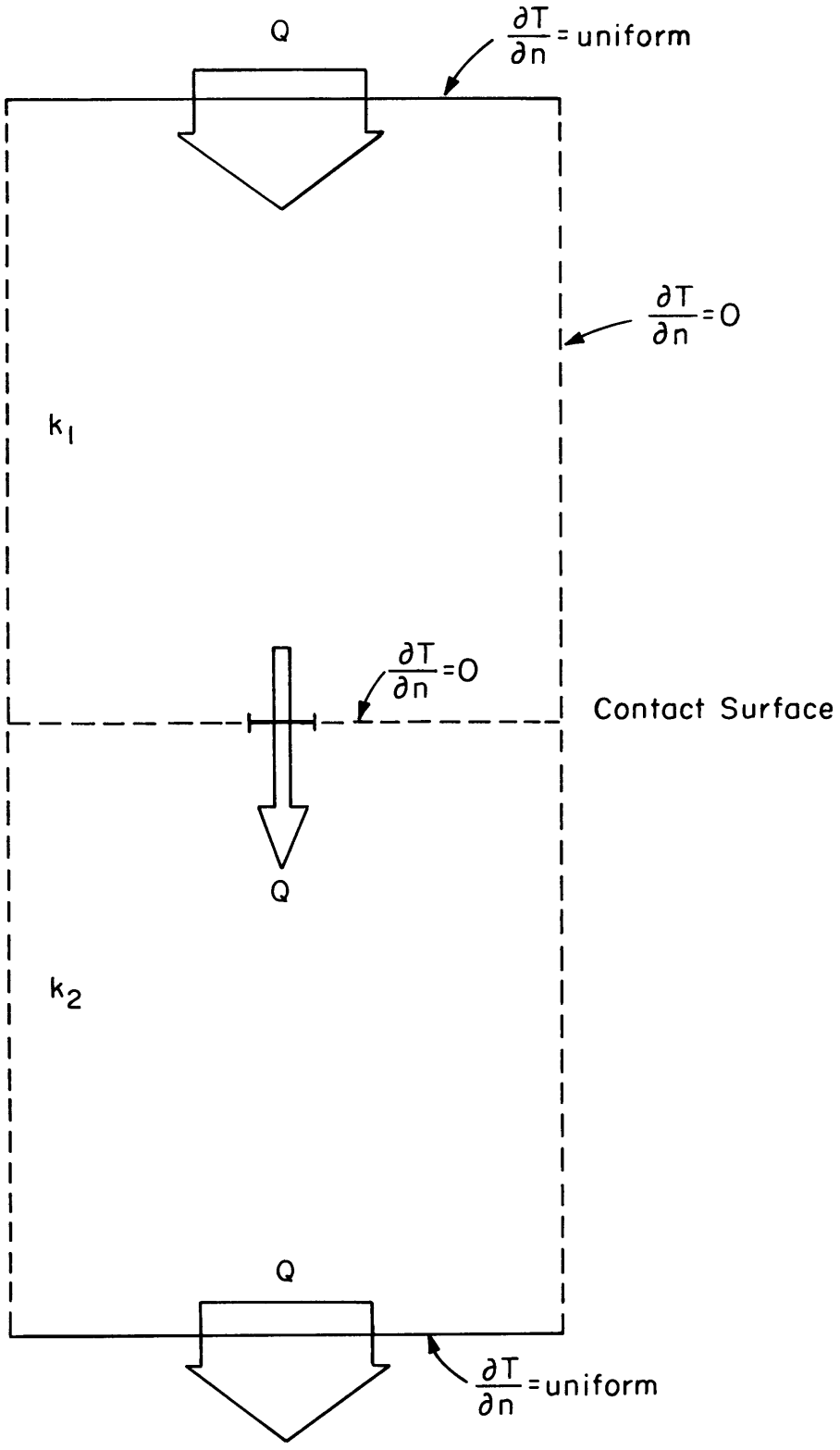

Fig. 9 Elemental Heat Flux Tube with One Contact Spot

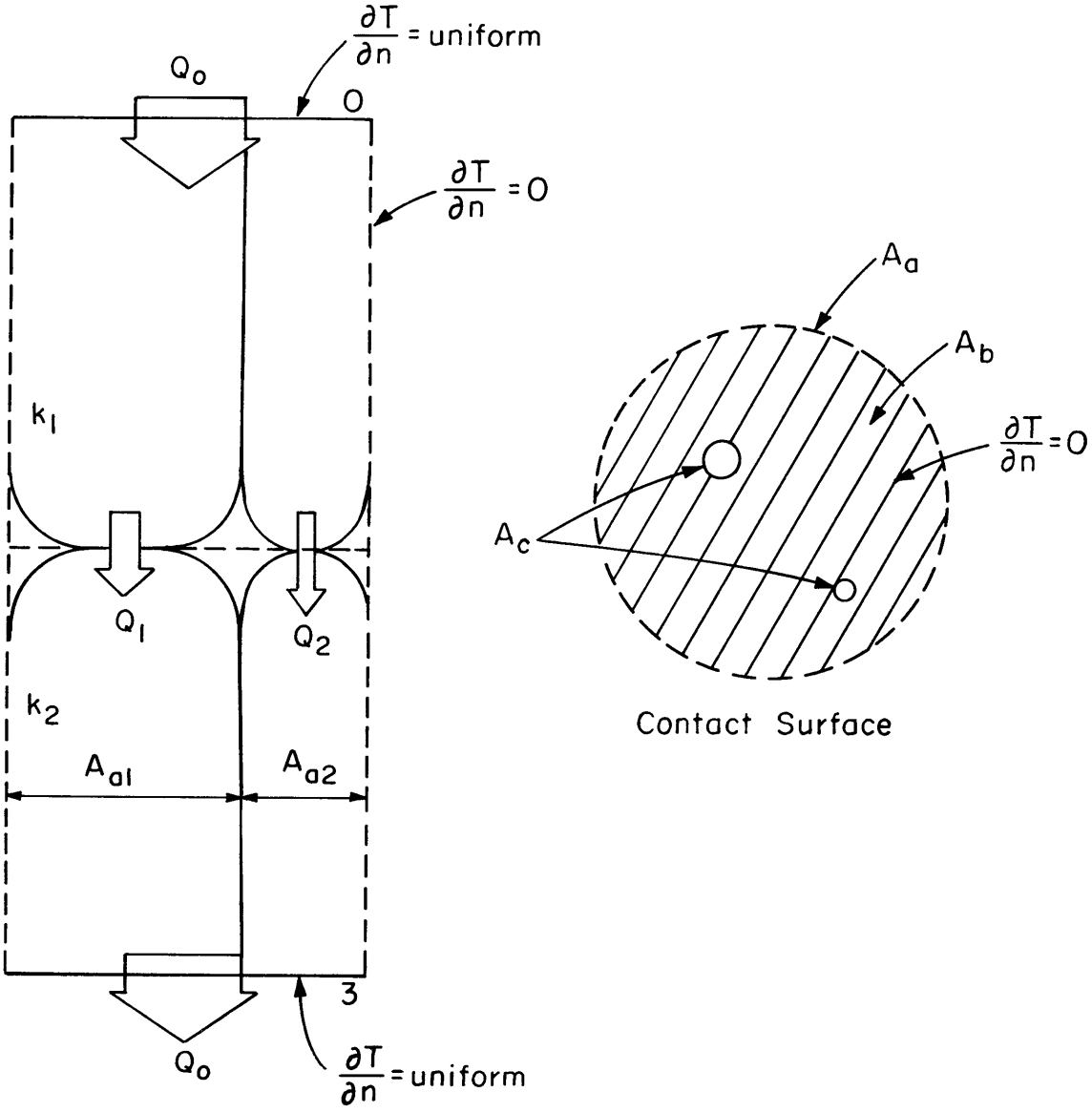

Fig. 10 Elemental Heat Channel with Two Unequal Contacts

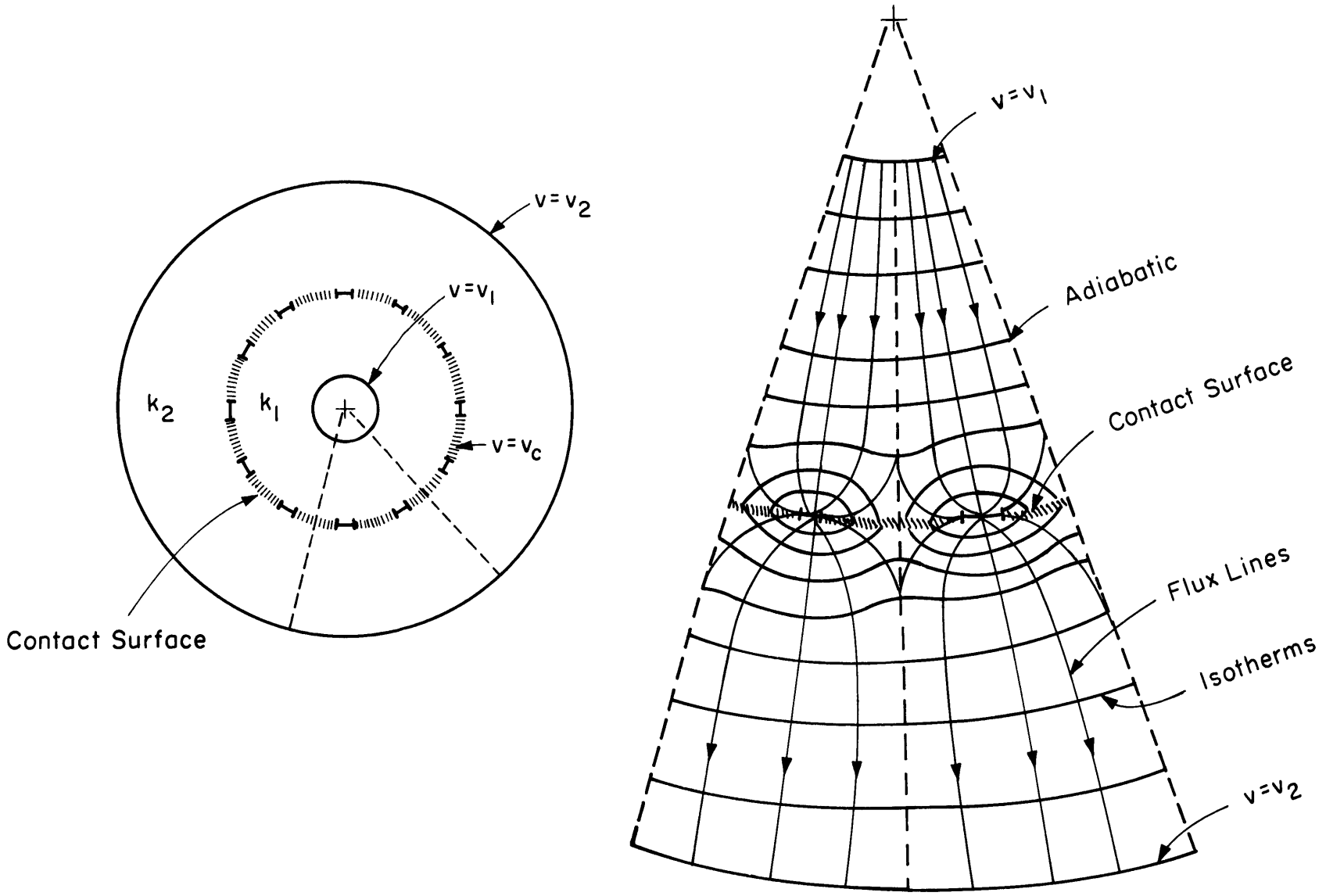

Fig. 11 Typical Heat Flux Channel for Cylindrical or Spherical Contact

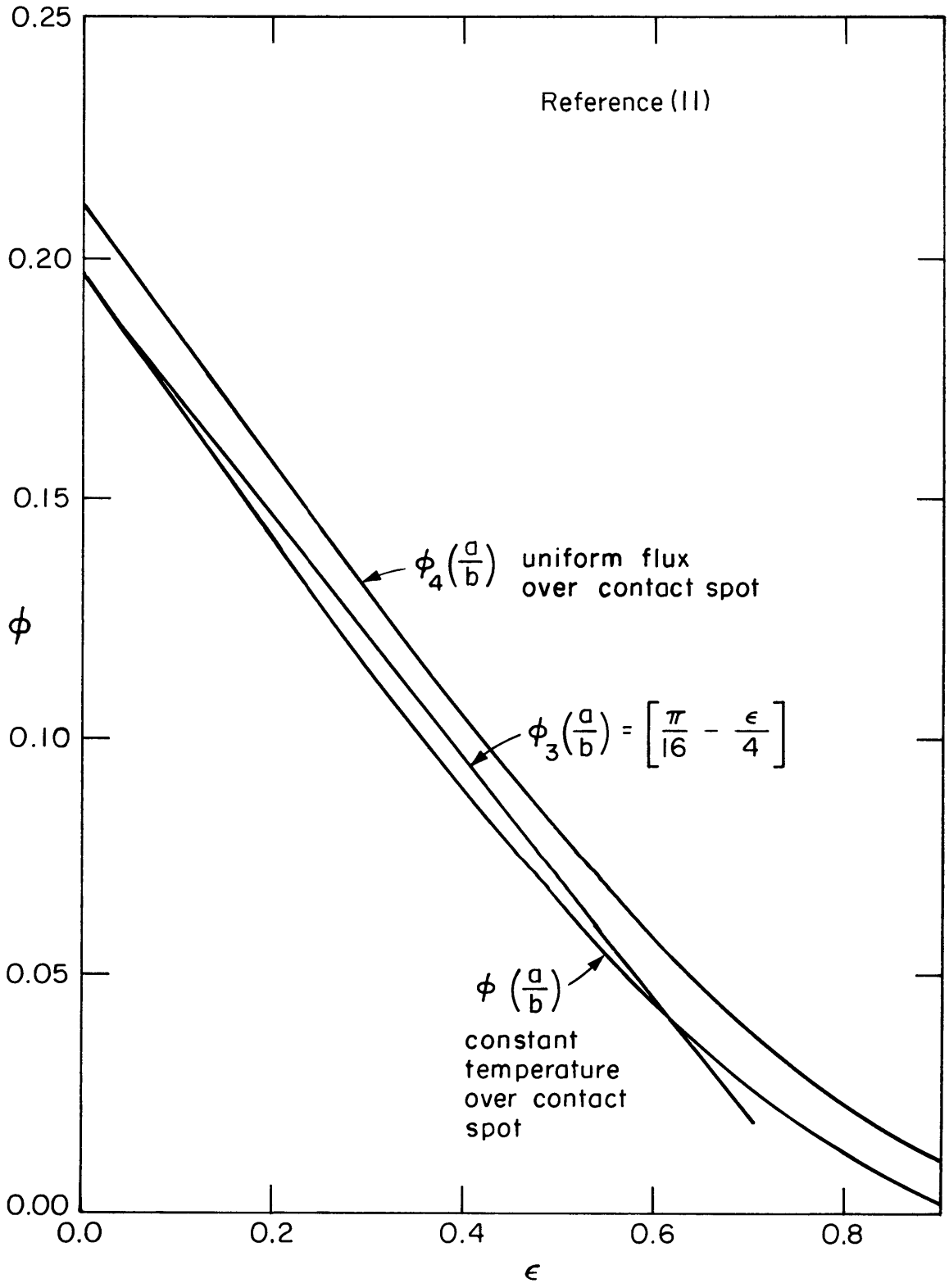

Fig. 12 Geometric Factor for Symmetric Contact

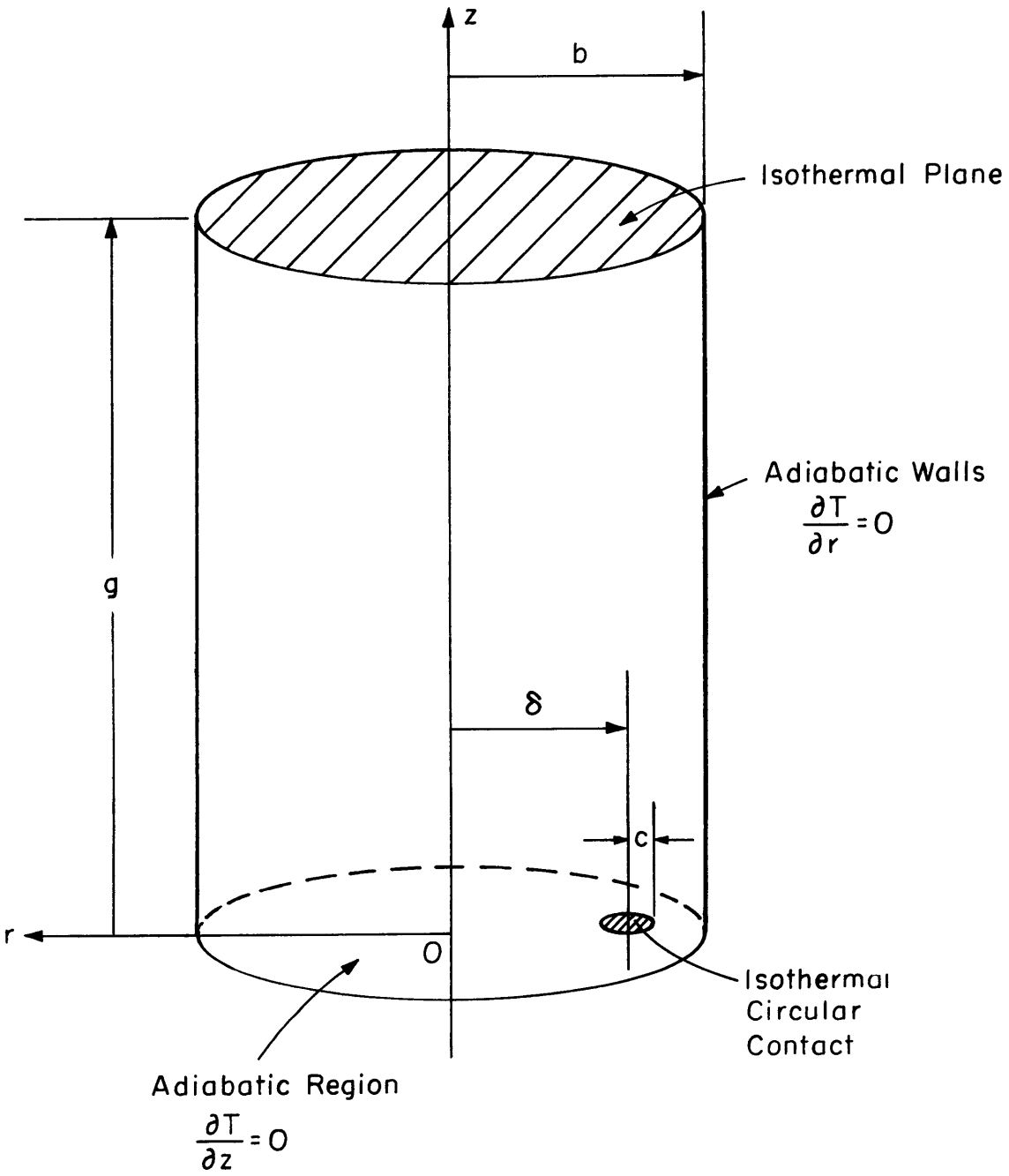

Fig. 13 Asymmetric Heat Flux Tube

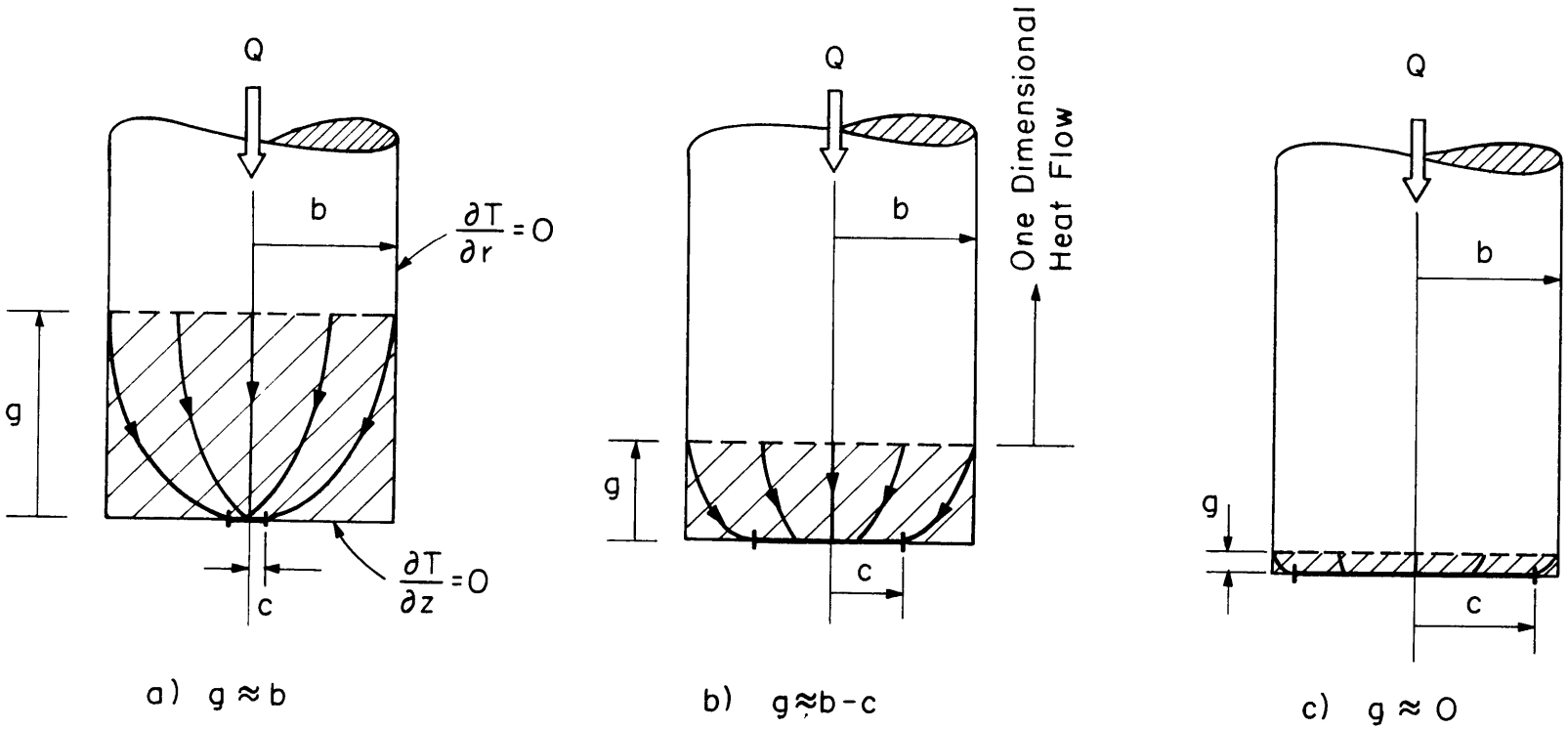

Fig. 14 Disturbed Temperature Regions

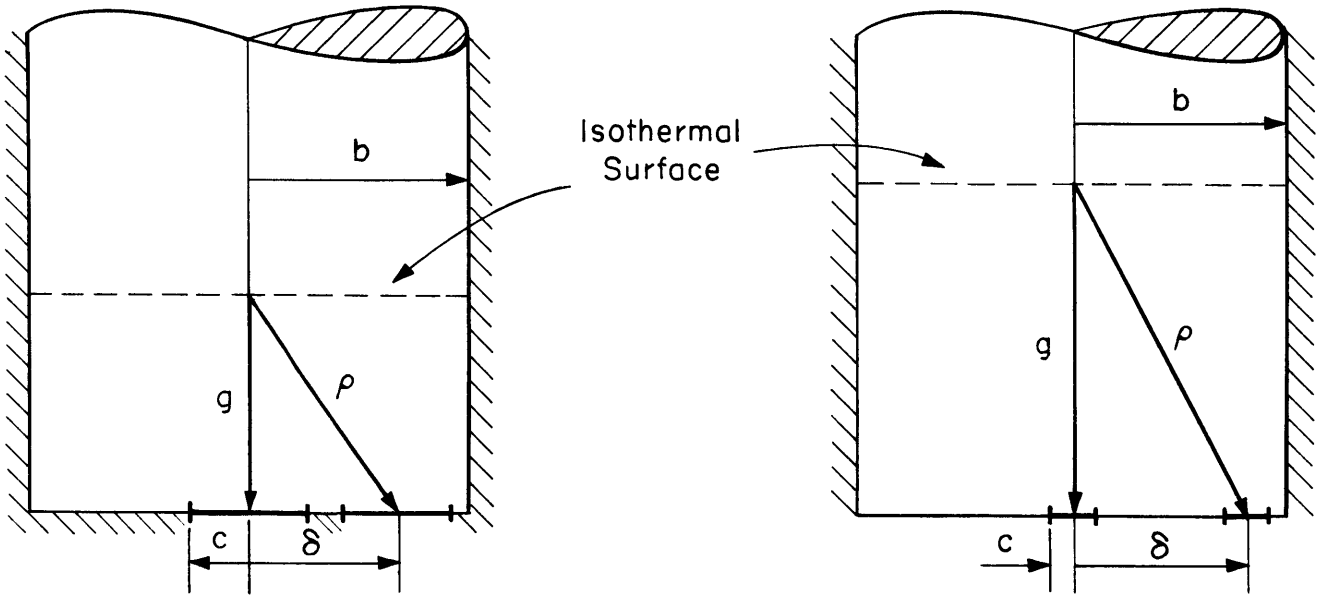

Fig. 15 Asymmetric Constriction Resistance Model

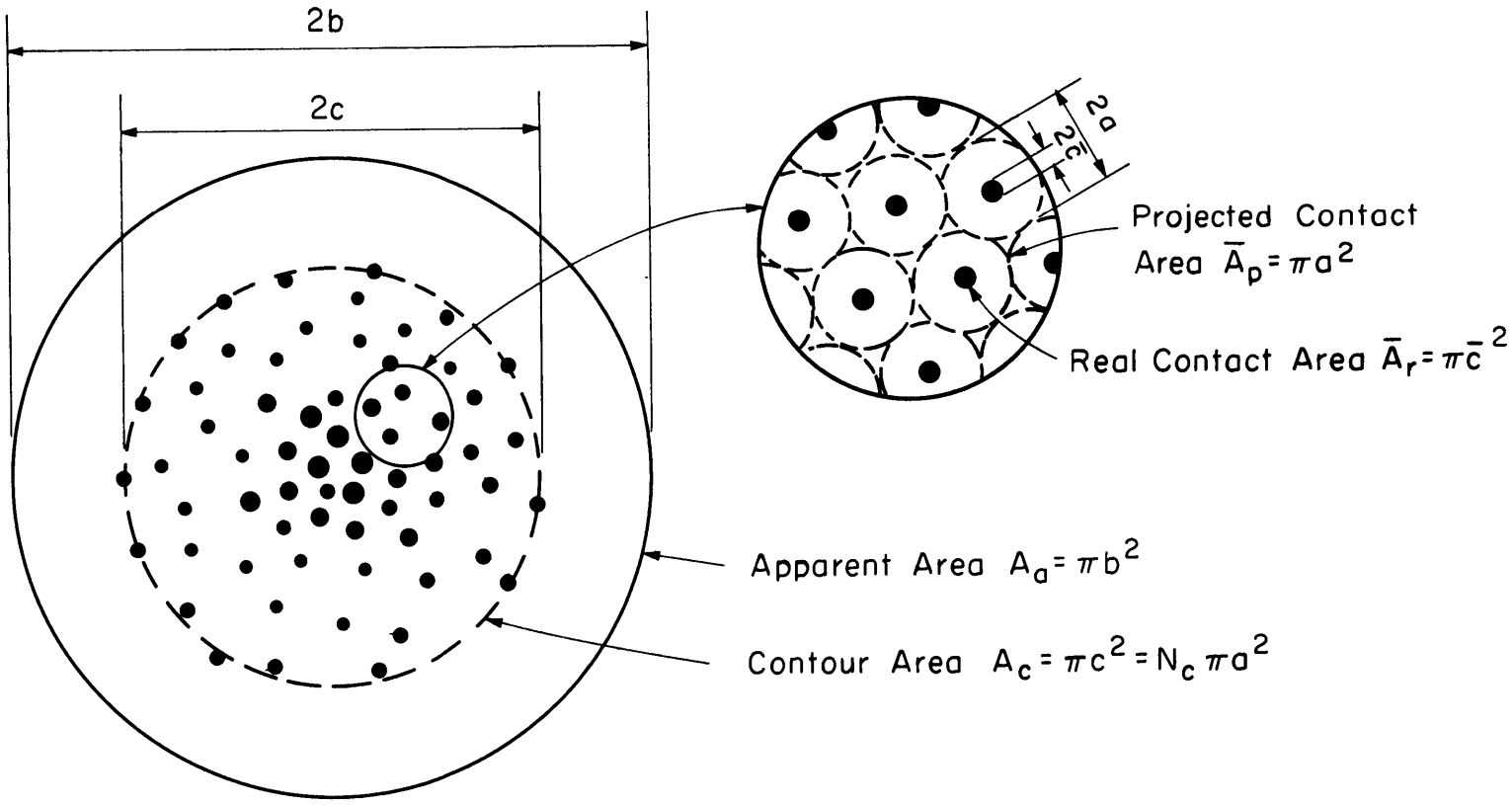

Fig. 16 Spherical Contact Model

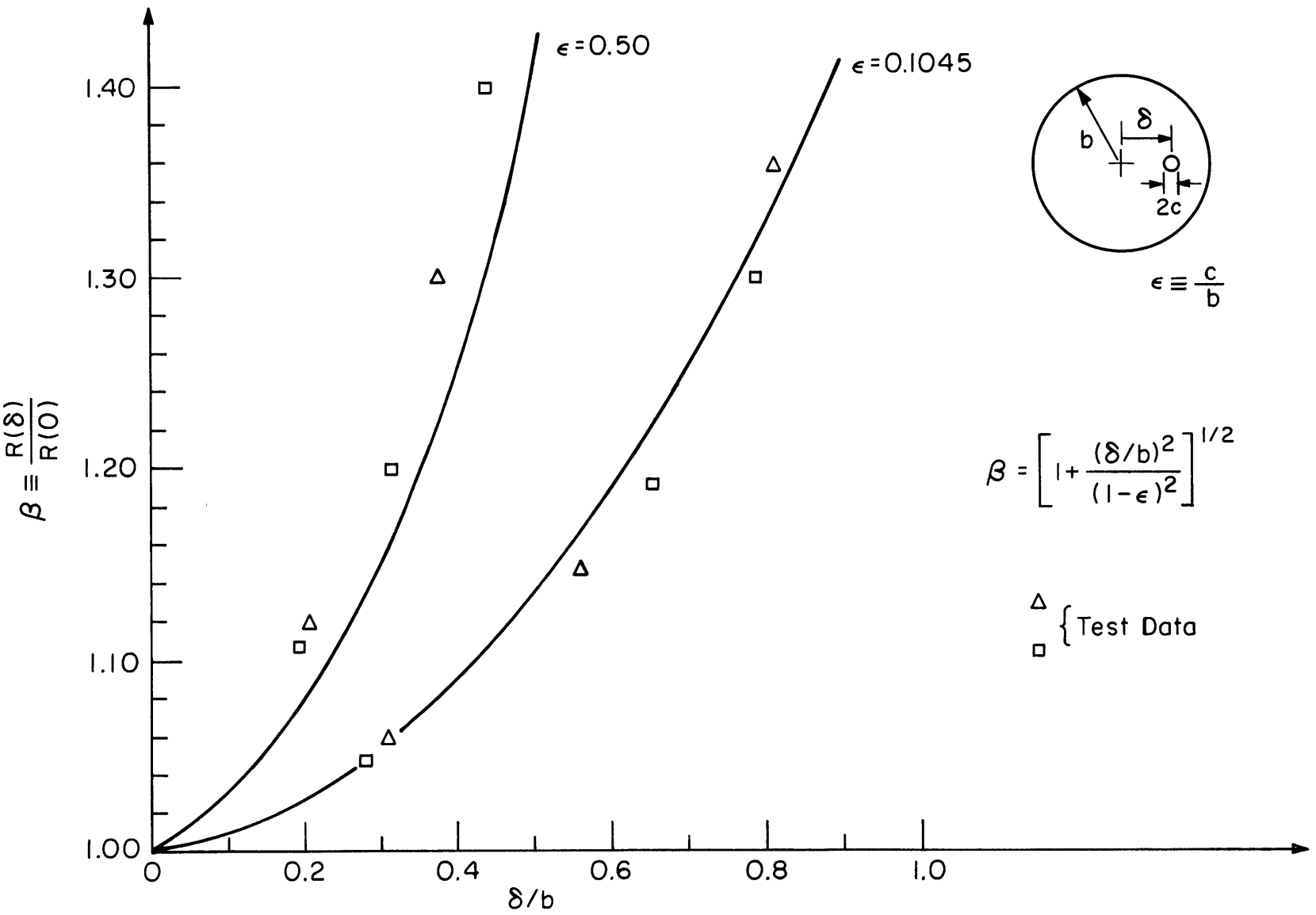

Fig. 17 Effect of Contact Spot Asymmetry

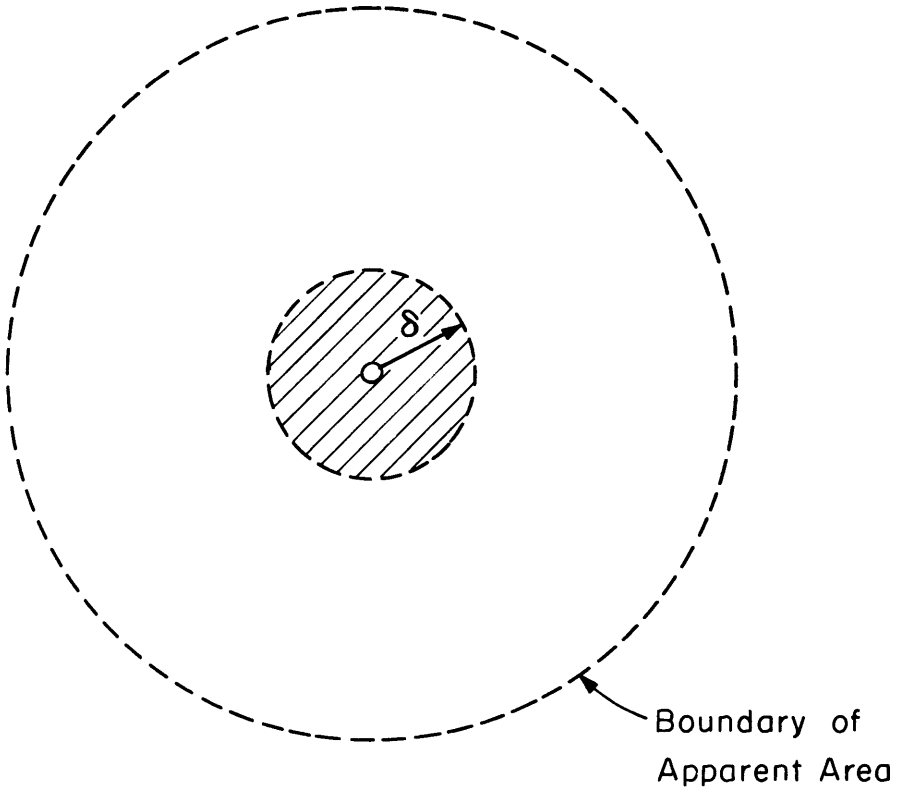

Fig.18 Displacement Region for Nominal Asymmetry Effect

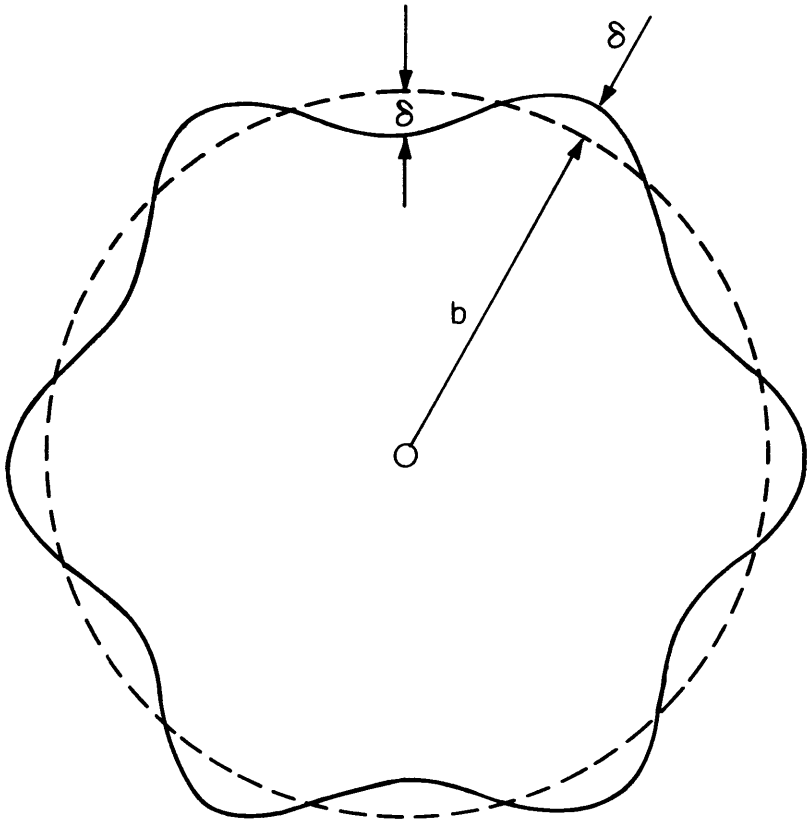

Fig. 19 Heat Flux Tube Boundary for Small Contact Spots

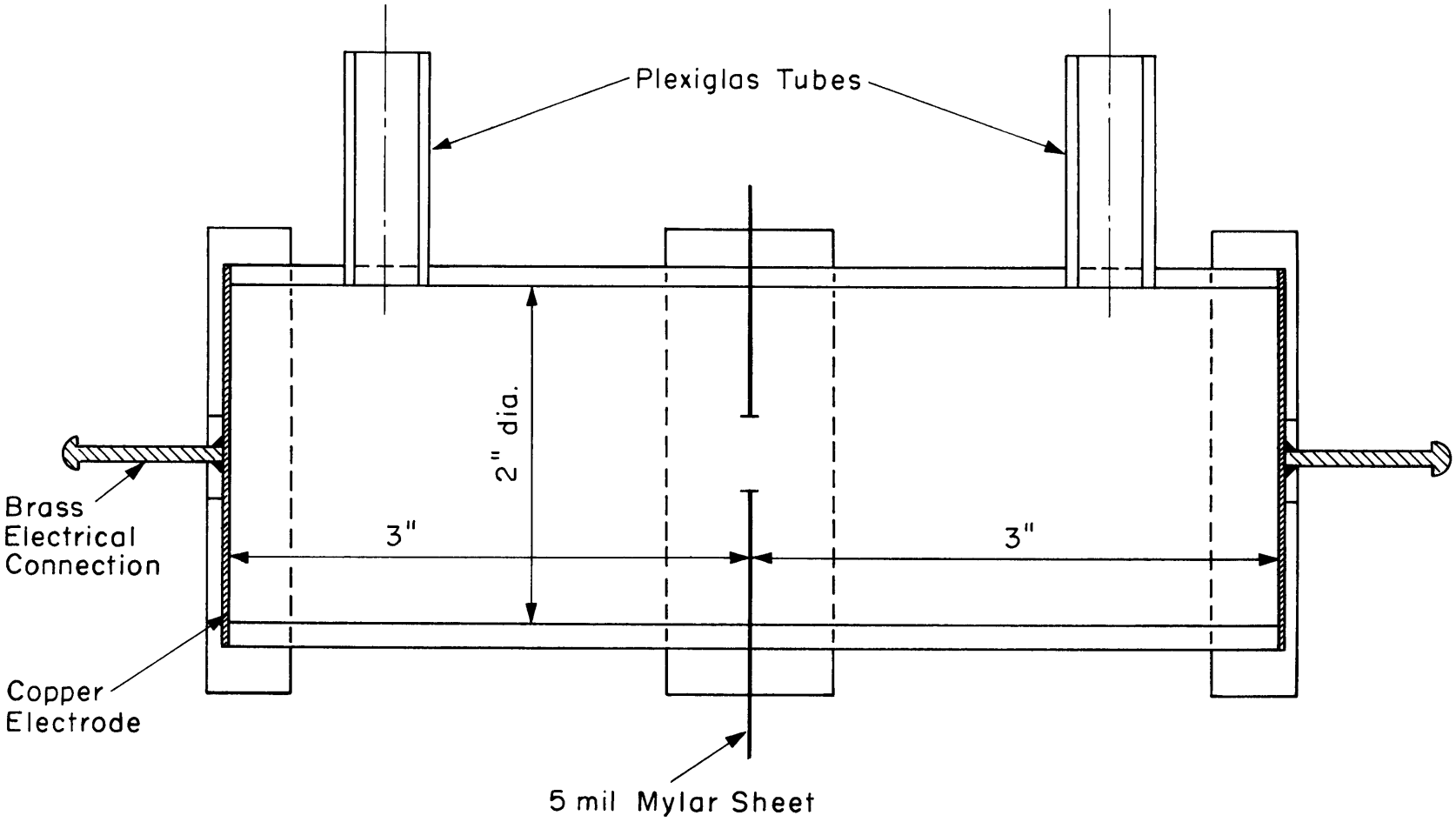

Fig. 20 Liquid Analog Apparatus to Test for Asymmetry

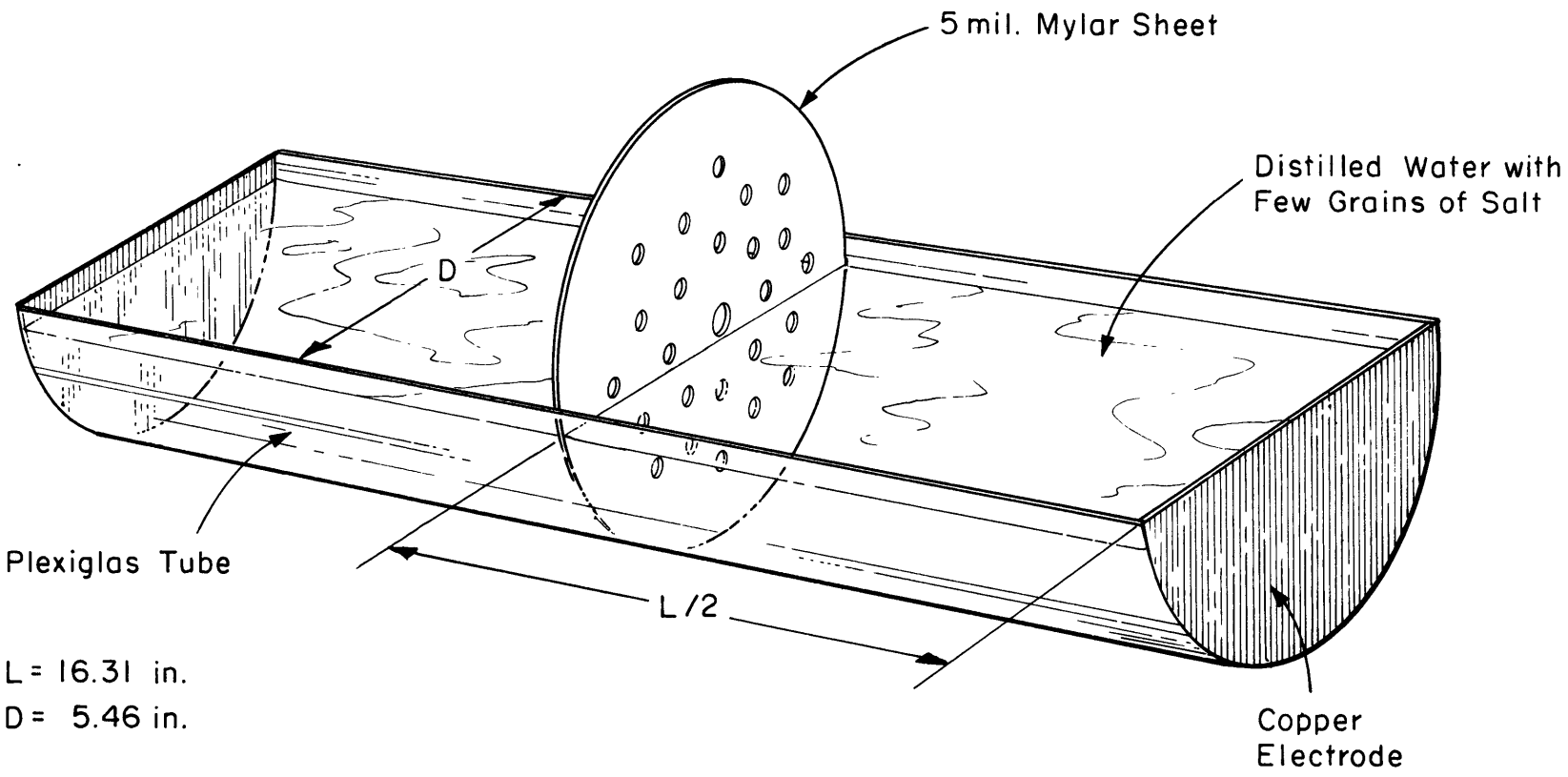

Fig. 21 Liquid Analog Apparatus to Test Variable Size Effect

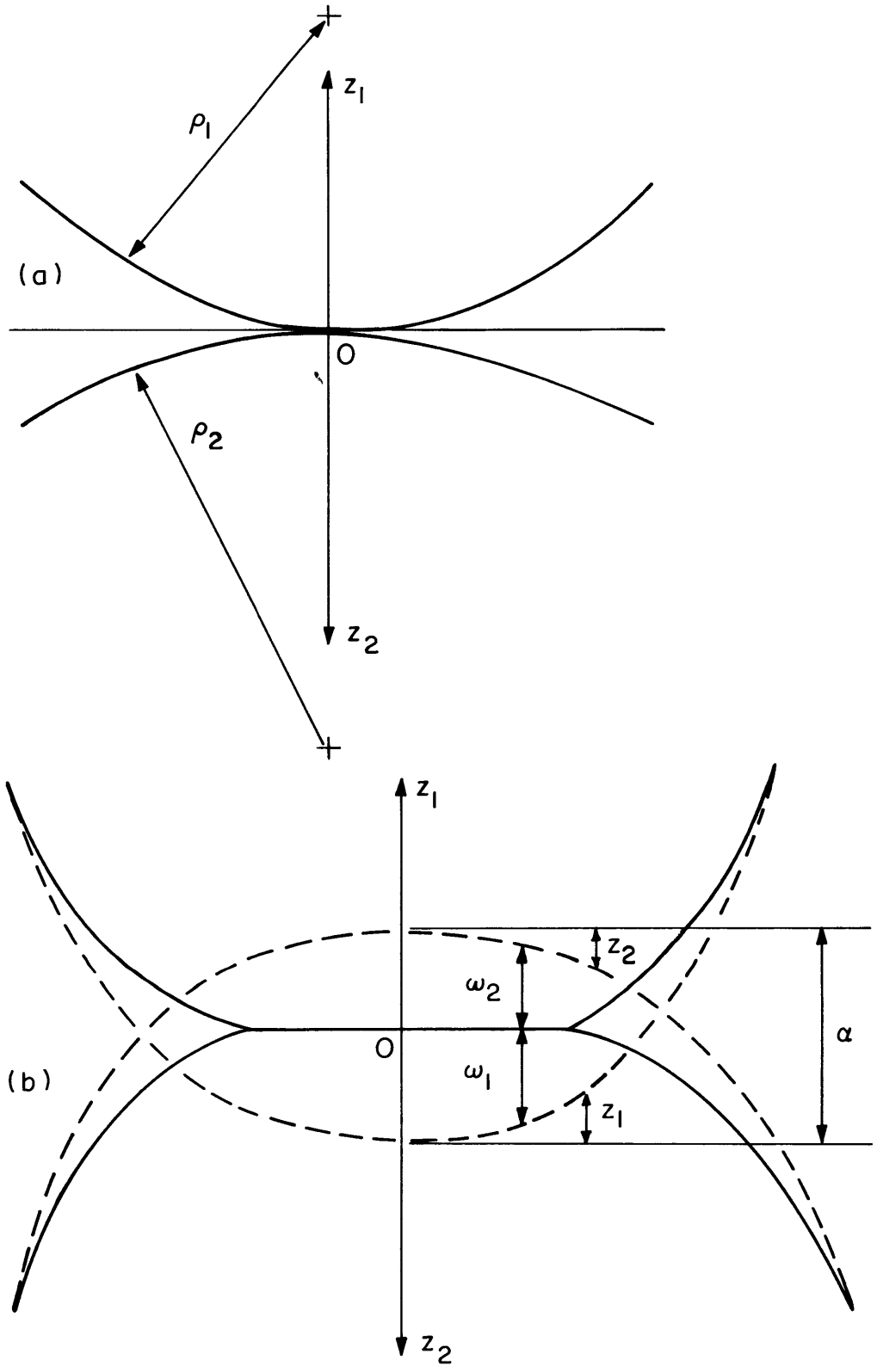

Fig. 22 Contact Between Smooth Hemispherical Solids

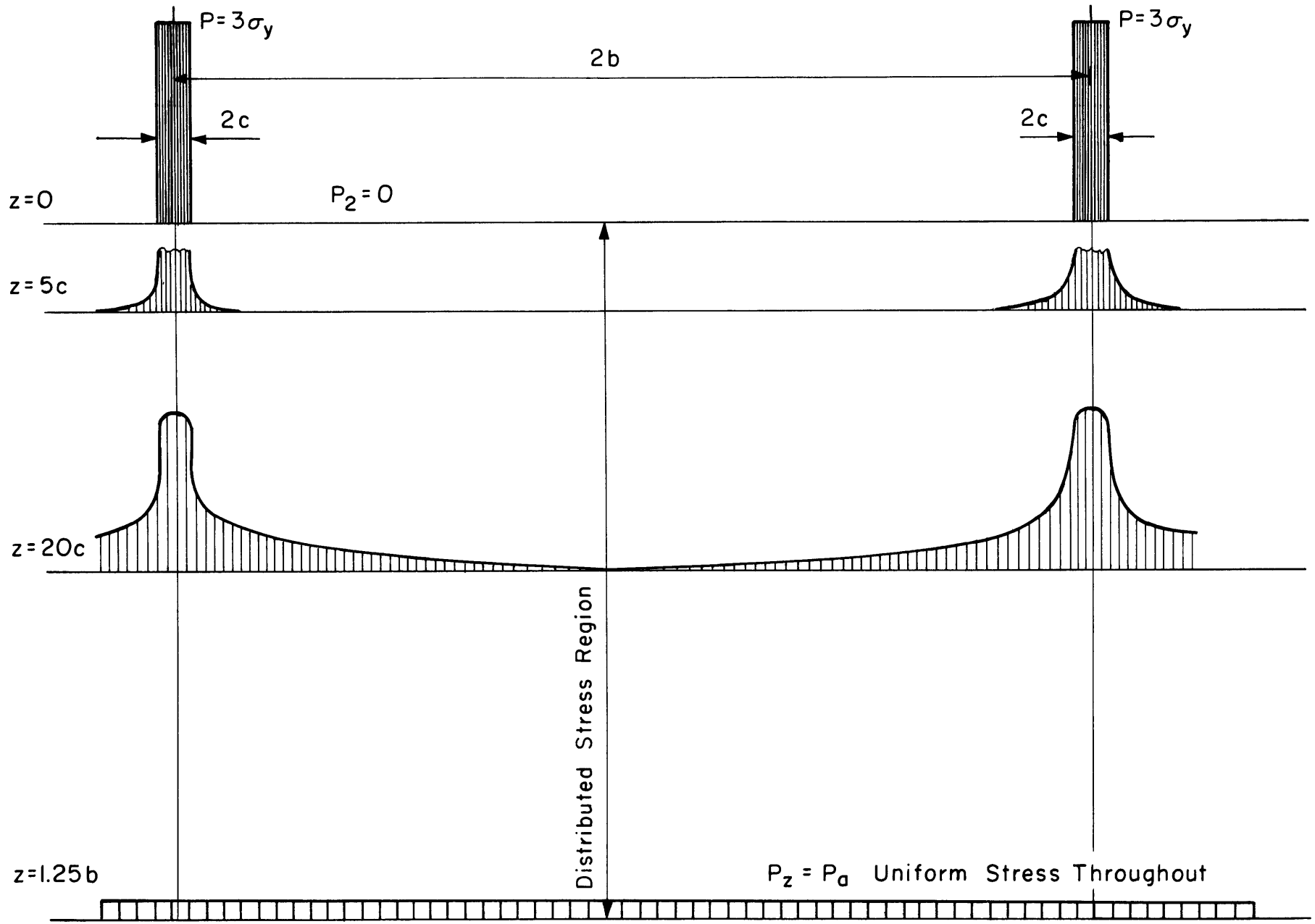

Fig. 23 Stress Distribution in Half Space Under a Rigid Circular Contact

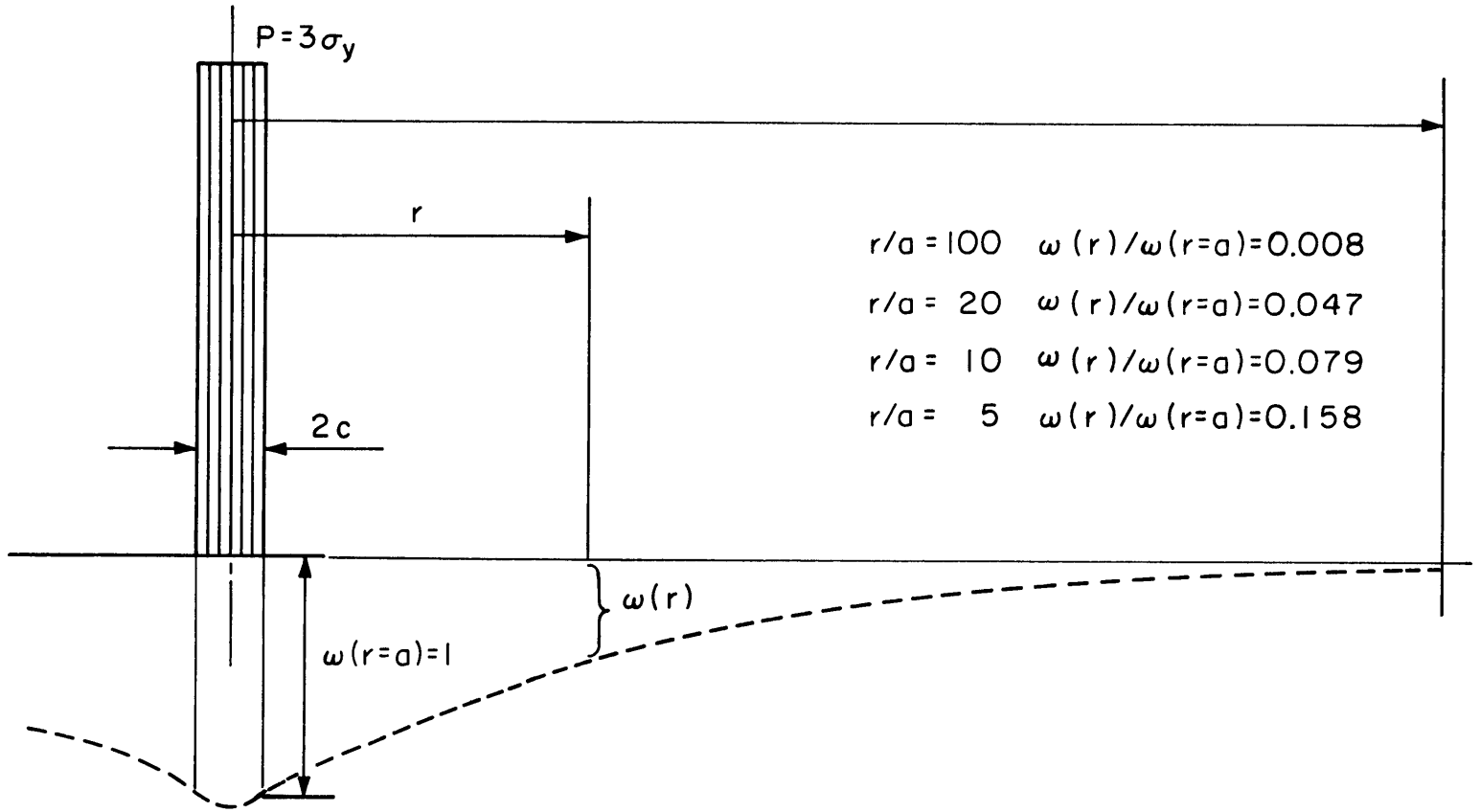

Fig. 24 Vertical Displacement of Free Surface Due to Rigid Circular Contact

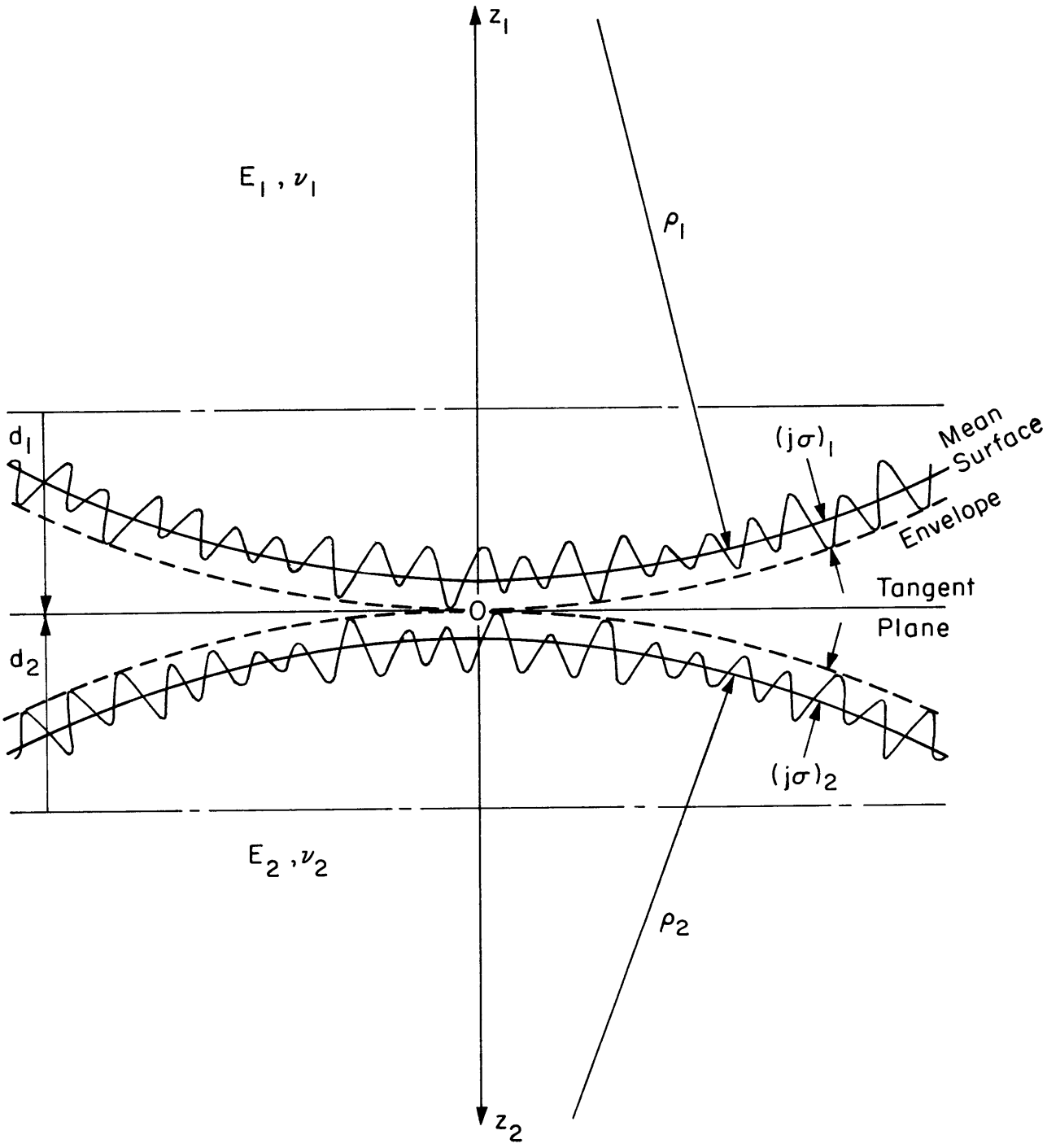

Fig. 25 Contact Between Two Rough Hemispherical Solids

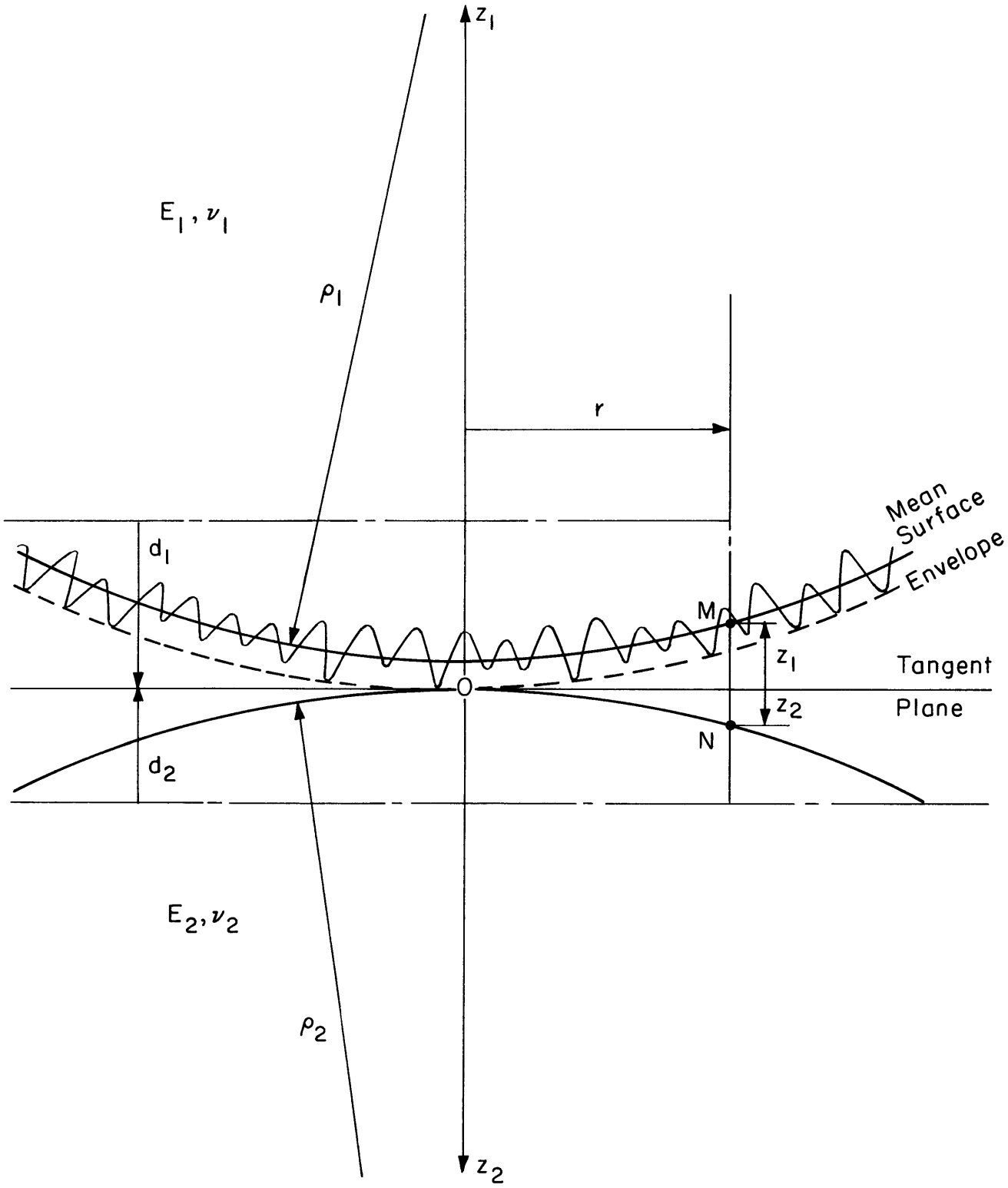

Fig. 26 Contact Model for Rough Hemispherical Solids

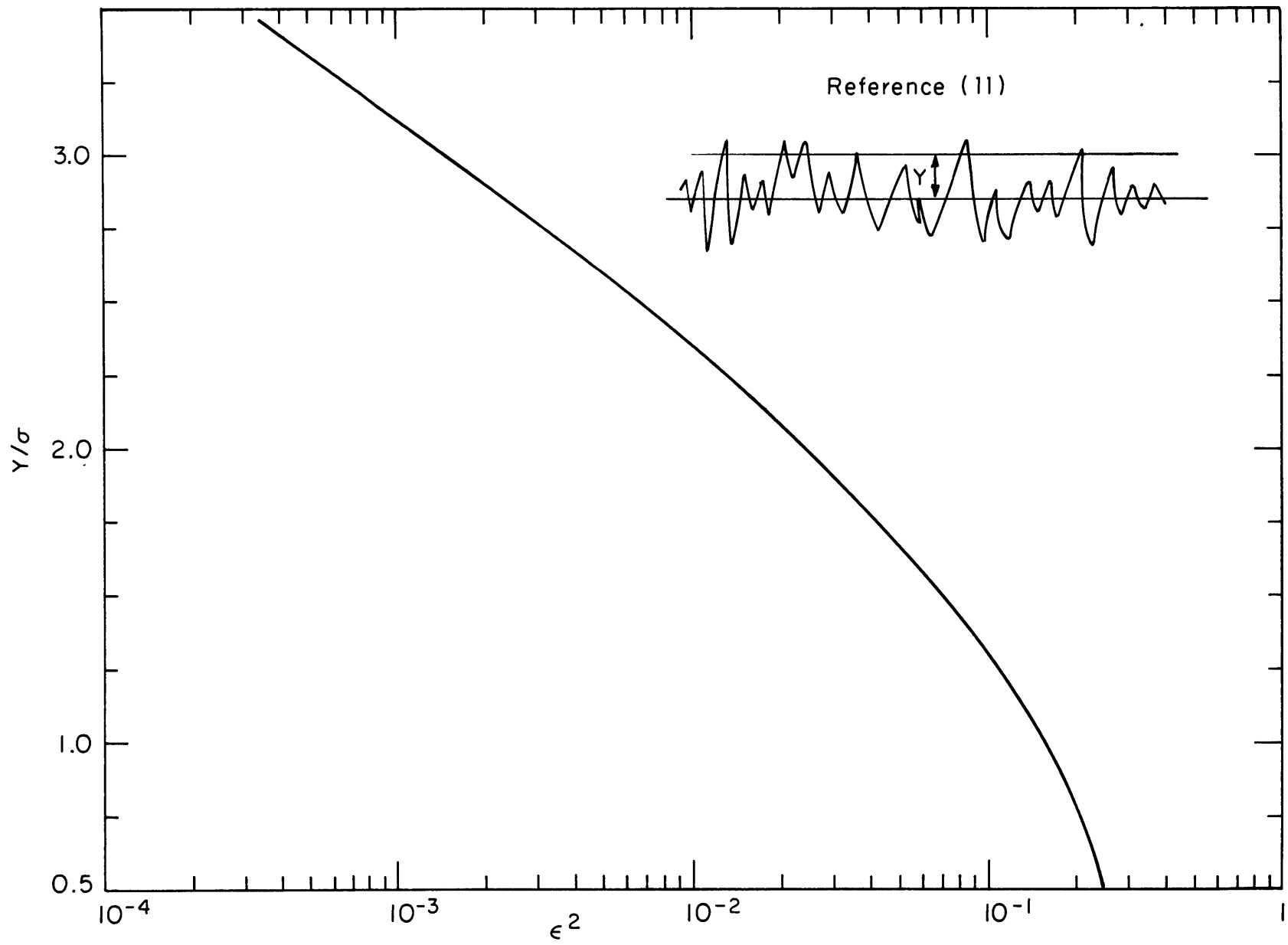

Fig. 27 Separation Between Mean Planes vs. Real Area Ratio

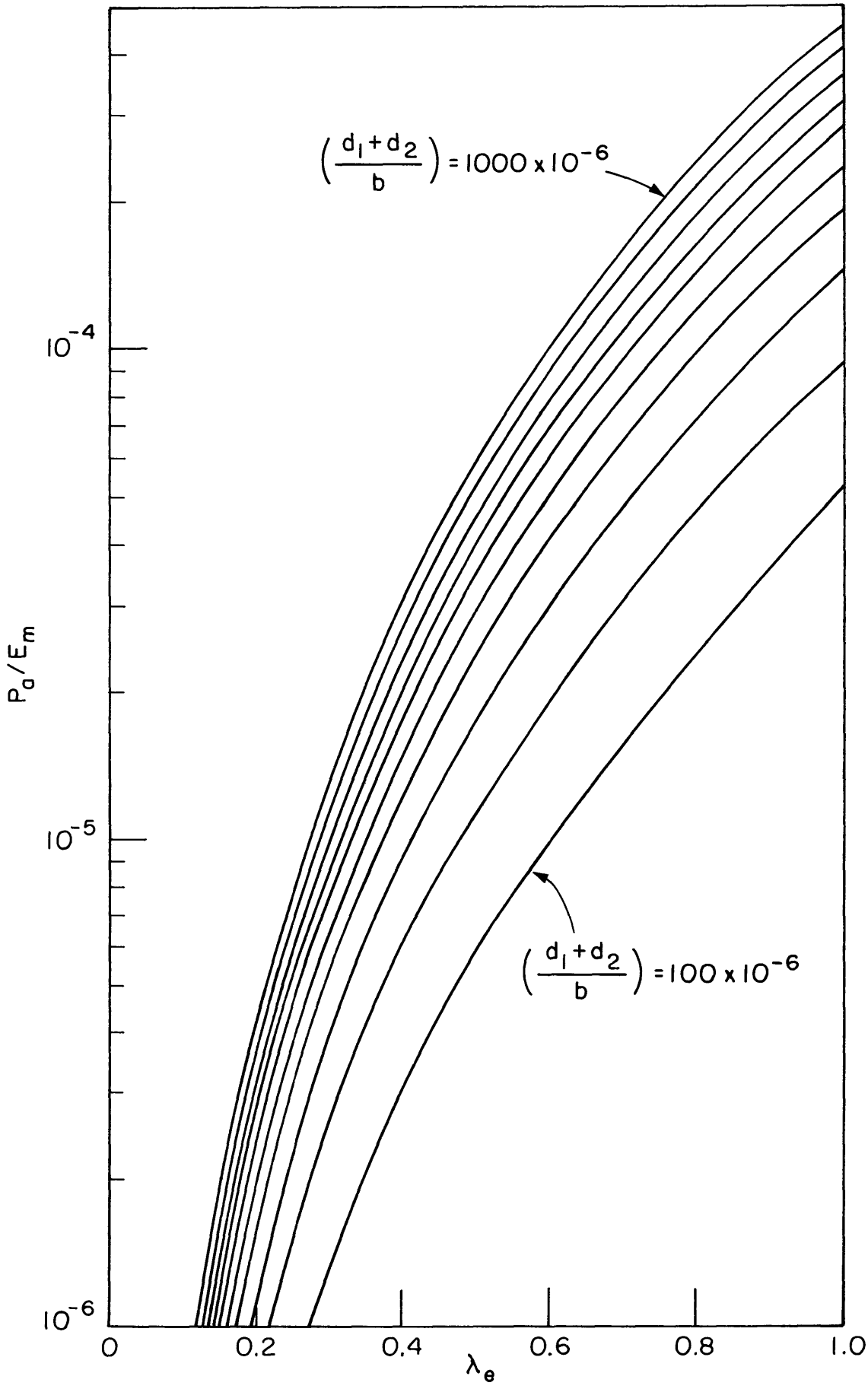

Fig. 28 Contour Ratio Based Upon Smooth Contact

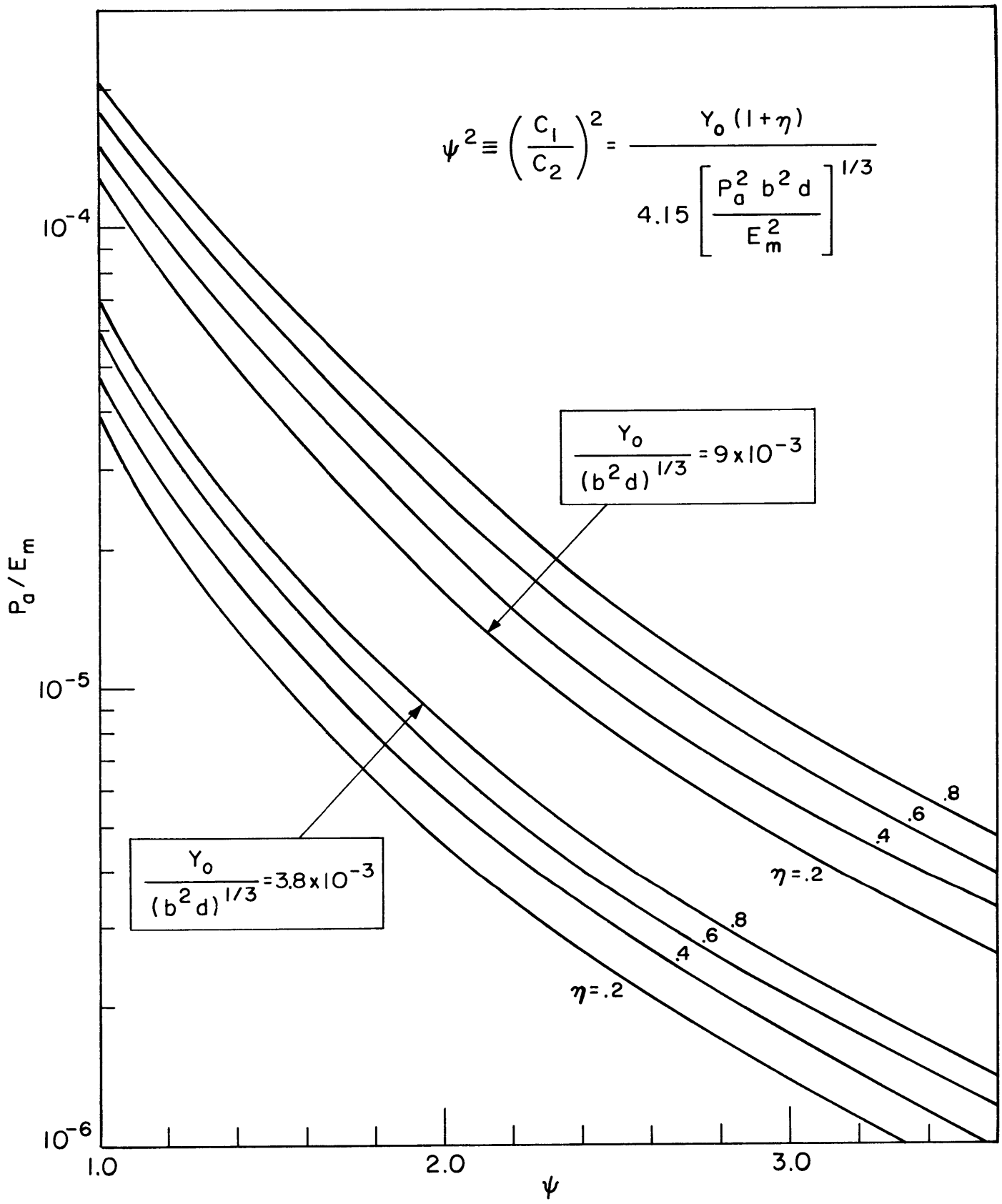

Fig. 29 Roughness Influence Factor

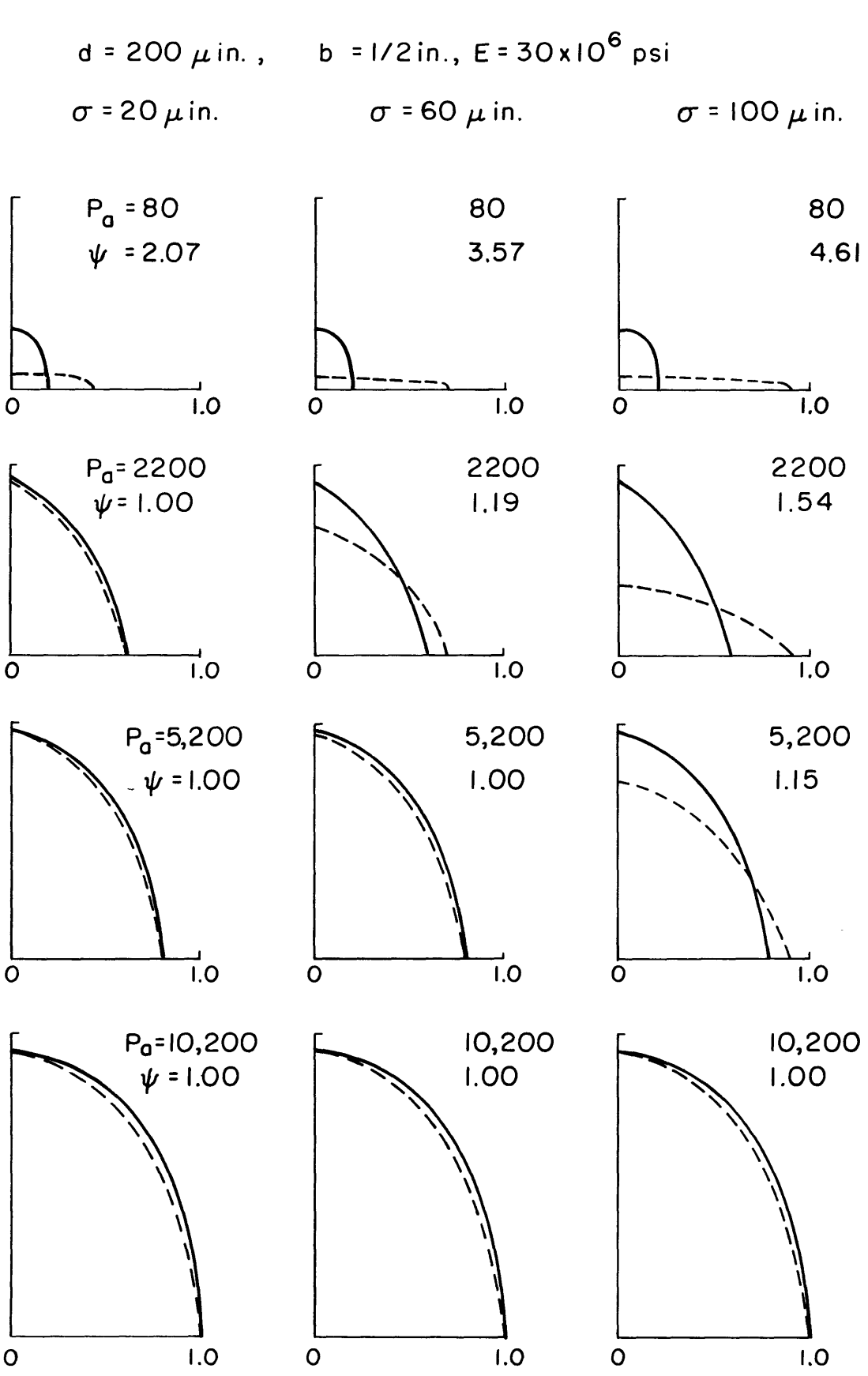

Fig. 30 Effect of Roughness on Contour Radius

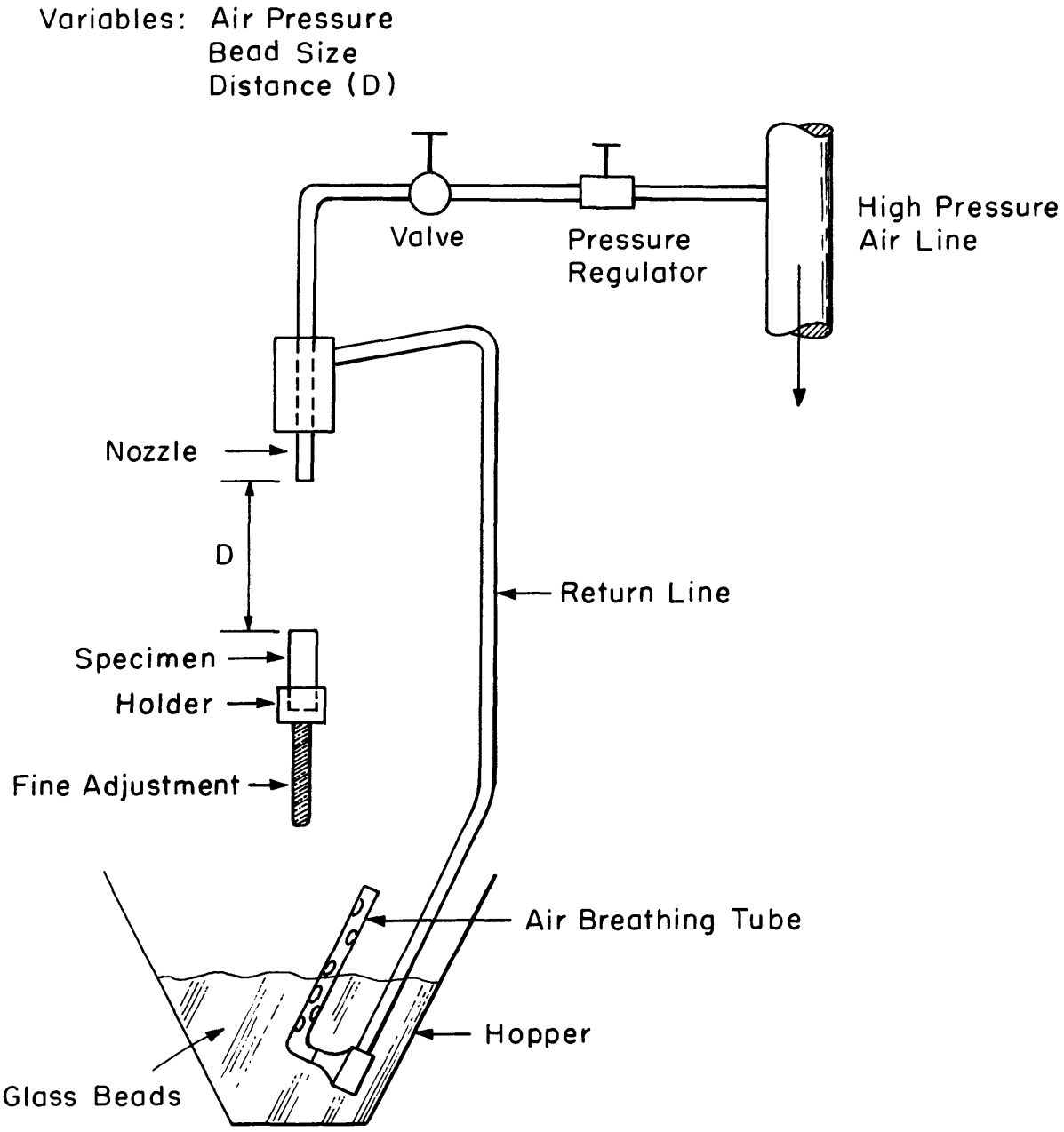

Fig. 31 Schematic of Glass Bead Blasting Device

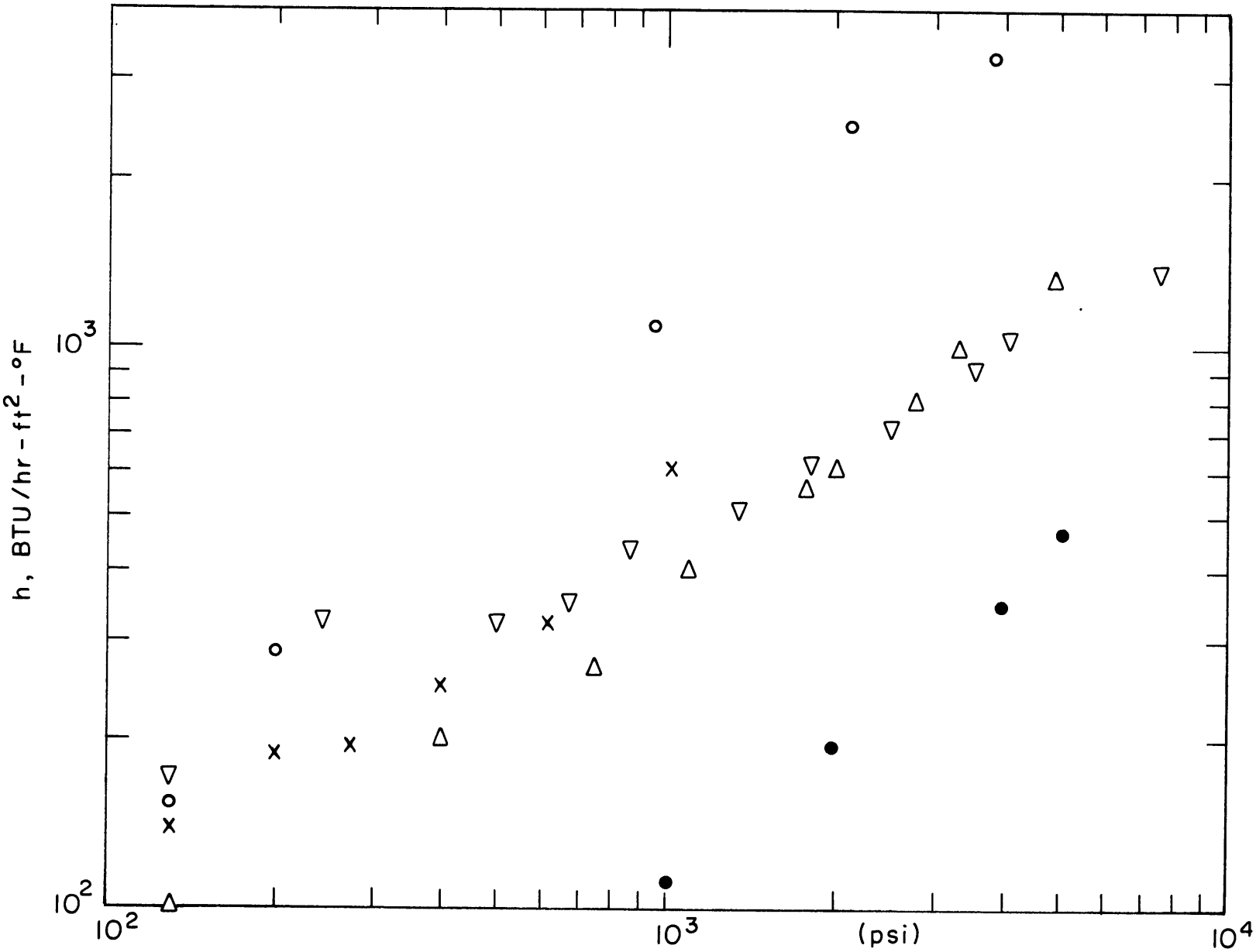

Fig. 32 Thermal Conductance Data vs. Apparent Pressure

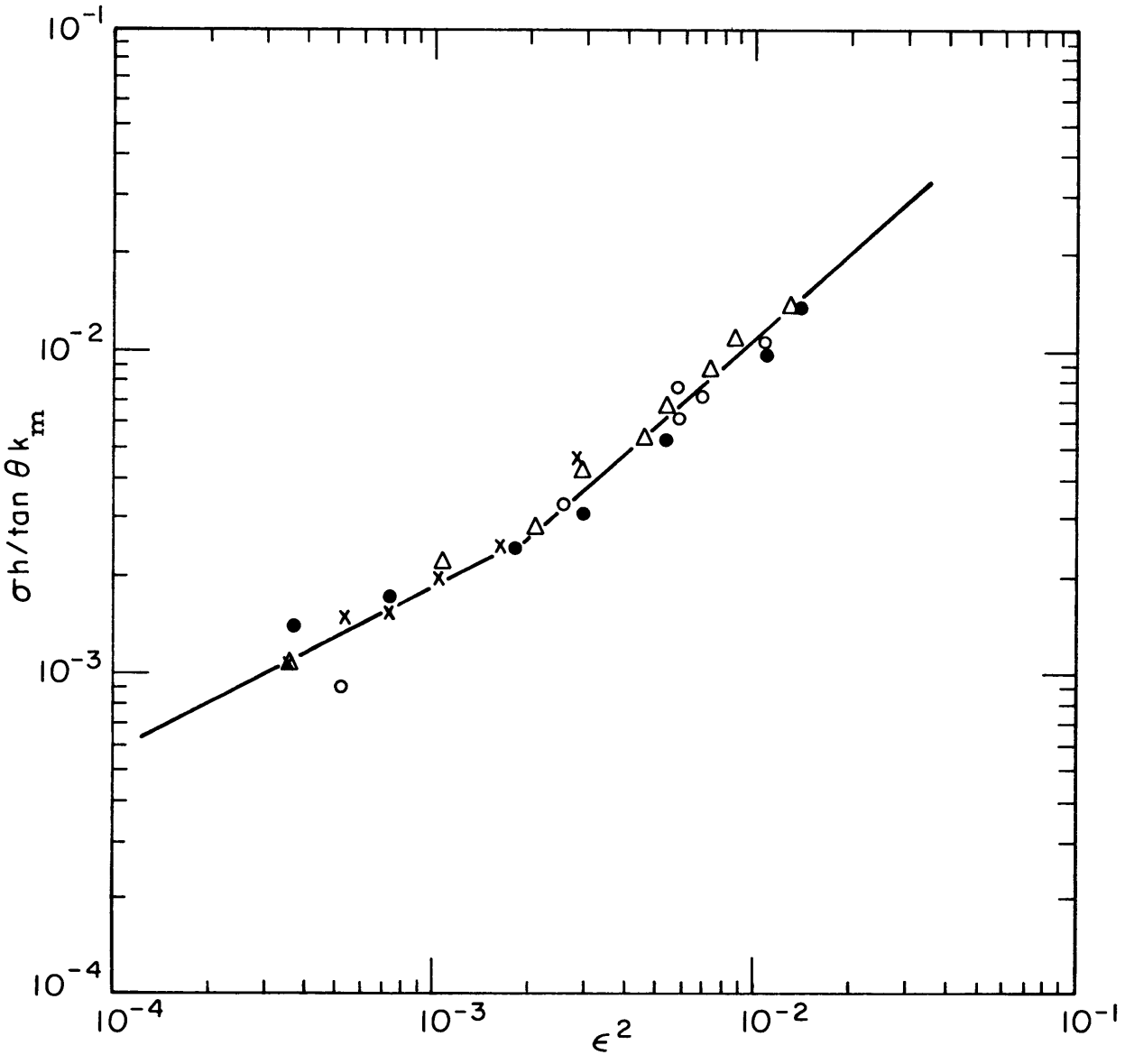

Fig. 33 Thermal Conductance Number vs. Area Ratio

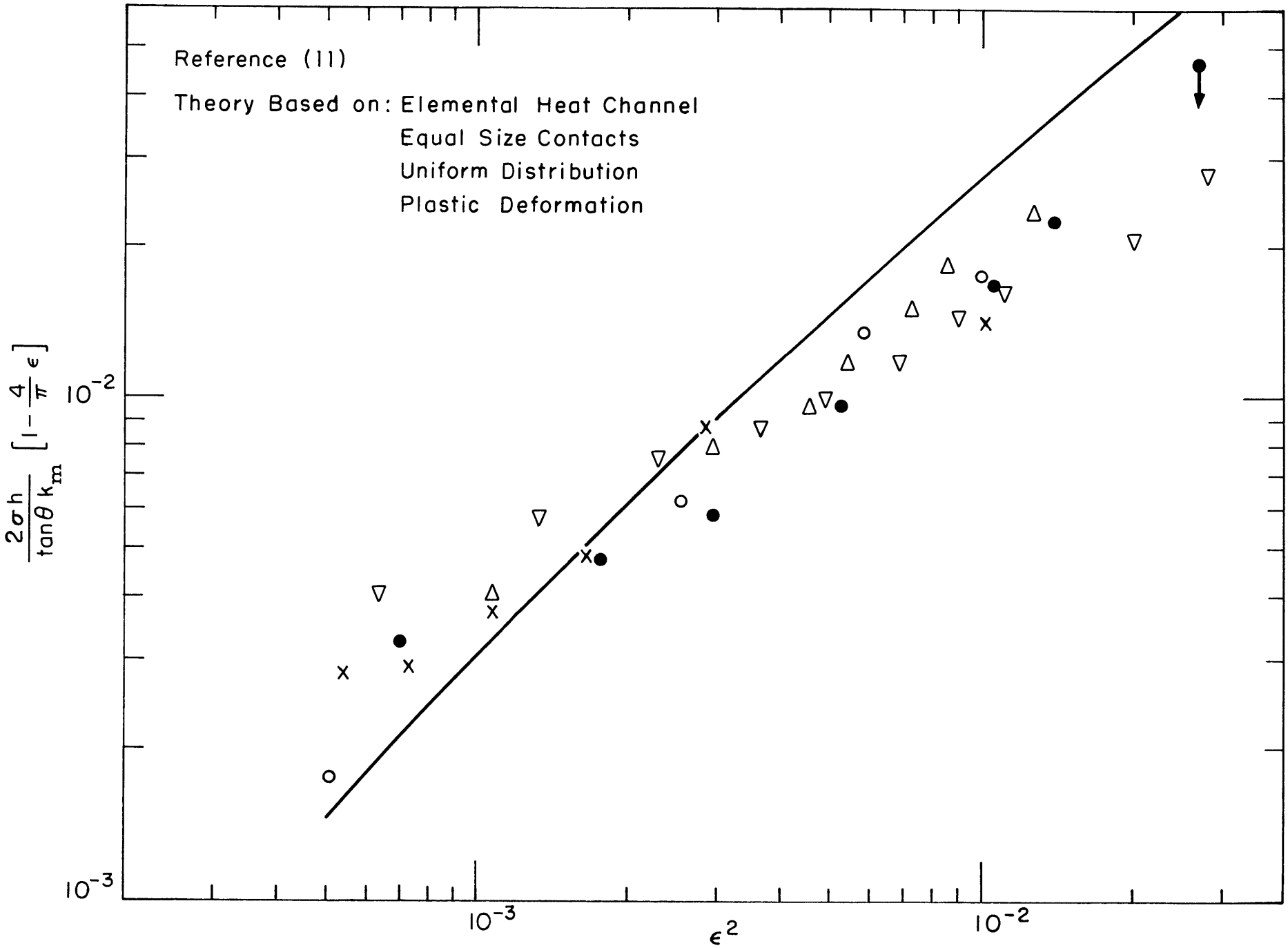

Fig. 34 Thermal Conductance Number vs. Area Ratio

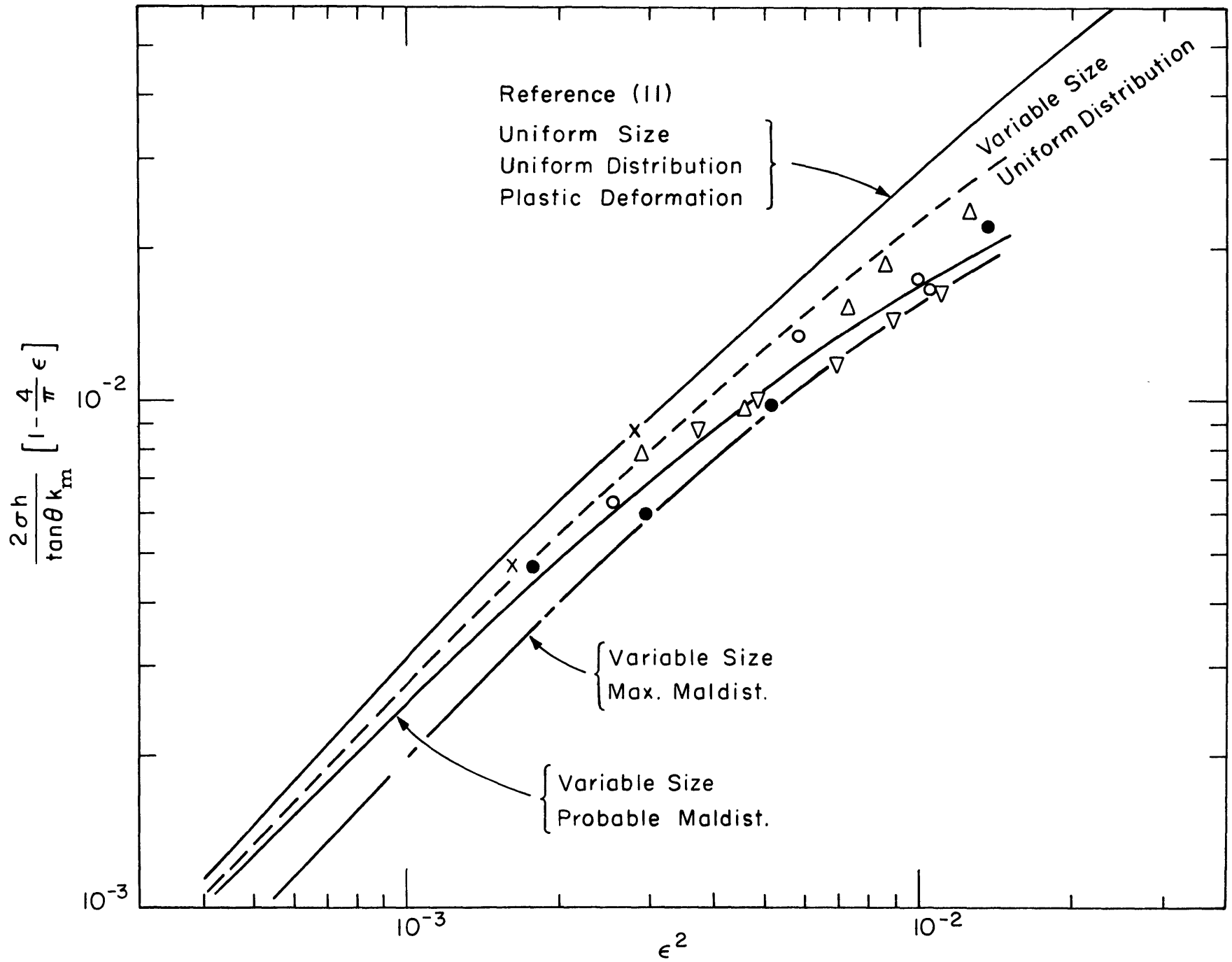

Fig. 35 Thermal Conductance Number vs. Area Ratio

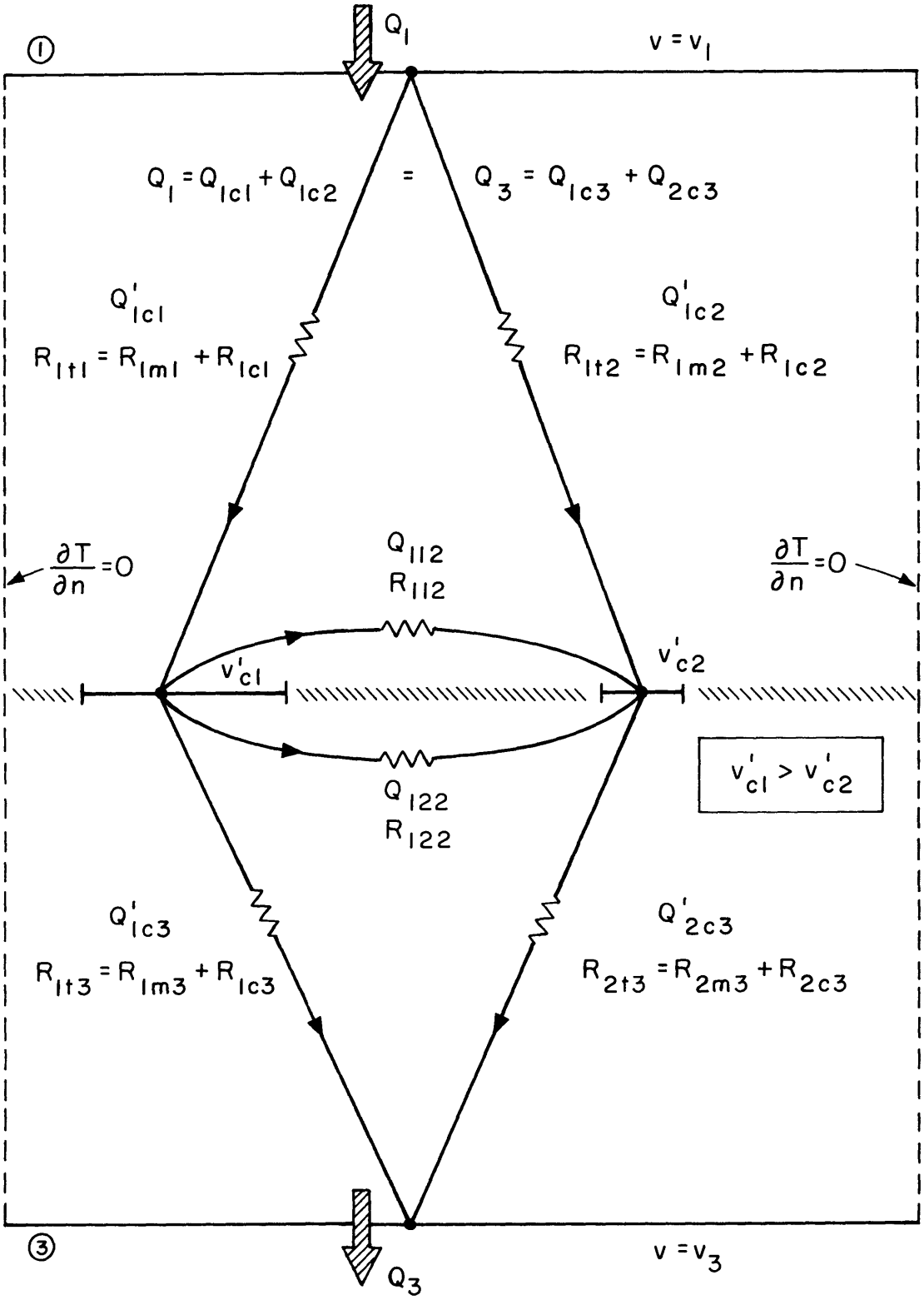

Fig. 36 Heat Flows Through Two Unequal Contact Spots

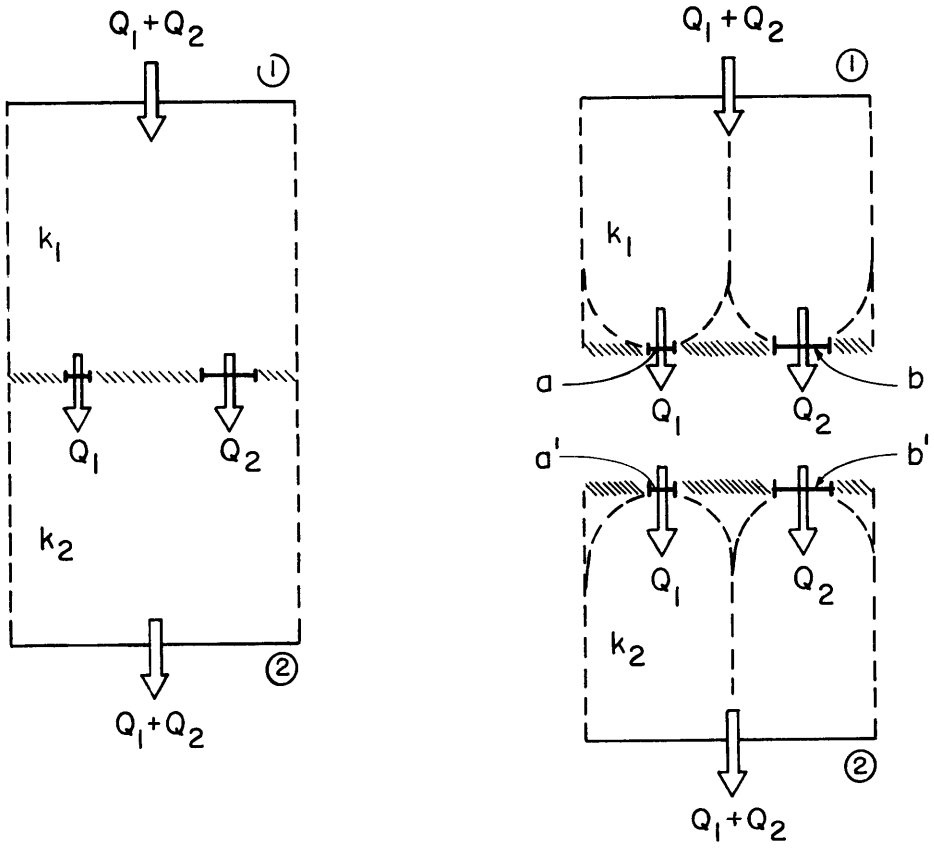

Fig. 37 Contact Model for Equal Contact Spot Temperatures